SACRAMENTO MUNICIPAL UTILITY DISTRICT

RANCHO SECO

NUCLEAR GENERATING STATION

DOCKET NUMBER 50-312

LICENSING REPORT FOR SPENT FUEL STORAGE CAPACITY EXPANSION

Licensing Report for High Density Spent Fuel Storage Racks

for

Rancho Seco Nuclear Generating Station

Sacramento Municipal Utilities District

Docket #50-312

June, 1982

TABLE OF CONTENTS

SECTION 13 - PRODUCTION CONTROL

SECTION 14 - COST/BENEFIT ASSESSMENT

LIST OF TABLES

SECTION 8

SECTION 9

SECTION 10

LIST OF FIGURES

LIST OF FIGURES (Continued)

1. INTRODUCTION

The purpose of this report is to provide descriptive information, and performance and safety analyses on the installation and use of high-density spent fuel storage racks at Rancho Seco Nuclear Generating Station, Unit Number 1. The corresponding requests to change the Rancho Seco Technical Specifications and Final Safety Analysis Report to allow for and describe the use of high-density spent fuel storage racks will be submitted to the USNRC in the near future.

Rancho Seco Nuclear Generating Station is a single unit B&W 177 fuel assembly design, owned and operated by Sacramento Municipal Utility District. The fuel storage pool is a reinforced concrete pool lined with stainless steel in the Fuel Storage Building. At the present time, the spent fuel storage pool has storage to accommodate 579 fuel assemblies. These storage racks are of the flux trap design and do not require the use of insoluble neutron absorber material. The center-to-center spacing between the fuel assembly storage location is 15 inches. The present fuel storage racks are replacements for the original 1 1/3 core designed storage capability.

Table 1.1 shows the previous and projected fuel discharge schedule for Rancho Seco. After each operating cycle approximately 59 fuel assemblies are transferred from the reactor to the spent fuel storage pool. Considering the current spent fuel storage capacity of 579 fuel assemblies, Table 1.1 indicates that following refueling at the end of cycle 8 (1987), insufficient fuel storage capacity will exist to receive a full core discharge of 177 fuel assemblies. Furthermore, following the refueling at the end of cycle 10 insufficient storage capacity will exist for refueling at the end of cycle 11. No further expansion of the Rancho Seco spent fuel storage capacity is possible using the presently approved spent fuel storage rack design (15 inch C-C flux-trap).

To efficiently increase the spent fuel storage capacity, the District proposes to replace the present spent fuel storage racks with new high-density spent fuel storage racks. This modification will utilize free-standing, self-supporting modules constructed of ASTM304 stainless steel and Boraflex, a neutron absorbing material to maintain K_{eff} less than 0.95. This design provides storage for 1080 fuel assemblies.

The specifications for design, construction and quality assurance for the high-density spent fuel storage racks were prepared by the District. The mechanical design, seismic/structural analysis, thermal-hydraulic analysis, and other related calculations as well as the fabrication of the hardware will be performed by Joseph Oat Corporation. Joseph Oat Corporation, based in Camden, N.J., possesses ASME Code stamps for Section III, Classes 1, 2, and 3 and MC pressure vessels and components. Southern Science Applications, Inc., of Dunedin, Florida, is serving as a consultant to Joseph Oat Corporation in the areas of criticality analysis and other radionuclide evaluations.

TABLE 1.1

RANCHO SECO NUCLEAR GENERATING STATION

FUEL ASSEMBLY DISCHARGES

Refueling		Discharged Assemblies		Remaining Storage Capabilities	
				Existing	
Cycle	Date	Cycle	Total	Racks	HD Racks
1	08/20/77	56	56	523	-
2	11/15/78	56	112	467	-
3	01/13/80	52	164	415	-
4	01/31/81	32	196	383	-
5	09/01/82	64	260	319	-
6	03/24/84	56	316	263	*764
7	08/15/85	56	372	207	708
8	01/06/87	56	428	151**	652
9	05/29/88	56	484	95	596
10	09/05/89	56	540	39	540
11	12/13/90	56	596	-	484
12	03/22/92	60	656	-	424
13	06/28/93	60	716	-	364
14	10/05/94	56	772	-	308
15	01/12/96	60	832	-	248
16	04/21/97	60	892	-	***188
17	07/28/98	56	948	-	**132

18	11/04/99	60	1008	-	72
19	02/11/01	60	1068	-	12
20	05/18/02	56	1124	-	-
21	08/25/03	60	1184	-	-
22	12/02/04	60	1244	-	-
23	03/09/06	56	1300	-	-
24	06/16/07	60	1360	-	-
EOL	10/15/08	177	1537		

* Approximate spaces available when change is made to high density racks.

** Full core discharge reserve lost.

*** To proceed beyond this point either off-site shipments or fuel consolidation will be necessary.

2. GENERAL ARRANGEMENT

The high density spent fuel racks consist of individual cells with approximately 9" x 9" square cross section, each of which accommodates a single PWR (Babcock and Wilcox) fuel assembly. The cells are arranged in modules of varying number of cells with a 10.50 inch center to center spacing. A total of 1080 cells are arranged in 11 distinct modules.

The high density racks are engineered to achieve the dual objective of maximum protection against structural loadings (arising from ground motion, thermal stresses, etc.) and the maximization of available storage locations. In general, a greater width to height aspect ratio provides greater margin against rigid body tipping. Hence the modules are made as wide as possible within the constraints of transportation and site handling capabilities. The rack modules will be installed in the Rancho Seco pool in the manner shown in Fig. 2.1.

As shown in Fig. 2.1, there are 11 discrete modules in 4 different types arranged in the fuel pool at 2.0" minimum inter-module gap. Table 2.1 gives the relevant physical data on each module type.

The modules are not anchored to the pool floor, to each other, or to the pool walls. A minimum gap of 2.0" gap is provided between the modules to ensure that kinematic movements of the modules during the Plant Design Basis Earthquake will not cause inter-module impact, or violate the minimum distance to ensure adequate margins for nuclear subcriticality. Adequate clearance with other pool hardware, eg. cask catcher, pool elevator, etc. is also provided.

Table 2.1 Module Data

Module Type	Quantity	Cells per module	Array Size	Approximate Weight (lb/module)
A	6	108	9x12	38500
B	3	90	9x10	32000
C	1	72	9x8	26000
D*	1	90+4*	9x10 1x4*	33500

* Module type D contains (4) four "defective fuel container" cells.

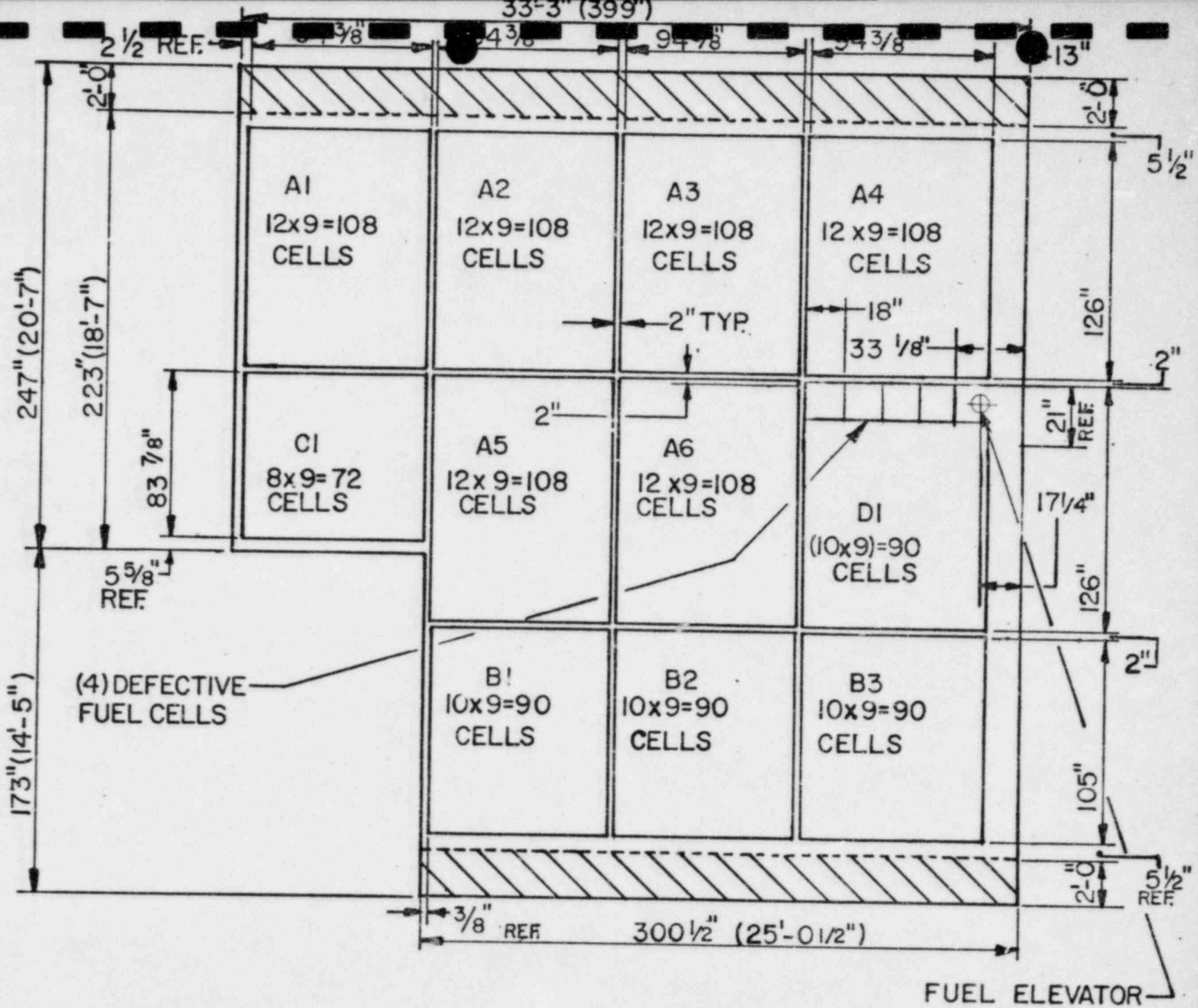

FIG. 2.1 TOTAL 1080 CELLS MODULE LAYOUT

3. RACK CONSTRUCTION

3.1 Fabrication Details:

The rack module is fabricated from ASTM 240-304 austenitic stainless steel plate material, and ASTM 182-F304 forging material. The stainless steel material is required to pass the intragrannular corrosion test specified by ASTM 262 Practice E to ensure high corrosion resistance of all structural components in the rack. Boraflex, a patented brand name product of BISCO serves as the neutron absorber material. Further details on this material may be found in Section 9.

A typical module contains storage cells which have an 8.874" minimum cross sectional opening. This dimension ensures that fuel assemblies with maximum expected axial bow can be inserted and removed from the storage cells without any damage to the fuel assemblies or the rack modules.

Fig. 3.1 shows a horizontal cross section of a 2x2 array. The cells pro ·ie a smooth and continuous surface for lateral contact with the fuel assembly. The anatomy of the rack modules is best exposed by describing the basic building blocks of the design, namely

(a) Internal square tube
(b) Boraflex envelope angular elements
(c) Angular structural element
(d) Base plate
(e) Support assembly
(f) Top bend-in

a. Internal square tube:
This element provides the lateral bearing surface to the fuel assembly. It is fabricated by joining two formed channels using a controlled seam welding operation. The weld penetration in the seam welded zone is required to be 90% minimum. This element is 8.874" square (minimum) cross section x 162.375" long.

b. Boraflex envelope angular elements:
Boraflex surrounds the square tube on all four sides over a length of 146" which completely envelopes the active fuel length of all fuel assemblies and provides for one inch of additional protection on the top and bottom.

c. Angular structural elements:
Two angular subelements, illustrated in Fig. 3.2 (a) and (b) comprise the structural support gridwork for the fuel racks. One set of large and small angular subelements is placed around the square tube with the poison material interposed in-between, as shown in the cross section in Fig. 3.3. Angular spacers and appropriately dimensioned boraflex sheets preclude any lateral sliding of the neutron absorber material. The fillet welds indicated in Fig. 3.3 are made while the angular subelements exert a contact pressure on the neutron absorber sheets in the welding fixture, thereby ensuring a continuous surface contact in a macroscopic sense, between the constituent elements of the sandwich. As shown in Fig. 3.4, bottom spacer sheets (also made for ASTM

240-304 material) position the boraflex sheets in the vertical direction. The top of the angular sub-elements is welded to the square tube using a suitable spacer. In this manner a composite box assembly is fabricated. An array of composite box assemblies welded as indicated in Fig. 3.1 form the "honey-comb" gridwork of cells which harnesses the structural strength of all sheet and plate type members in an efficient manner. The array of composite boxes has overall bending, torsional and axial rigidities which are an order of magnitude greater than configurations utilizing grid bar type of construction.

(d) Base Plate:

The base plate is a 5/8" thick plate type member which has 6" diameter holes concentrically located with respect to the internal square tube. These holes provide the primary path for coolant flow. Secondary flow paths are available between adjacent cells via the lateral flow holes (1.0" diameter) near the root of the "honey-comb". The honey comb is welded to the base plate with 1/8" fillet welds.

(e) Support Assembly:

Each module has 4 support legs. One support leg is of fixed height,(Fig. 3.6) the other three can be adjusted in length to enable leveling of the rack. The variable height support assembly consists of a flat-footed spindle which rides into an internally threaded cylindrical member. The cylindrical member is attached to the underside of the base plate through a full penetration weld. The base of the flat-footed spindle sits on the pool floor. Leveling of the rack modules is accomplished

by turning the square sprocket in the spindle using a long arm (approximately 17' long) square head wrench. Fig 3.5 shows a vertical cross section of the adjustable support assembly.
The supports elevate the module base plate 8.88" above pool floor, thus creating the water plenum for coolant flow. The lateral holes in the spindle provide the coolant entry path leading into the bottom of the storage locations.

(f) Top Lead-In:
Contiguous walls of adjacent cells are flared and seam welded to provide a smooth lead-in for fuel assembly insertion. These conical joints also aid in reducing the lateral deflection of the inner square tube due to the impact of fuel assemblies during the ground motion (postulated seismic motion specified in the FSAR). This construction procedure leads to natural venting locations for the inter-cell space where the neutron absorber material is located. The fabrication of the rack modules is performed under a strict quality assurance system suitable for ASME Section III, Class 1, 2 and 3 manufacturing which has been in place at Joseph Oat Corporation for over 10 years. The essentials of the Q.A. production and design interface systems are abstracted in Sections 11 through 13.

3.2 Codes, Standards, and Practices for the Spent Fuel Pool Modification

The following are the public domain codes, standards, and practices to which the fuel storage racks are designed, constructed and assembled, and/or pool structure analyzed. Additional problem-specific references related to detailed analyses are given at the end of each section.

I. Design Codes

(a) AISC Manual of Steel Construction, 8th Edition, 1980 including supplements 1, 2 and 3 to the AISC Specification.

(b) ANSI N210-1976 Design Objectives for Light Water Reactor Spent Fuel Storage Facilities at Nuclear Power Stations.

(c) ASME, Section III, Appendix (1980).

II. Material Codes

(a) American Society for Testing and Materials (ASTM) Standards

(b) American Society of Mechanial Engineers (ASME), Section III, Div. 1, Subsection NF (1980).

III. Welding Codes

(a) ASME Boiler and Pressure Vessel Code, Section IX-1980 Welding and Brazing Qualifications.

IV. Quality Assurance, Cleanliness, Packaging, Shipping, Receiving, Storage, and Handling Requirements

The quality assurance program for the design and installation of the new spent fuel storage racks will be consistent with the plant Q.A. program.

V. Other References

(a) NRC Regulatory Guides, division 1, regulatory guides 1.13, 1.29, 1.71, 1.85, 1.92, and 1.124 (revisions effective as of April 1980).

(b) General Design Criteria for Nuclear Power Plants, Code of Federal Regulations, Title 10, Part 50, Appendix A (GDC Nos. 1, 2, 61, 62, and 63).

(c) NUREG-0800, Standard Review Plan (1981).

(d) "NRC Position for Review and Acceptance of Spent Fuel Storage and Handling Applications," dated April 14, 1978, and the modifications to this document of January 18, 1979.

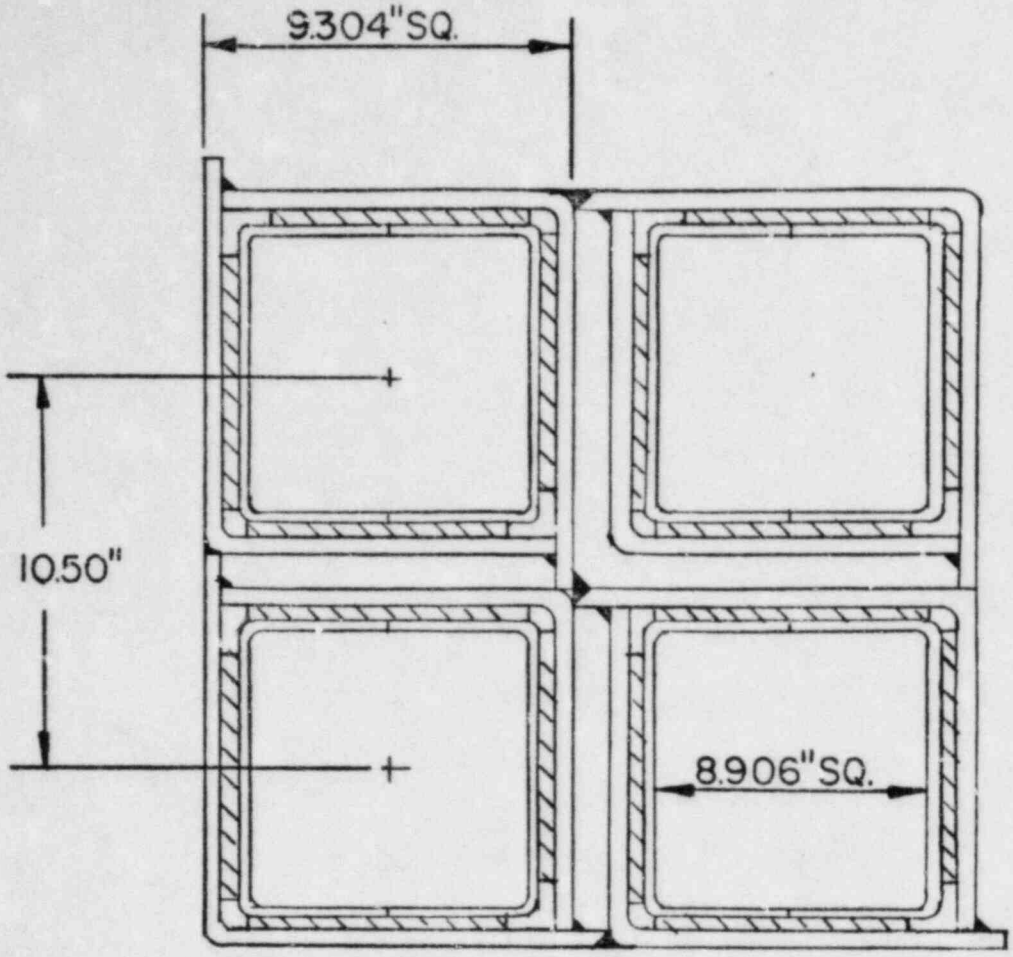

FIG. 3.1 2X2 CELLS

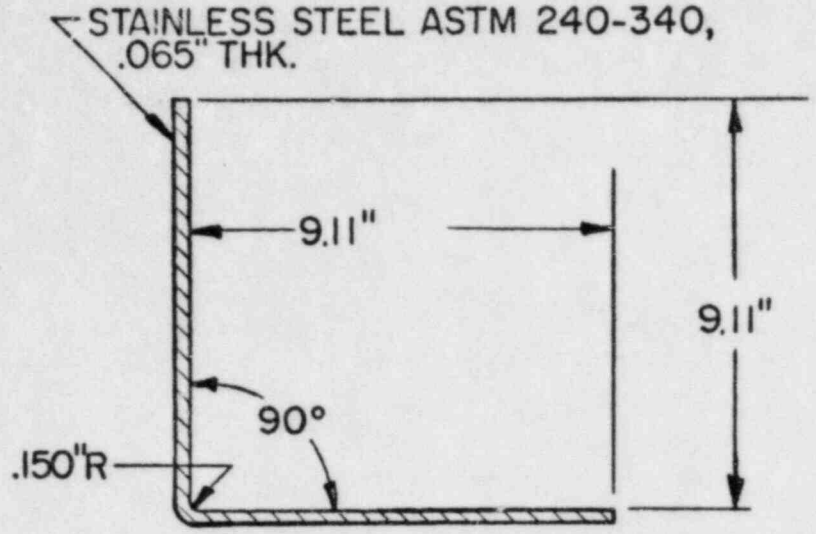

FIG 3.2A-SMALL ANGULAR SUB ELEMENT

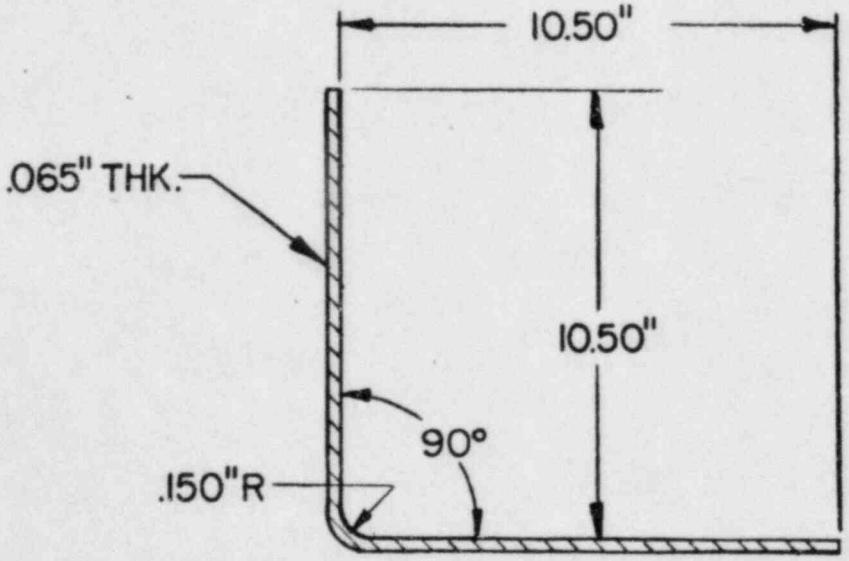

FIG 3.2B LARGE ANGULAR SUB ELEMENT

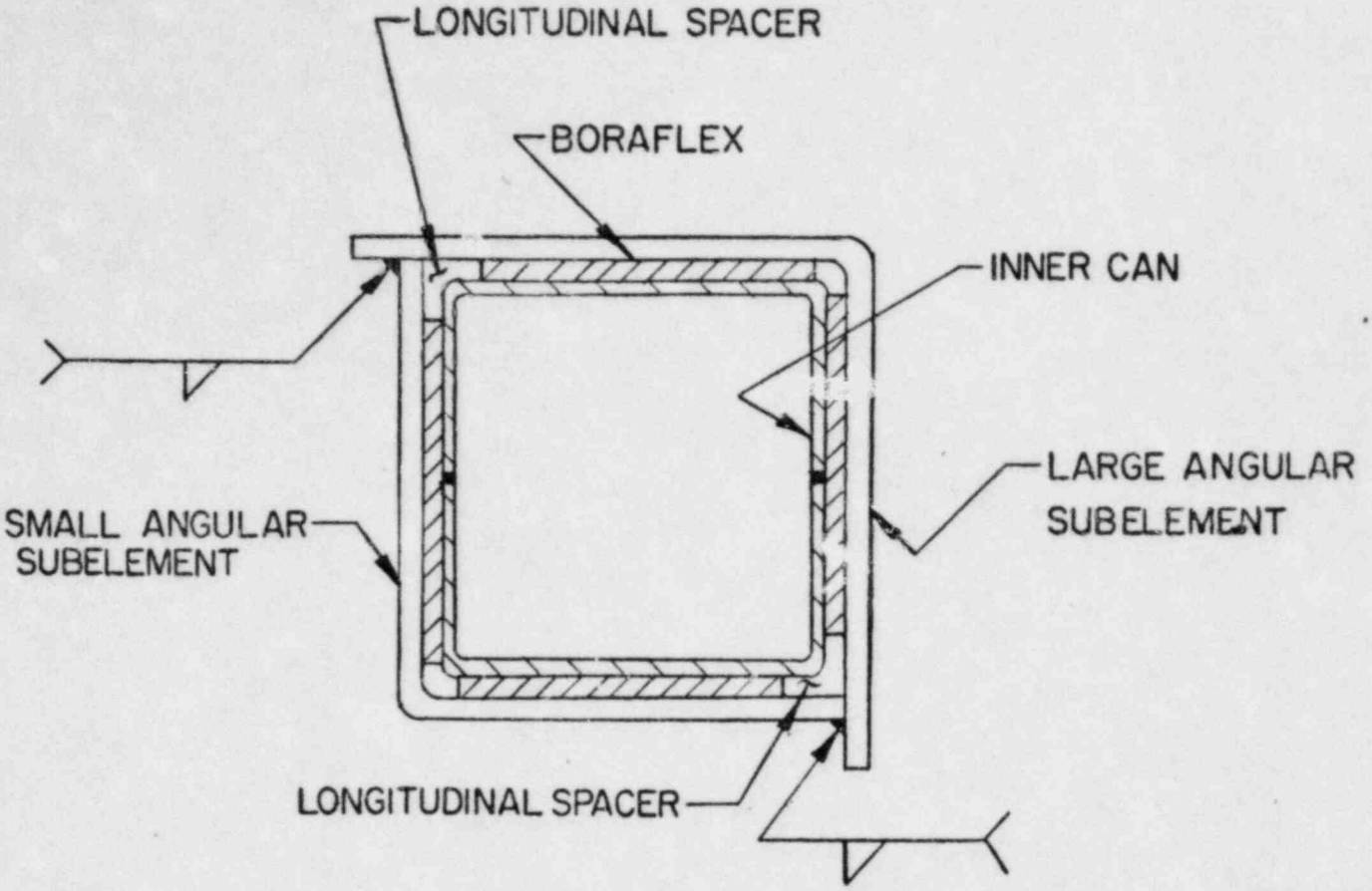

FIG 3.3 COMPOSITE BOX ASSEMBLY

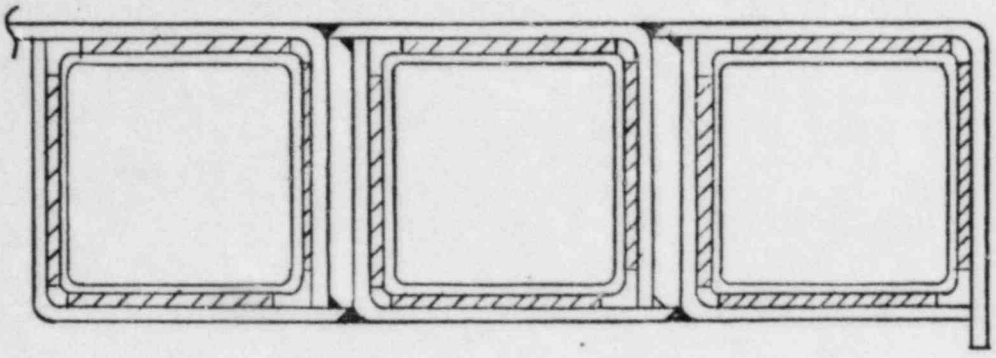

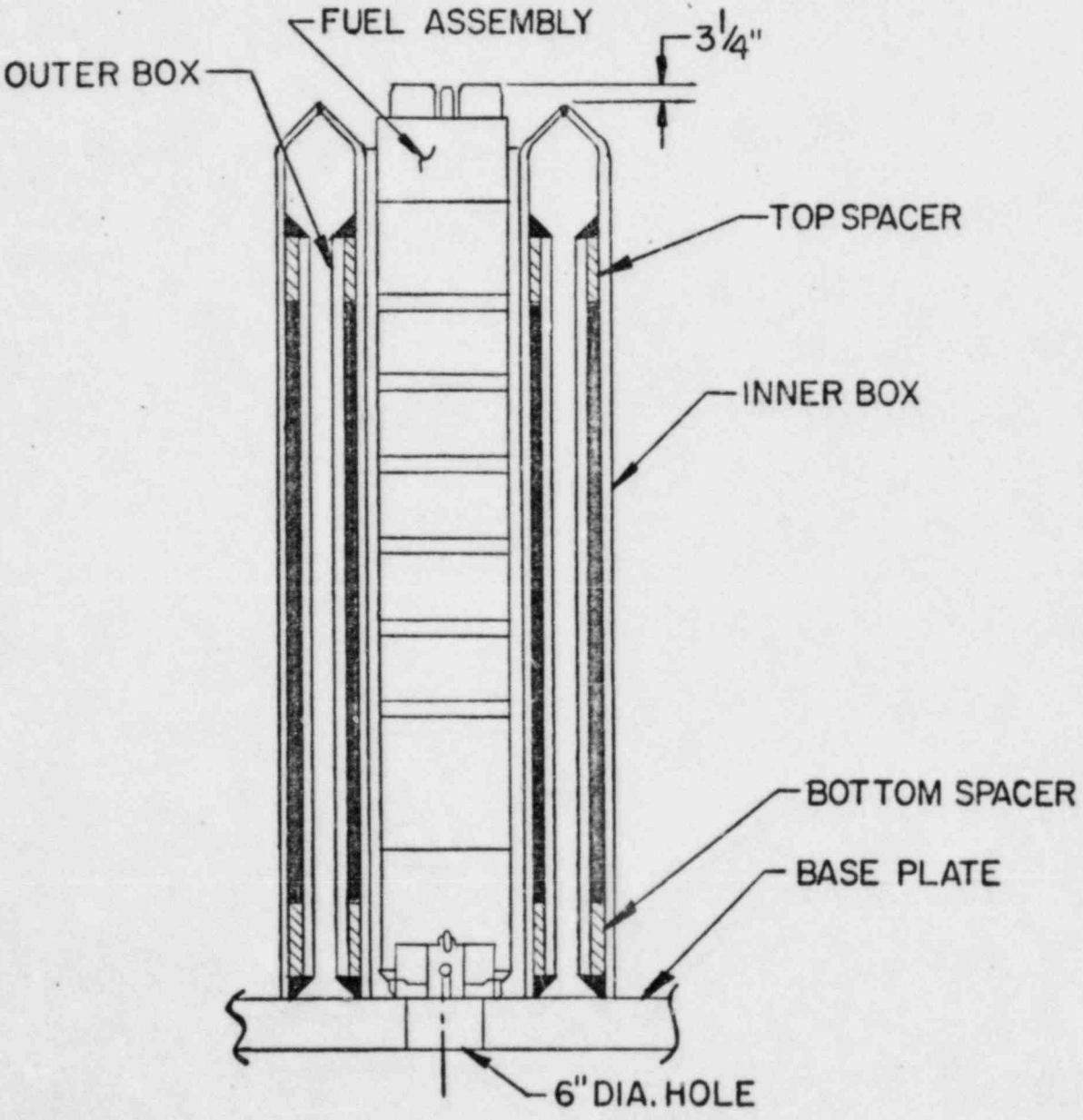

FIG 3.4 TYPICAL CELL ELEVATION

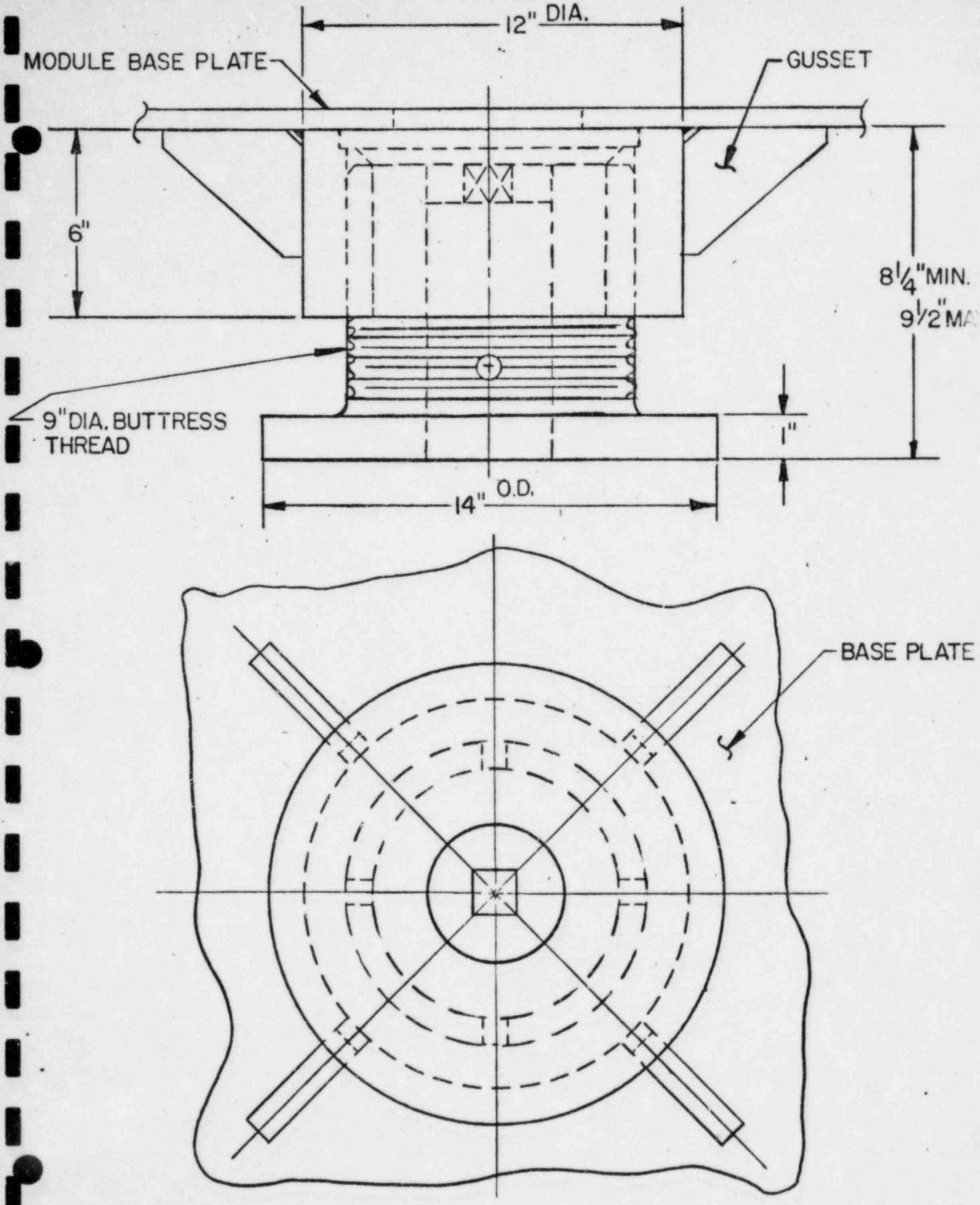

FIG. 3.5 ADJUSTABLE SUPPORT

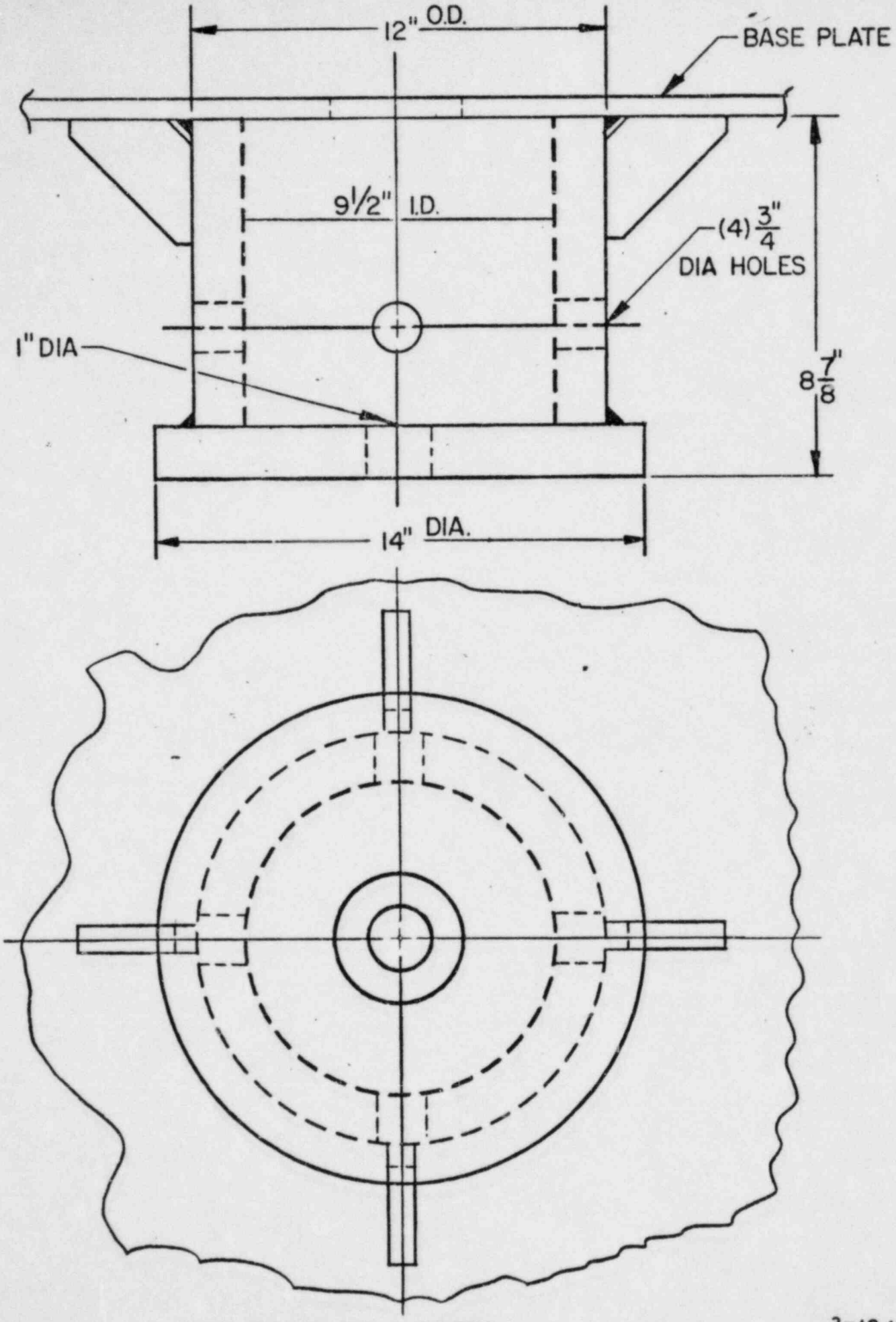

FIG. 36 FIXED SUPPORT

4. NUCLEAR CRITICALITY ANALYSIS

4.1 Design Bases

The high density spent fuel storage racks for the Rancho Seco Plant are designed to assure that a k_{eff} equal to or less than 0.95 is maintained with the racks fully loaded with fuel of the highest anticipated reactivity and flooded with unborated water at a temperature corresponding to the highest reactivity. The maximum calculated reactivity includes a margin for uncertainty in reactivity calculations and in mechanical tolerances, statistically combined, such that the true k_{eff} will be equal to or less than 0.95 with a 95% probability at a 95% confidence level.

Applicable codes, standards and regulations or pertinent sections thereof include the following:

- General Design Criterion 62 - Prevention of Criticality in Fuel Storage and Handling.
- NRC letter of April 14, 1978, to all Power Reactor Licensees - OT Position for Review and Acceptance of Spent Fuel Storage and Handling Applications, including modification letter dated January 18, 1979.
- USNRC Standard Review Plan, NUREG-0800, Section 9.1.2, Spent Fuel Storage.
- Regulatory Guide 1.13, Spent Fuel Storage Facility Design Basis (proposed), December 1981.
- Regulatory Guide 3.41, Validation of Calculational Method for Nuclear Criticality Safety (and related ANSI N16.9-1975).
- ANSI N210-1976, Design Objectives for Light Water Reactor Spent Fuel Storage Facilities at Nuclear Power Plants.
- ANSI N18.2-1973, Nuclear Safety Criteria for the Design of Stationary Pressurized Water Reactor Plants.

The design basis fuel assembly is a 15 x 15 array of fuel rods (Babcock & Wilcox Mark B designs) containing UO_2 at a maximum uniform enrichment of 4.0% U-235 by weight, corresponding to 51.5 to 52.5 grams U-235 per axial centimeter of fuel assembly (0.110 to 0.112 g/cm^3).

The high density spent fuel storage racks are also designed, should the need arise, to accommodate "consolidated" fuel pin storage, i.e., fuel elements which have been dismantled and individual pins placed in storage cells on a more close-packed lattice than in the original fuel elements. A separate licensing submittal will be made if consolidation is to be used.

To assure the true reactivity will always be less than the calculated reactivity, the following conservative assumptions were made.

- Moderator is pure, unborated water at a temperature corresponding to the highest reactivity.
- Lattice of storage racks is infinite in all directions; i.e., no credit is taken for axial or radial neutron leakage (except in the assessment of certain abnormal/accident conditions).
- Neutron absorption in minor structural members is neglected; i.e., spacer grids are replaced by water.
- Pure zirconium is used for cladding, control rod guide tubes and instrument thimbles; i.e., higher neutron absorption of alloying materials in Zircaloy is neglected.

4.2 Geometric and Calculational Models

4.2.1 Reference Fuel Assembly

The reference design basis fuel assembly, illustrated in Fig. 4.1, is a 15 x 15 array of fuel rods with 17 rods replaced by 16 control rod guide tubes and one instrument thimble.

Minor variations in fuel pellet diameter and UO_2 density

exist between the different batches of replacement fuel. Table 4-1 summarizes the fuel assembly design specifications and expected range of fuel parameters. In all cases, the cladding is Zircaloy of 0.430-inch O.D. and 0.377-inch I.D.

4.2.2. Analytical Methods

Nuclear criticality analyses of the high density spent fuel storage rack were performed with the AMPX[1]-KENO[2] computer package, using the 123-group GAM-THERMOS cross-section set and the NITAWL subroutine for U-238 resonance shielding effects (Nordheim integral treatment). AMPX-KENO has been extensively benchmarked against a number of critical experiments (e.g., Refs. 3, 4, 5 and 6).

For investigation of small reactivity effects (e.g., mechanical tolerances), a four-group diffusion/blackness theory method of analysis (NULIF-CNROD-PDQ7) was used (Ref. 5) to calculate small incremental reactivity changes. This model has been used previously with good results and is normally used only to evaluate trends and small incremental reactivity effects that would otherwise be lost in the KENO statistical variation. Where possible, trends calculated by AMPX-KENO and by diffusion/blackness were compared and found to be in good agreement, within the statistical uncertainty of KENO calculations, over the range of interest.

Table 4-1 FUEL ASSEMBLY DESIGN SPECIFICATIONS

Fuel Rod Data	
Outside dimension, in.	0.430
Cladding thickness, in.	0.0265
Cladding material	Zr-4
Pellet diameter, in.	0.3648 - 0.3700
UO_2 density, % T.D.	92.5 - 96.5
Enrichment, wt. % U-235	4.00
Fuel Assembly Data	
Number of fuel rods	208 (15 x 15 array)
Fuel rod pitch, in.	0.568
Control rod guide tube	
Number	16
O.D., in.	0.530
Thickness, in.	0.016
Material	Zr-4
Instrument thimble	
Number	1
O.D., in.	0.493
Thickness, in.	0.026
Material	Zr-4
U-235	
g/axial cm of assembly	51.5 - 52.5
g/cm^3 of assembly	0.110 - 0.112

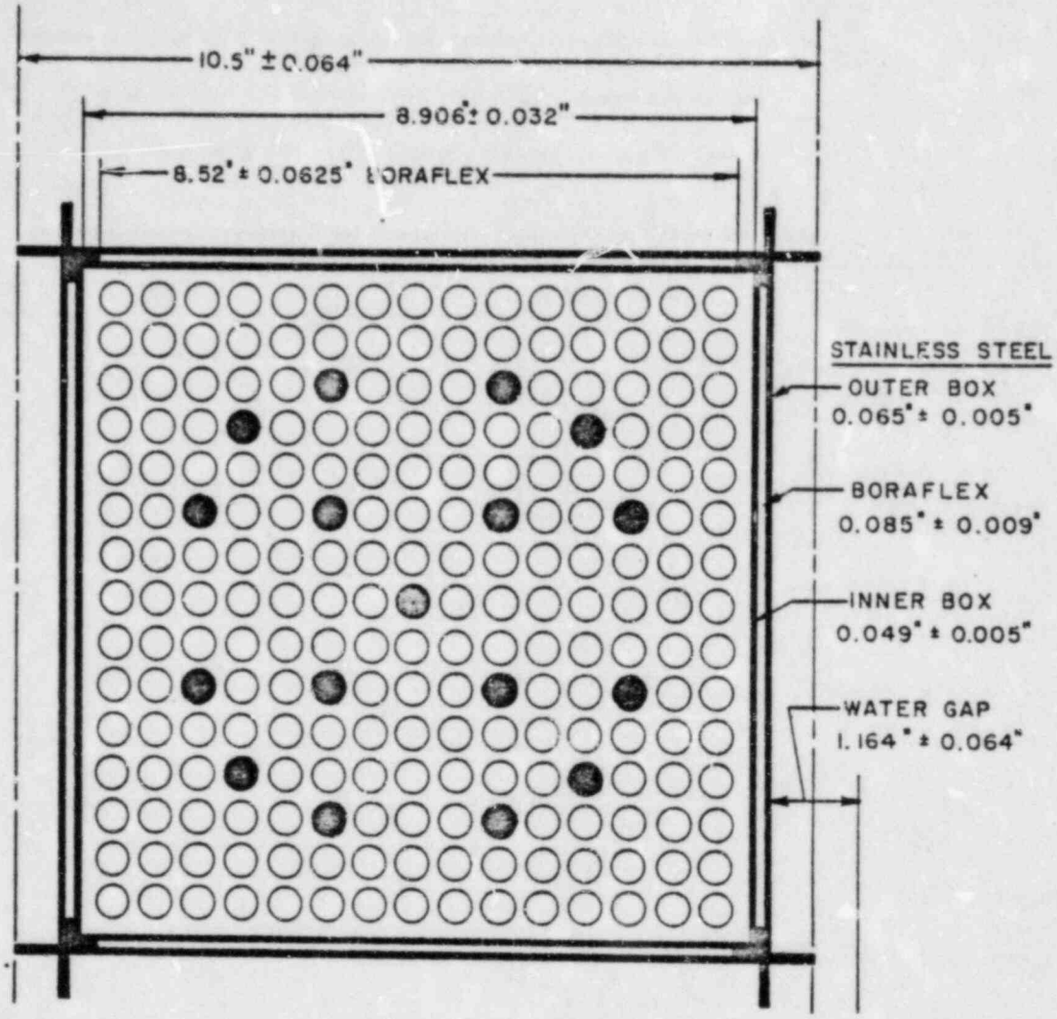

FUEL ASSEMBLY: 15 x 15 Square Array
208 Fuel Rods
16 Control Rod Thimbles
1 Instrument Tube

Fig. 4.1 Reference design configuration.

4.2.3 Calculational Bias and Uncertainty

Results of benchmark calculations[5,6] on a series of critical experiments, indicate a calculational bias of 0, with an uncertainty of ±0.003 (95% probability at a 95% confidence level). In addition, a small correction in the calculational bias is necessary to account for the water gap thickness (0.486 inches) between fuel assemblies in the Rancho Seco spent fuel rack compared to the corresponding thickness (0.644 inches) in the benchmark critical experiments. Based upon the correlation developed in Ref. 6, the correction for water-gap thickness in the Rancho Seco spent fuel storage rack indicates a small overprediction of 0.002 Δk. For conservatism, the overprediction is neglected and the net calculational bias is taken as 0.000 ± 0.003, including the effect of the water-gap thickness.

4.2.4 Trend Analysis

Trend analysis[6] of benchmark calculations on critical experiments with varying boron content in the absorber plate between fuel assemblies indicates a tendency to overpredict k_{eff} with higher reactivity worth of the boron absorber. In the Rancho Seco spent fuel rack, the boron worth is about 31% Δk, or approximately twice the highest boron worth (15.9% Δk) in the critical experiments analyzed in Ref. 6. Based upon extrapolation of the trend analysis, AMPX-KENO calculations of the Rancho Seco rack would be expected to overpredict k_∞ by an estimated 1.8 ± 0.8 (95% probability at 95% confidence limit). Thus, to the extent extrapolation of the linear regression analysis is valid, the AMPX-KENO calculation of the Rancho Seco rack will conservatively overpredict the reactivity. Calculations with the ORNL 218-group SCALE cross-section library confirm the conservatism of the calculational model. No credit is taken for the expected overprediction other than to indicate an additional level of conservatism in the criticality analysis of the Rancho Seco spent fuel storage rack.

4.2.5 Reference Fuel Storage Cell

The nominal spent fuel storage cell model used for the criticality analyses is shown in Fig. 4.1. The rack is composed of Boraflex absorber material sandwiched between a 0.049-inch inner stainless steel box and a 0.065-inch outer stainless steel box. The fuel assemblies are centrally located in each storage cell on a nominal lattice spacing of approximately 10.5 inches. Stainless steel tabs connect one storage cell box to another in a rigid structure and define an outer water space between boxes. This outer water space constitutes a flux-trap between the two Boraflex absorber plates that are essentially opaque (black) to thermal neutrons. The Boraflex absorber has a nominal thickness of 0.085 inches and a nominal B-10 areal density of 0.02646 grams B-10 per cm^2. For two-dimensional X-Y analysis, a zero current (white albedo) boundary condition was applied in the axial direction and at the centerline through the outer water space (flux-trap) on all four sides of the cell, effectively creating an infinite array of storage cells.

4.3 Reference Subcriticality and Mechanical Tolerance Variations

4.3.1 Nominal Design Case

Under normal conditions, with nominal dimensions, the calculated k_∞ is 0.9247 ± 0.0034 (1σ with 100 generations of 500 neutrons each) for the nominal case. For a one-sided tolerance factor[7] of 1.924, corresponding to 95% probability at a 95% confidence limit with 100 generations, the maximum deviation of k_∞ is ±0.0065. A mid-range UO_2 density of 94.5% theoretical density with a pellet diameter of 0.370 inches was used for the nominal case in the criticality analysis.

The outer stainless steel tabs, shown in Fig. 4.1, connecting to adjacent storage cells are not necessarily all present in every storage cell. A KENO calculation with all tabs removed showed a very small decrease in k_∞ (-0.0014 Δk) from the reference configuration. Thus, the presence or absence of the tabs does not significantly affect reactivity and the reference configuration represents the higher reactivity.

An independent KENO check calculation was made using both the more recent 218-group and derivative 27-group SCALE cross-section libraries[8,9] developed by ORNL for criticality safety analysis. Both of these libraries yielded a k_∞ that was 0.020 ± 0.005 Δk lower than the reference calculation with the 123-group GAM-THERMOS library. These calculations confirm the trend toward overprediction identified in Ref. 6 (discussed in Section 4.2.4 above) and indicate the analysis presented herein is conservative by ~2% Δk .

4.3.2 Consolidated Fuel Pin Storage

For purposes of criticality safety evaluation, it was assumed that two fuel assemblies are dismantled and all 416 fuel rods placed in a single storage cell. For the very low water-to-

fuel volume ratio ("dry" lattice) of such an arrangement, the k_∞ is expected to be substantially subcritical. This has been confirmed by an AMPX-KENO calculation,* yielding a k_∞ of 0.597. Thus, the reference design with a single intact fuel assembly has a higher reactivity and is the limiting case. "Consolidated" fuel can be safely stored in the storage rack without encountering any potential criticality problem.

4.3.3 Boron Loading Variation

The Boraflex absorber plate is nominally 0.085 inches thick with a B-10 areal density of 0.02646 g/cm^2. Independent manufacturing tolerance limits are ±0.009 inch in thickness and ±0.00185 g/cm^2 in boron-10 content. This assures that, at any point where the minimum boron loading (0.02461 g B-10/cm^2) and minimum Boraflex thickness (0.076 inch) may coincide, the boron areal density will not be less than 0.022 g B-10/cm^2.

Calculations were made of k_∞ with variations in Boraflex absorber loading and thickness. Results of these calculations, given in Fig. 4.2, indicate that the k_∞ can be described by the following regression fit (least squares) to the data over the range of B-10 loading from 0.015 to 0.030 g/cm^2.

$$\ln k_\infty = -0.03835 \ln (\text{B-10, } g/cm^2) - 0.2158$$

*For this calculation, the fuel pins were assumed to be uniformly positioned within the storage cell, and the XSDRNPM routine in AMPX used to generate a 123-group set of weighted cross-sections for the homogenized fuel region for subsequent use in KENO.

Within the precision of the calculations, this relationship indicates that the tolerance limits result in an incremental reactivity change (uncertainty) of ±0.0026 Δk for boron content and ±0.0041 for Boraflex thickness variations. The trend calculated both by AMPX-KENO and by diffusion/blackness theory is the same within analytical uncertainty over the applicable range.

4.3.4 Storage Cell Lattice Pitch Variations

The design storage cell lattice spacing between fuel assemblies is approximately 10.5 inches. An increase in storage cell lattice spacing may or may not reduce reactivity depending upon other dimensional changes that may be associated with the increase in lattice spacing. Increasing lattice spacing by increasing the outer (flux-trap) water thickness reduces reactivity, although increasing the inner water thickness (between the fuel and the inner stainless steel box) results in a small increase in reactivity for the same increase in lattice spacing. The reactivity effect of the outer (flux-trap) water thickness, however, is considerably more significant. Both of these effects have been evaluated for the independent design tolerances.

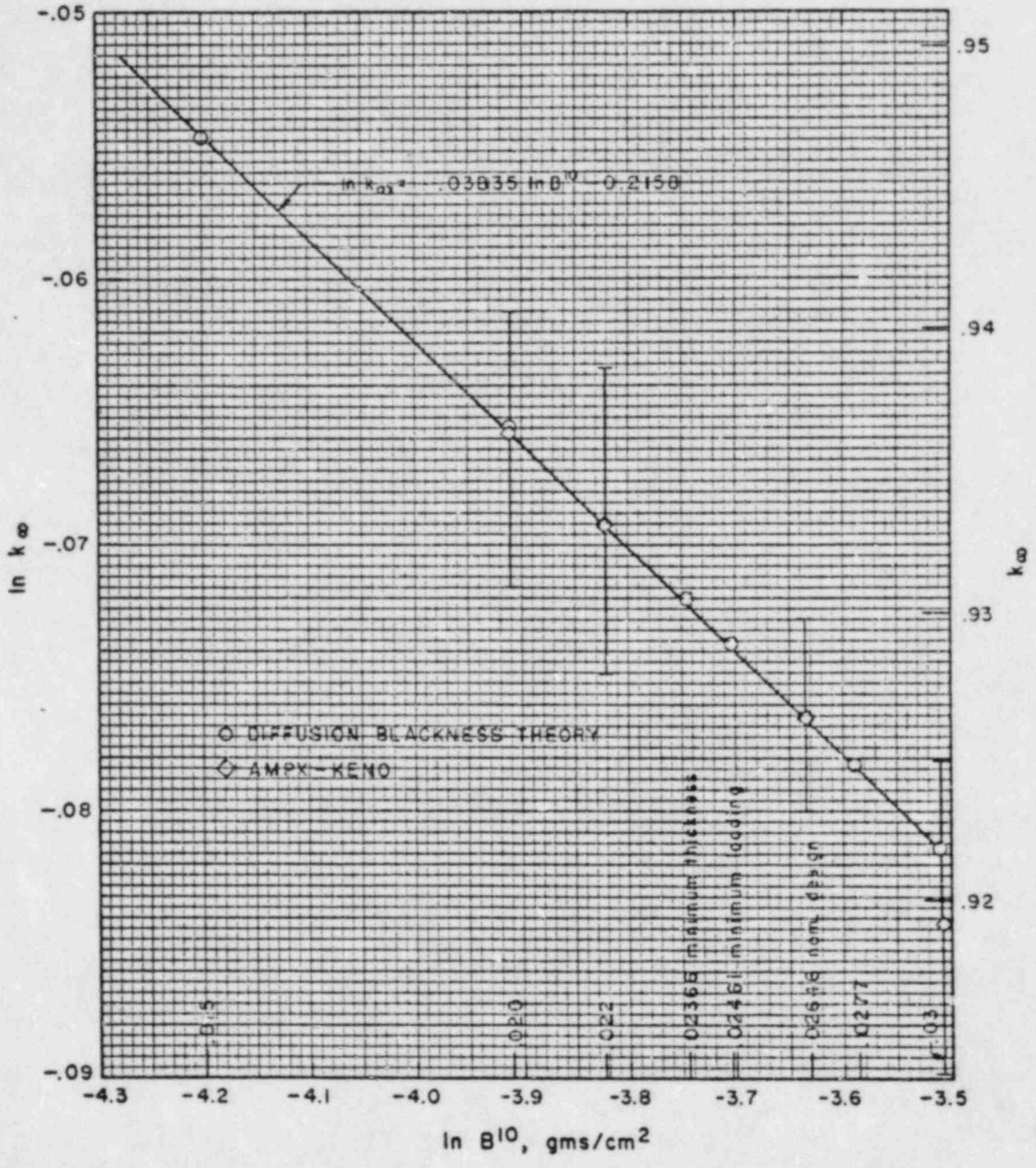

Fig. 4.2 Log-log plot of calculated k_∞ versus B-10 loading.

4.3.4.1 Inner Water Thickness Variations

The inner stainless steel box dimension, 8.906 ± 0.032 inches, defines the inner water thickness between the fuel and the inside box. For the stated tolerance limit, the calculated uncertainty in reactivity is ±0.0006 Δk, with k_∞ increasing as the inner stainless steel box dimension (and derivative lattice spacing) increases.

4.3.4.2 Outer (Flux-trap) Water Thickness Variation

The design outer (flux-trap) water thickness is 1.164 ± 0.064 inches, which results in an uncertainty of ±0.007 Δk due to the tolerance in flux-trap water thickness. Increasing the flux-trap thickness reduces reactivity.

4.3.5 Stainless Steel Thickness Variations

The nominal stainless steel thickness is 0.049 inches for the inner box and 0.065 inches for the outer box. The maximum positive reactivity effect of the expected stainless steel thickness tolerance variation (±0.005 inches) was calculated to be ±0.0006 Δk (by diffusion/blackness theory, since the reactivity increment is too small to be calculated by AMPX-KENO).

4.3.6 Fuel Enrichment and Density Variation

The design maximum enrichment is 4.00 ±0.013 wt.% U-235. Calculations of the sensitivity to small enrichment variations by diffusion/blackness theory yielded a coefficient of 0.0045 Δk per 0.1 wt% U-235 at the design enrichment. For the tolerance on U-235 enrichment of ±0.013 in wt.%, the uncertainty on k_∞ is ±0.0006 Δk.

Calculations were made with the UO_2 fuel density ranging from the minimum of 92.5% theoretical density to a maximum

(compacted) value of 96.5% theoretical density. For the mid-range value (94.5% T.D.), used for the reference design calculations, the uncertainty in reactivity is ±0.0024 Δ k over the maximum range of UO_2 densities expected.

4.3.7 Boraflex Width Tolerance Variation

The reference storage cell design (Fig. 4.1) uses a Boraflex blade width of 8.52 ± 0.0625 inches. A positive increment in reactivity occurs for a decrease in Boraflex absorber width. For the width tolerance of -0.0625 inches, the maximum calculated reactivity increment is + 0.0003 Δ k. Increasing the Boraflex width decreases reactivity.

4.3.8 Summary of Statistical Variations

Calculated reactivity increments from mechanical and fabrication tolerances are summarized in Table 4-2.

Table 4-2 CALCULATED STATISTICAL VARIATIONS IN REACTIVITY (MECHANICAL)

Case	Tolerance	Incremental Reactivity, Δk
Boron concentration	±0.00185 g B-10/cm^2	∓0.0026
Boraflex thickness	±0.0009 inch	∓0.0041
Lattice pitch		
inner water thickness	±0.032 inch	±0.0006
outer water thickness	±0.064 inch	∓0.0070
SS tolerance	±0.005 inch	±0.0006
Fuel enrichment	±0.013% U-235	±0.0006
Fuel density	92.5% - 96.5% T.D.	±0.0024 (at mid-range of 94.5% T.D.)
Boraflex width	±0.0625 inch	±0.0003
Statistical combination (root-mean-square of reactivity increments)		±0.0089

4.4 Abnormal and Accident Conditions

4.4.1 Eccentric Positioning of Fuel Assembly in Storage Rack

The fuel assembly is normally located in the center of the storage rack cell with bottom fittings and spacers that mechanically limit lateral movement of the fuel assemblies. Nevertheless, calculations were made with adjacent fuel assemblies (each assumed to be positioned in an eccentric location) on one side of a cell with the fuel rods touching the stainless steel Boraflex plate. For this case, the calculated reactivity was slightly less than the nominal design case (by 0.006 Δ k). Calculations made with the fuel assemblies moved into the corner of the storage rack cell (four-assembly cluster at closest approach) also resulted in a negative reactivity effect (0.005 Δ k). Fuel assembly bowing will produce a small negative reactivity effect locally. Thus, the nominal case, with the fuel assembly positioned in the center of the storage rack cell, yields the maximum reactivity.

4.4.2 Temperature and Water Density Effects

Increasing temperature from the nominal 40°F (water density of 1.000) is calculated to monotonically decrease reactivity as indicated in Table 4-3 (reactivity effects calculated by diffusion/blackness theory). Introducing voids in the water internal to the storage cell (to simulate boiling) decreased reactivity, as shown in the table. Voids due to boiling will not occur in the outer (flux-trap) water region.

Table 4-3 EFFECT OF TEMPERATURE AND VOID ON CALCULATED REACTIVITY OF STORAGE RACK

Case	Δk_∞	Comment
39°F (Reference)	0	Maximum water density
68°F (20°C)	-0.001	ρ (H_2O) = 0.998
104°F (40°C)	-0.005	ρ (H_2O) = 0.992
176°F (80°C)	-0.015	ρ (H_2O) = 0.972
212°F (100°C)	-0.021	ρ (H_2O) = 0.958
212°F with 50% void	-0.275	Simulates boiling

4.4.3 Abnormal Positioning of Fuel Assembly Outside Storage Rack

A fresh fuel assembly of the highest initial reactivity, assumed to be positioned outside a fuel rack and adjacent to the outer Boraflex-steel wall, is calculated to increase k to 0.939 ± 0.011, with neutron leakage (infinite water reflector) considered in the axial direction and the side of the rack module where the extra fuel assembly was postulated to be positioned. A fuel element which had accumulated some burnup prior to discharge would, of course, result in a lower value of reactivity. In addition, the fuel racks are designed so that the space between the fuel rack and the pool wall (< 5 inches) is not sufficient to permit a fuel assembly being abnormally positioned outside a fuel rack. Furthermore, soluble boron is normally present in the spent fuel pool (for which credit is permitted for this condition) and would reduce the maximum k to substantially less than 0.95. Therefore, it is concluded that the abnormal positioning of a fuel assembly outside and immediately adjacent to the storage rack is not a credible occurrence and, even should it occur, would not increase reactivity unacceptably.

4.4.4 Missing Absorber Plate

Should a Boraflex absorber plate be missing from between fuel assemblies, the reactivity will be slightly higher than the reference case. Calculations performed in two dimensions (PDQ7) indicate the reactivity increment is +0.012 Δk due to the loss of a single plate. Because of mesh size limitations in PDQ7, symmetry considerations (with reflective boundary conditions) effectively resulted in the loss of an absorber plate from one side of every 25 storage cells. Thus, the calculated incremental reactivity addition due to the loss of an absorber plate should be conservative.

A missing Boraflex absorber plate could potentially increase the k_∞ (locally) to 0.935 ±0.011, including credit (-0.002 Δk) for axial neutron leakage. Thus, a missing Boraflex absorber will not result in an unacceptable increase in reactivity above that of the reference design storage rack. Manufacturing QA and QC programs will minimize the possibility of a missing plate.

4.4.5 Dropped Fuel Assembly Accident

To investigate the possible reactivity effect of a postulated fuel assembly drop accident, calculations were made for unpoisoned assemblies separated only by water. Figure 4.3 shows the results of these calculations. From these data, the reactivity (k_∞) will be less than 0.95 for any water-gap spacing greater than ~6 inches in the absence of any absorber material other than water between assemblies. For a drop on top of the rack, the fuel assembly will come to rest horizontally on top of the rack with a minimum separation distance of >12 inches. Maximum expected deformation under seismic or accident conditions (see Sections 6 and 7) will not reduce the minimum spacing between fuel assemblies to less than 12 inches. Consequently, fuel assembly drop accidents will not result in an increase in reactivity above that calculated for the infinite nominal design storage rack.

4.4.6 Lateral Rack Movement

Lateral motion of the rack modules under seismic conditions could alter the spacing between rack modules. However, the lateral motion is not of sufficient magnitude to reduce the spacing to less than the nominal spacing (1.164 inches) between absorber plates in the reference storage cell. In addition, soluble boron would substantially reduce the k_∞ under the postulated conditions.

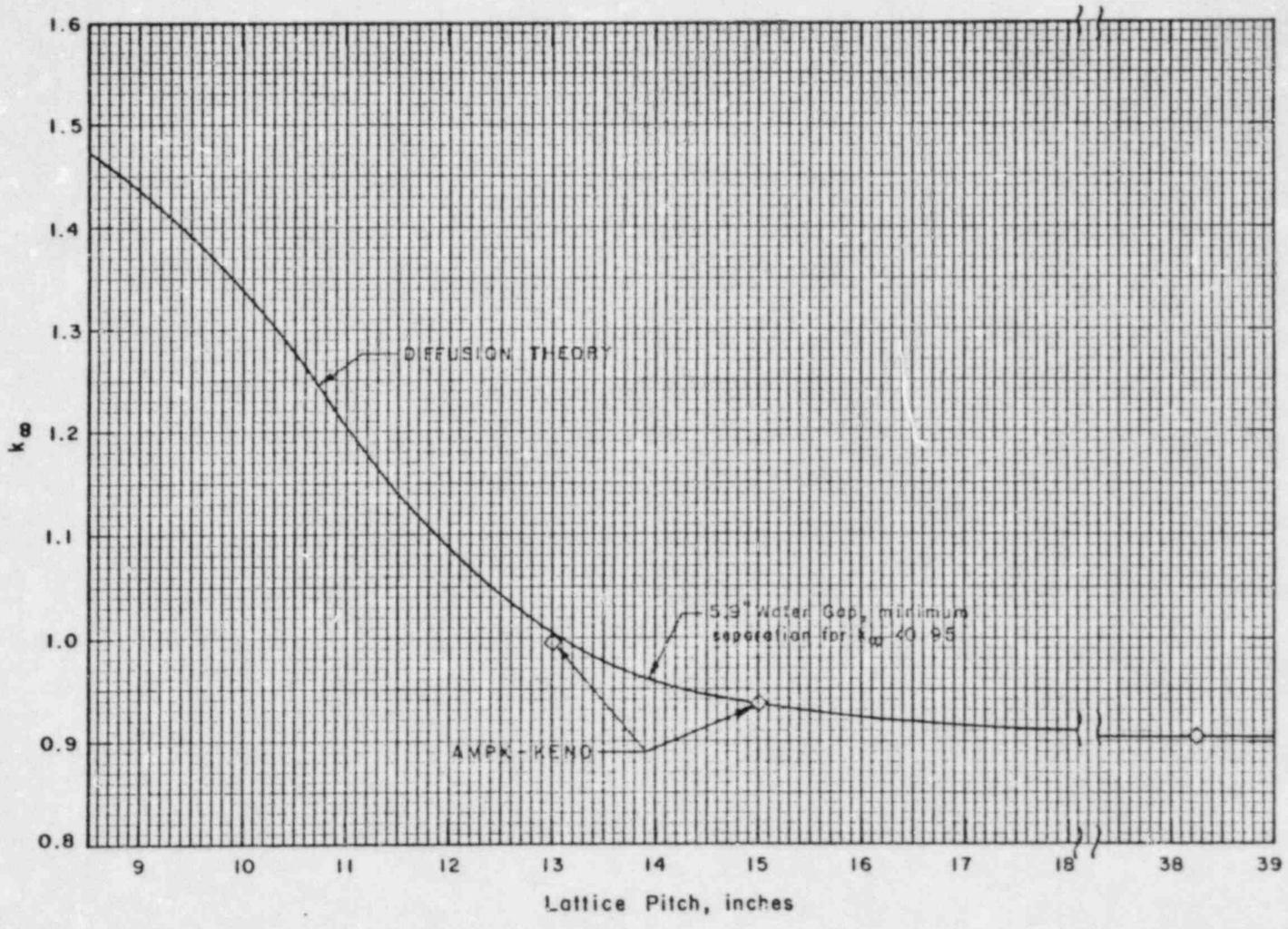

Fig. 4.3 Reactivity effect of separation between fuel assemblies (unpoisoned).

4.5.1 Nominal Design Criticality Summary

The criticality analyses of the spent fuel storage rack under normal and abnormal conditions are summarized in Table 4-4.

Table 4-4 SUMMARY OF CRITICALITY CALCULATIONS

Case		k_∞ or Δk_∞	Comment
Normal Condition			
k_∞, reference		0.9247	Section 4.3.1
Calculational bias		+0.000	Includes gap correction
Uncertainties			
Bias	±0.003		Section 4.2.3
Calculational	±0.0065		Section 4.3.1
Mechanical	±0.0089		Section 4.3.8 Table 4-2
	±0.0114		Statistical combination
Total		0.9247 ± 0.0114	
Maximum k_∞		0.936	
Abnormal and Accident Conditions			
Increased temperature or void		negative	
Fuel element eccentric positioning		negative	
Lost/missing absorber plate		+0.010	With credit for axial leakage
Assembly outside rack (not credible occurence)		+0.014	With credit for leakage
Fuel handling accident		negligible	
Lateral rack movement		negligible	

Thus, a k_∞ of 0.936 is conservatively estimated to be the maximum k_∞ under the worst combination of calculational and mechanical uncertainties (normal conditions), with a 95% probability at a 95% confidence level. Credible abnormal or accident conditions will not result in exceeding the limiting reactivity of 0.950.

REFERENCES

1. Green, Lucious, Petrie, Ford, White, Wright, PSR-63/AMPX-1 (code package), AMPX Modular Code System for Generating Coupled Multigroup Neutron-Gamma Libraries from ENDF/B, ORNL-TM-3706, Oak Ridge National Laboratory, March 1976.

2. L. M. Petrie and N. F. Cross, KENO-IV, An Improved Monte Carlo Criticality Program, ORNL-4938, Oak Ridge National Laboratory, November 1975.

3. S. R. Bierman et al., Critical Separation Between Subcritical Clusters of 4.29 wt% U^{235} Enriched UO_2 Rods in Water with Fixed Neutron Poisons, NUREG/CR-0073, Battelle Pacific Northwest Laboratories, May 1978, with errata sheet issued by the USNRC August 14, 1979.

4. M. N. Baldwin et al., Critical Experiments Supporting Close Proximity Water Storage of Power Reactor Fuel, BAW-1484-7, The Babcock & Wilcox Company, July 1979.

5. S. E. Turner and M. K. Gurley, Benchmark Calculations for Spent Fuel Storage Racks, Report SSA-127 (Rev. 5), Southern Science Applications, Inc., May 1981.

6. S. E. Turner and M. K. Gurley, Evaluation of AMPX-KENO Benchmark Calculations for High Density Spent Fuel Storage Racks, Nuclear Science and Engineering; 80, 230-237 (1982).

7. M. G. Natrella, Experimental Statistics National Bureau of Standards, Handbook 91, August 1963.

8. R. M. Westfall et al., "SCALE: A Modular Code System for Performing Standardized Computer Analyses for Licensing Evaluation," NUREG/CR-0200 (1979).

9. W. E. Ford III et al., "A 218 Neutron Group Master Cross Section Library for Criticality Safety Studies," ORNL/TM-4 (1976).

5. THERMAL-HYDRAULIC CONSIDERATIONS

A central objective in the design of the high-density fuel rack is to ensure adequate cooling of the fuel assembly cladding. In the following, a brief synopsis of the design basis, the method of analysis, and computed results is given.

5.1 Decay Heat Calculations for the Spent Fuel

This report section covers requirement III.1.5(2) of the NRC "OT Position for Review and Acceptance of Spent Fuel Storage and Handling Applications" issued on April 14, 1978. This requirement states that calculations for the amount of thermal energy removed by the spent fuel cooling system shall be made in accordance with Branch Technical Position APCSB 9-2 "Residual Decay Energy for Light Water Reactors for Long Term Cooling"[2]. The calculations contained herein have been made in accordance with this requirement.

5.1.1 Basis

The Rancho Seco reactor is rated at 2772 Megawatt-Thermal (MWT). The core contains 177 fuel assemblies. Thus, the average operating power per fuel assembly, P_o, is 15.66 MW. The fuel assemblies are assumed to be removed from the reactor after a nominal burn-up of 50,000 Megawatt-days per short ton of uranium (MWD/STU). This burn-up is considerably higher than the current burn-up rate. An upper bound on the burn-up rate has been assumed herein to maximize the residual heat load estimate. The fuel discharge can be made in one of the following two modes:

(i) Normal discharge - Mode (i)

(ii) Full Core discharge - Mode (ii)

The average fuel assembly removal batch size for Mode (i) is 59 fuel assemblies. The fuel transfer begins after 120

hours of cool-off time in the reactor (time after shut down). It is assumed that the time period of discharge of this batch is 10 days.

Mode (ii) corresponds to a full core discharge (177 assemblies). It is assumed that the total time period for the discharge of one full core is 9 days (after 120 hours of shut down time in the reactor). The discharge rate to the pool is assumed to be continuous and uniform.

The heat dissipation from the pool is accomplished by an independent fuel pool cooler loop equipped with a pump rated at 1000 gpm. In addition, the Decay Heat removal (DHR) heat exchangers may be used in conjunction with the fuel pool cooler to boost the heat removal rate.

In the following, all relevant performance data for the spent fuel pool and DHR heat exchangers is given.

a. Spent Fuel Pool Heat Exchanger:

Type	Tube and shell
Quantity	1
Performance data	
o Heat transferred	9.0×10^6 Btu/hr
Tube Side	
o Fluid flow	1,000 gpm
o Entering temperature	120 f
o Outlet temperature	102 F
Shell Side	
o Fluid flow	1000 gpm
o Entering temperature	95 F
o Outlet temperature	113 F
o Fouling factor	min. 0.0005

b. Decay Heat Removal Cooler:

o Applicable code (tube/shell):	ASME III/ASME VIII; TEMA-R
o Quantity	2

Performance data

o Type	Shell and tube
o Capacity (at 140 F)	33.75×10^6 Btu/hr
o Reactor coolant flow	3,000 gpm
o Nuclear Service Cooling water flow	3,000 gpm
o Nuclear Service cooling Water inlet temperature	95 F
o Material (Shell/tube)	CS/SS
o Design Pressure (Shell/ Tube)	150/450 psig
o Design Temperature (Shell/Tube)	300/300 F
o Cooler, UA	1.9×10^6 Btu/h-F

The above data enables complete characterization of the thermal performance of the heat exchangers.

Reference(2) is utilized to compute the heat dissipation requirements in the pool. The total decay power consists of "fission products decay" and "heavy element decay". Total decay power P for a fuel assembly is given as a linear function of P_o and an exponential function of t_o and t_s.

i.e.: $P = P_o\ f(t_o, t_s)$

where

P = linear function of P_o

P_o=average operating power per fuel assembly

t_o=cumulative exposure time of the fuel assembly in the reactor

t_s=Time elapsed since reactor shutdown

The uncertainty factor K, which occurs in the functional relationship f (t_o, t_s) is set equal to 0.1 for $t_s > 10^7$ sec in the interest of conservatism. Furthermore, the operating power P_o is taken equal to the rated power, even though the reactor may be operating at a fraction of its total power during most of the period of exposure of the batch of fuel assemblies. Finally, the computations and results reported here are based on the discharge taking place when the inventory of fuel in the pool will be at its maximum resulting in an upper bound on the computed decay heat rate.

The equilibrium cycle for the Rancho Seco reactor is 335 Full Power Days (FPD) which corresponds to approximately 15 calendar months. The cycle burn-up is 11300 MWD/MTU which in turn relates to a discharge burn-up of 34,000 MWD/MTU, and a cumulative exposure period of approximately 45 calendar months. It can be shown that the function f (t_o, t_s) is a weak monotonically increasing function of t_o. Hence, using a larger than actual value of t_o (t_o = 4.7 years) yields an upper bound on f (t_o, t_s), and hence an upper bound on the decay heat release rate.

Having determined the heat dissipation rate, the next task is to evaluate the time temperature history of the pool water. Table 5.1.1 identifies the loading cases examined. The pool bulk temperature time history is determined using the first law of thermodynamics (conservation of energy).

A number of simplifying assumptions are made to render the analysis conservative. The principal ones are:

1. The cooling water temperature in the fuel pool cooler and the DHR heat exchangers are based on the maximum postulated values given in the FSAR.

2. The heat exchangers are assumed to have maximum fouling. Thus, the temperature effectiveness, s, for the heat exchangers utilized in the analysis are the lowest postulated values: S= 0.72 for fuel pool coolers, 0.5 for DHR heat exchangers. S is calculated from FSAR and heat exchanger technical data sheets.No heat loss is assumed to take place through the concrete floor.

4. No credit is taken for the improvement in the film coefficients of the heat exchangers as the operating temperature rises. Thus, the film coefficient used in the computations are lower bounds.

5. No credit is taken for evaporation of the pool water.

The basic energy conservation relationship for the pool heat exchanger system yields:

$$C_t \frac{dt}{d\tau} = Q_1 - Q_2 - Q_3 \qquad (5.1.2)$$

where

C_t: Thermal capacity of stored water in the pool.

t: Temperature of pool water at time, τ

Q_1: Heat generation rate due to stored fuel assemblies in the pool. Q_1 is a known function of time, τ from the preceding section.

Q_2: Heat removed in the fuel pool cooler.

Q_3: Heat removed in the DHR heat exchanger (Q_3=0 if DHR is not used).

The pool has total water inventory of 61455 cubic feet when all racks are in place in the pool and every storage location is occupied.

5.1.2 Decay Heat Calculation Results:

The calculations were performed for the pool disregarding the additional thermal capacity and cooling system available in the transfer channel.

For a specified coolant inlet temperature and flow rate, the quantities Q_2 and Q_3 are shown to be linear function of t in a recent paper by Singh (3). As stated earlier, Q_1, is an exponential function of τ. Thus Equation (5.1.2) can be integrated to determine t directly as a function of τ. The results are plotted in Figures (5.1.1) to (5.1.6). The results show that the pool water never approaches the boiling

TABLE 5.1.1

LIST OF CASES ANALYZED

Case No.	Condition	No. of fuel assemblies discharged N	No. of spent fuel pool HXS	No. of DHR's in-service	Total Time to transfer fuel into the pool t_h, hrs.	Cool off time before transfer begins, hrs.
1	Normal discharge	59	1	0	240	120
2	Full core discharge	177	1	1	216	120
3	Full core discharge	177	0	1	216	120

TABLE 5.1.2

MAXIMUM POOL BULK TEMPERATURE t, COINCIDENT TOTAL POWER Q_1 and

COINCIDENT SPECIFIC POWER FOR THE HOTTEST ASSEMBLY

Case No.	No. of Assemblies	Time to transfer fuel into pool, hrs.	Maximum pool bulk temp.°F	Coincident time (since initiation of fuel transfer, hrs.	Coincident specific power q, BTU/sec.	$Q_1 \times 10^{-6}$ BTU/hour
1	59	240	113.9	255	34.02	10.4
2	177	216	120.3	222	35.21	28.1
3	177	216	132.4	222	35.21	28.1

TABLE 5.1.3

TIME (Hrs) TO BOILING AND BOILING VAPORIZATION RATE

FROM THE INSTANT ALL COOLING IS LOST

Case No.	CONDITION 1 Loss of Cooling at maximum pool bulk temperature		CONDITION 2 Loss of Cooling at maximum power discharge rate	
	Time (Hrs)	Vap. Rate lb./hr.	Time (Hrs)	Vap. Rate lb./hr.
1	36	10476	41.	10540
2	13	28000	12.5	28782
3	12	28638	10.	28857

point under the most adverse conditions. These figures also give Q_1 as a function of τ. Two plots are generated for each case. The first plot for each shows temperature and power generation for a period extending from $\tau = 0 \rightarrow \tau = 2\tau_n$ where τ_n is the total time of fuel transfer. The second plot shows the same quantities over a long period. The long-term plots are produced to indicate the required operating time for the heat exchangers. Summarized results are given in Table 5.1.2.

Finally, computations are made to determine the time interval to boiling after all heat dissipation paths are lost. Computations are made for each case under the following two assumptions:

(i) All cooling sources lost at the instant pool bulk temperature reaches the maximum value.

(ii) All cooling paths lost at the instant the heat dissipation power reaches its maximum value in the pool.

Results are summarized in Table 5.1.3. Table 5.1.3 gives the bulk boiling vaporization rate for both cases at the instant the boiling commences. This rate will decrease with time due to reduced heat emission from the fuel.

5.2 Thermal-Hydrulics Analyses for Spent Fuel Cooling

This report section covers requirement III.1.5(3) of the NRC "OT Position for Review and Acceptance of Spent Fuel Storage and Handling Applications" issued on April 14, 1978. Conservative methods have been used to calculate the maximum fuel cladding temperature as required therein. Also, it has been determined that nucleate boiling or voiding of coolant on the surface of the fuel rods does not occur.

5.2.1 Basis:

In order to determine an upper bound on the maximum fuel cladding temperature, a series of conservative assumptions are made. The most important assumptions are listed below:

a. As stated above, the fuel pool will contain spent fuel with varying "time-after-shutdown" (t_s). Since the heat emission falls off rapidly with increasing t_s, it is obviously conservative to assume that <u>all</u> fuel assemblies are fresh (t_s = 120 hours).

   and they all have had 4.5 years of operating time in the reactor. The heat emission rate of each fuel assembly is assumed to be equal.[2]

b. As shown in Figures 2.1 and 2.2 in Section 2, the modules occupy an irregular floor space in the pool. For purposes of the hydrothermal analysis, a circle circumscribing the actual rack floor space is drawn. It is further assumed that the cylinder with this circle as its base is packed with fuel assemblies at the nominal pitch of 10.5 inches (see Figure 5.2.1).

c. The downcomer space around the rack module group varies, as shown in Figure 5.2.1. The nominal downcomer gap available in the pool is assumed to be the total gap available around the idealized cylindrical rack; thus, the maximum resistance to downward flow is incorporated into the analysis.

d. No downcomer flow is assumed to exist between the rack modules.

In this manner, a conservative idealized model for the rack assemblage is devised. The water flow is axisymmetric about the vertical axis of the circular rack assemblage, and thus, the

flow is two-dimensional (axisymmetric three-dimensional). The governing equation to characterize the flow field in the pool can now be written. The resulting integral equation can be solved for the lower plenum velocity field (in the radial direction) and axial velocity (in-cell velocity field), by using the method of collocation. It should be added that the hydrodynamic loss coefficients which enter into the formulation of the integral equation are also taken from well-recognized sources[4] and wherever discrepancies in reported values exist, the conservative values are consistently used.

After the axial velocity field is evaluated, it is a straight-forward matter to compute the fuel assembly cladding temperature. The knowledge of the overall flow field enables pinpointing the storage location with the minimum axial flow (i.e. maximum water outlet temperature). This is called the most "choked" location. It is recognized that some storage locations, where rack module supports are located, have some additional hydraulic resistance not encountered in other cells. In order to find an upper bound on the temperature in such a cell, it is assumed that it is located at the most "choked" location. Knowing the global plenum velocity field, the revised axial flow through this choked cell can be calculated by solving the Bernoulli's equation for the flow circuit through this cell. Thus, an absolute upper bound on the water exit temperature and maximum fuel cladding temperature is obtained. It is believed that in view of the preceding assumption, the temperatures calculated in this manner overestimate the temperature rise that will actually be obtained in the pool.

The maximum pool bulk temperature t is computed in Section 5.1.3 and reported in Table 5.1.2. The corresponding average power output from the hottest fuel assembly, q is also reported in that table. The maximum radial peaking factor ranges from 1.6 to 1.8 for the Rancho Seco installation. Thus, it is conservative to assume that the maximum specific power of a fuel assembly is given by

$$q_A = q\ \alpha_r$$

where $\alpha_r = 1.8$

The maximum temperature rise of pool water in the most disadvantageously placed fuel assembly is given in Table 5.2.1 for all loading cases. Having determined the maximum "local" water temperature in the pool, it is now possible to determine the maximum fuel cladding temperature. It is conservatively assumed that the total peaking factor α_T is 3.12. Thus, a fuel rod can produce 3.12 times the average heat emission rate over a small length. The axial heat dissipation in a rod is known to reach a maximum in the central region, and taper off at its two extremities. For the sake of added conservatism it is assumed that the peak heat emission occurs at the top where the local water temperature also reaches its maximum. Furthermore, no credit is taken for axial conduction of heat along the rod. The highly conservative model thus constructed leads to simple algebraic equations which directly give the maximum local cladding temperature, t_c.

5.2.2 Results:

Table 5.2.1 gives the maximum local cladding temperature, t_c, at the instant the pool bulk temperature has attained its maximum value. It is quite possible, however, that the peak cladding temperature occurs at the instant of maximum value of q_A, i.e., at the instant when the fuel assembly is first placed in a storage location. Table 5.2.2 gives the maximum local cladding temperature at $\tau = 0$. It is to be noted that there are wide margins to local boiling in all cases. The local boiling temperature near the top of the fuel cladding is 240°F. Furthermore, the cladding temperature must be somewhat higher than the boiling temperature to initiate and sustain nucleate boiling. The above considerations indicate that a

comfortable margin against the initiation of localized boiling exists in all cases.

TABLE 5.2.1

MAXIMUM LOCAL POOL WATER TEMPERATURE AND LOCAL FUEL

CLADDING TEMPERATURE

Case No.	Max. Local Pool Water Temperature °F	Maximum Coincident Local Cladding Temperature °F	Case Identified
1	131.7	175.4	59 Assemblies Cooling Mode A
2	138.5	183.6	177 Assemblies Cooling Mode B
3	150.5	195.6	177 Assemblies Cooling Mode C

* Cooling Mode A mean only one fuel pool Hx working.

Cooling Mode B means one fuel pool Hx and one DHR working.

Cooling Mode C means one DHR Hx working.

TABLE 5.2.2

POOL AND MAXIMUM CLADDING TEMPERATURE AT THE INSTANCE FUEL ASSEMBLY TRANSFER BEGINS

Case No.	Cladding Temp. °F	Coincident Pool Temp, °F	
		Bulk	Local
1	182.2	93.8	117.6
2	188.5	100.1	123.9
3	190.9	102.5	126.3

REFERENCES TO SECTION 5

1. FSAR, Rancho Seco Nuclear Generating Station Unit No. 1.

2. U.S. Nuclear Regulatory Commission, Standard Review Plan, Branch Technical Position, APCSB 9-2, Rev. 1, November 1975.

3. Journal of Heat Transfer, Transactions of the ASME August,1981, Vol. 103, "Some Fundmental Relationships for Tubular Heat Exchanger Thermal Performance," K.P. Singh.

4. General Electric Corporation, R&D Data Books, "Heat Transfer and Fluid Flow, " 1974 and updates.

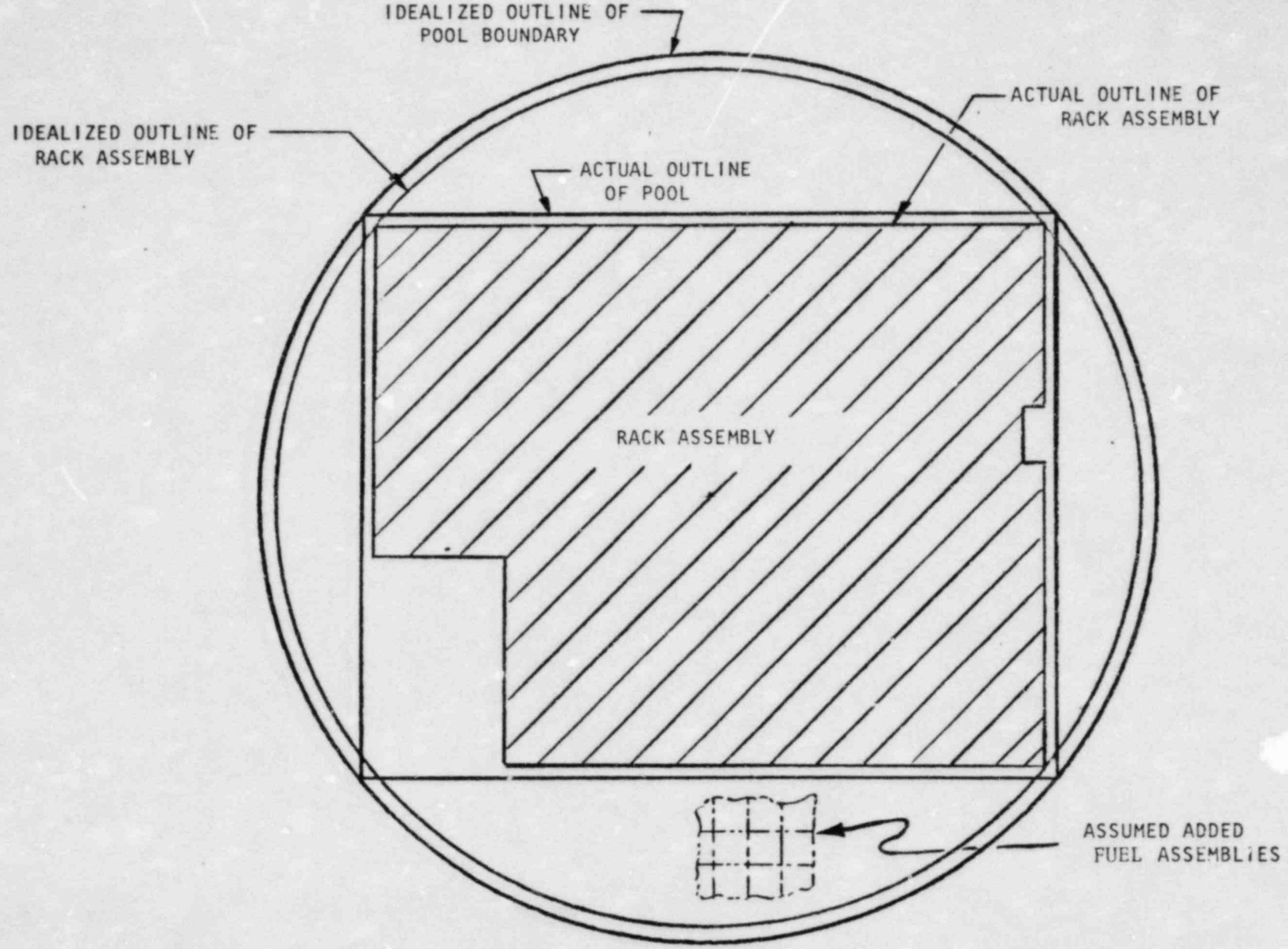

Figure 5.2.1 Rack Space Enveloping Cylinder
(Rancho SECO Nuclear Station)

SACRAMENTO MUNICIPAL UTILITY DISTRICT

J-2452

P.O. 8486

LICENSING DOC. SECTION 5

(Doc. 700K rev 0)

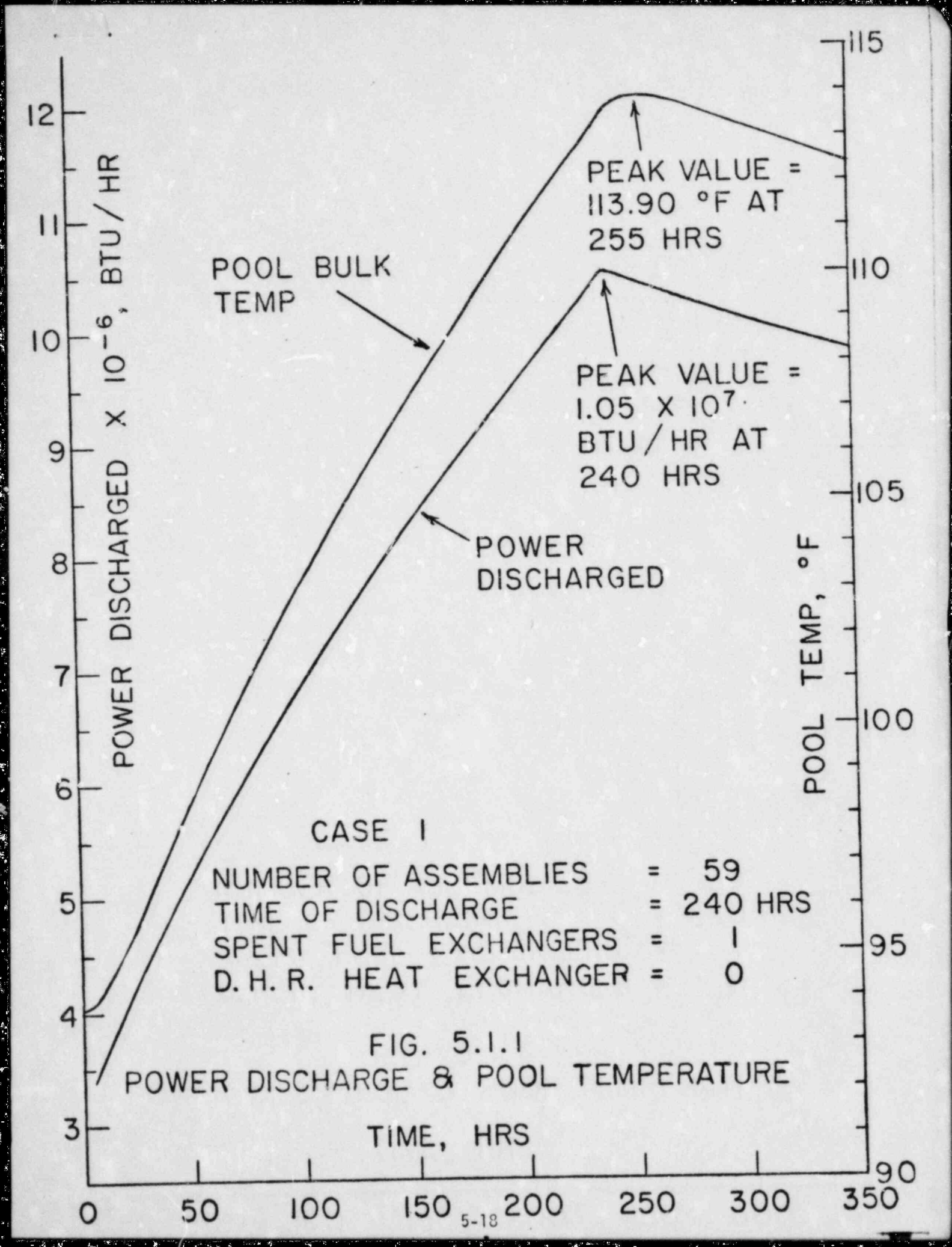

FIG. 5.1.1
POWER DISCHARGE & POOL TEMPERATURE

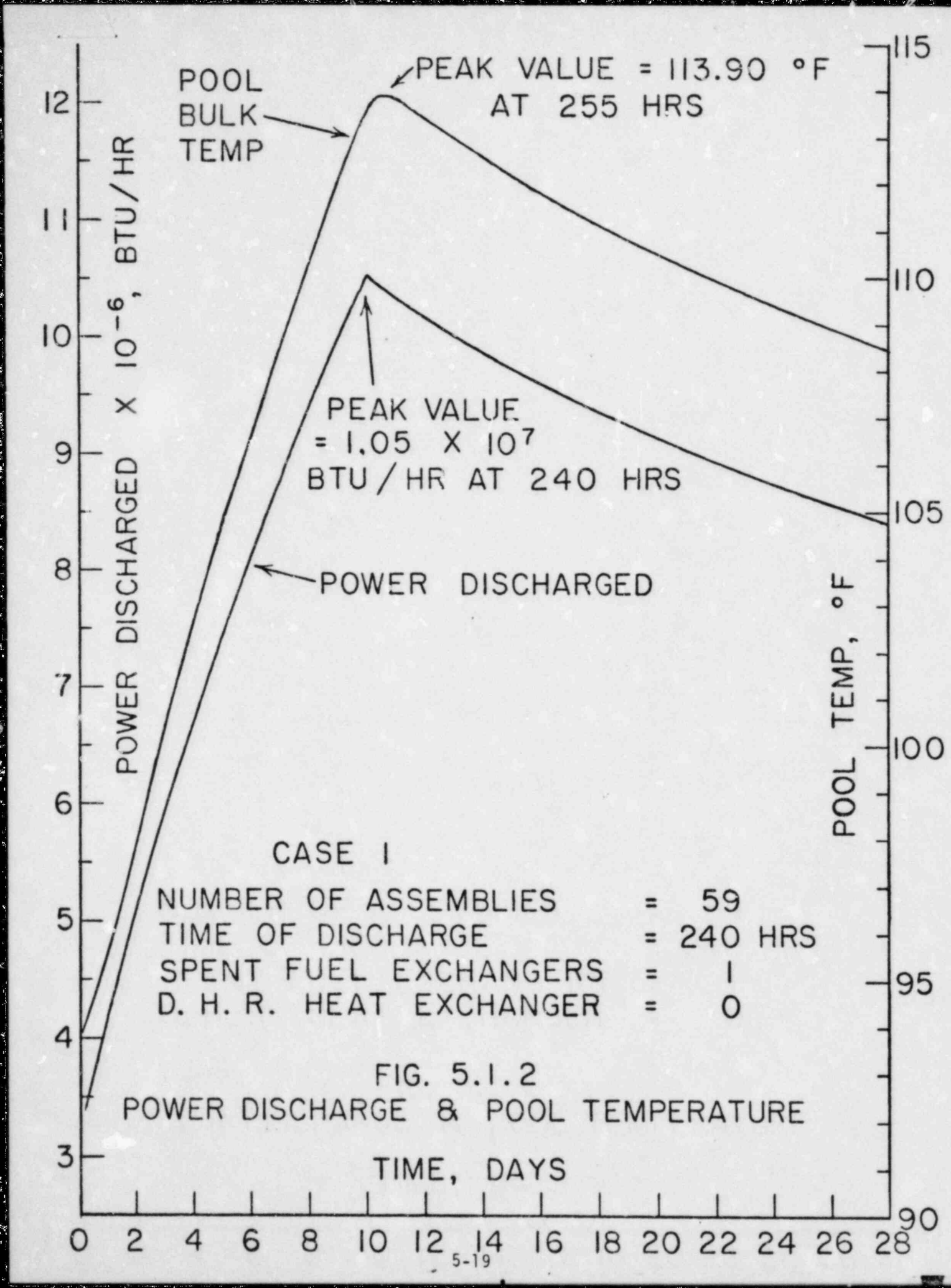

FIG. 5.1.2
POWER DISCHARGE & POOL TEMPERATURE

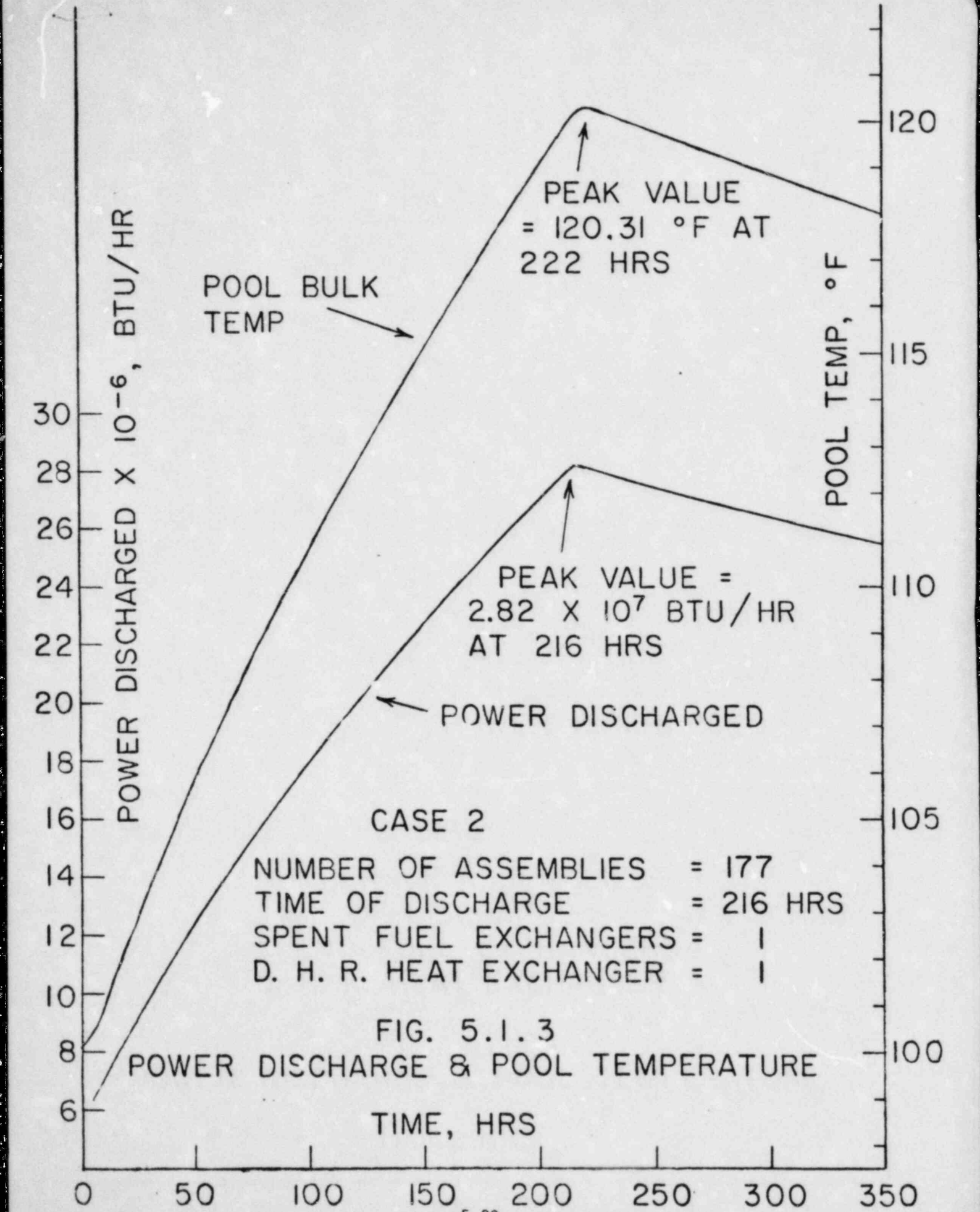

FIG. 5.1.3
POWER DISCHARGE & POOL TEMPERATURE

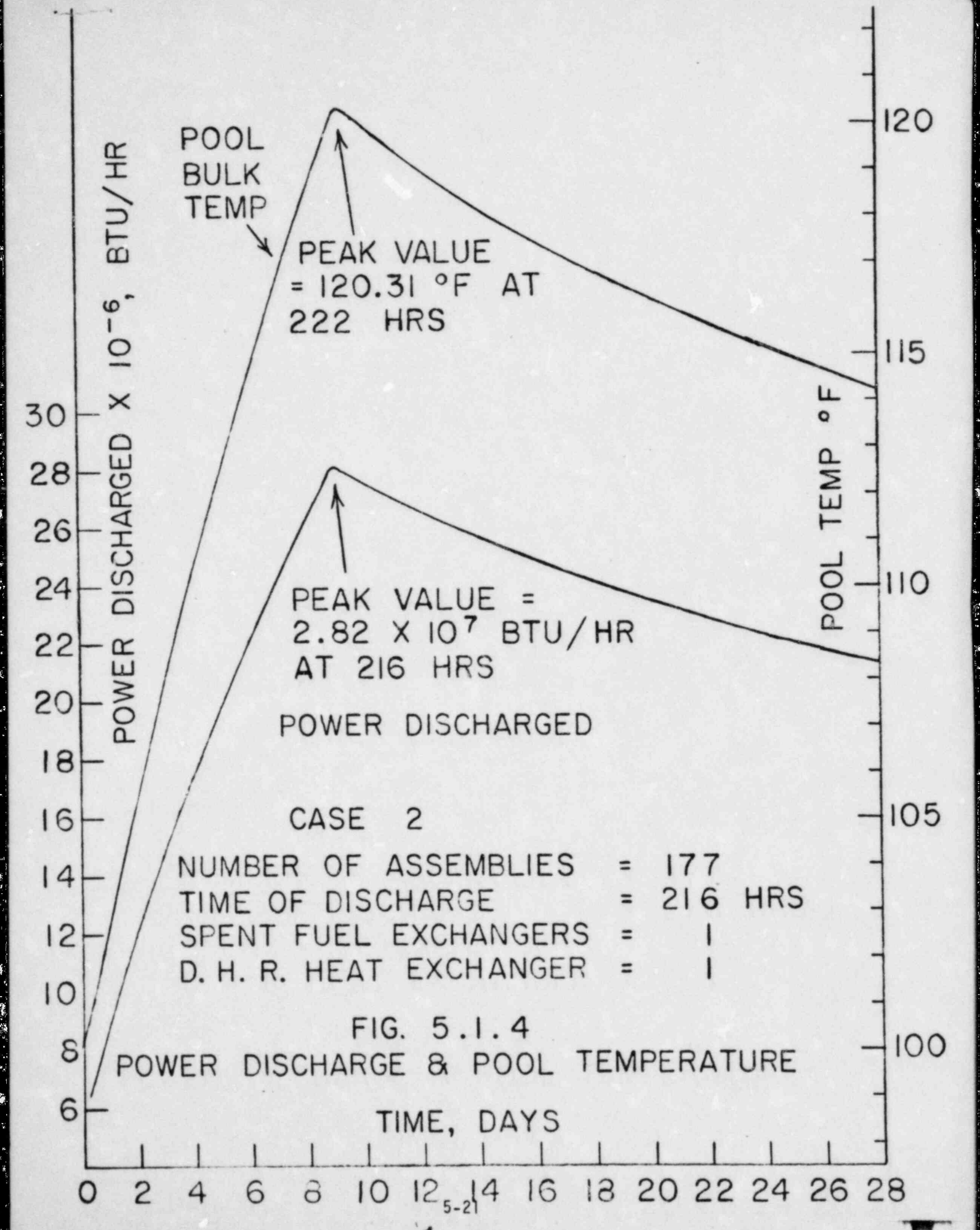

FIG. 5.1.4
POWER DISCHARGE & POOL TEMPERATURE

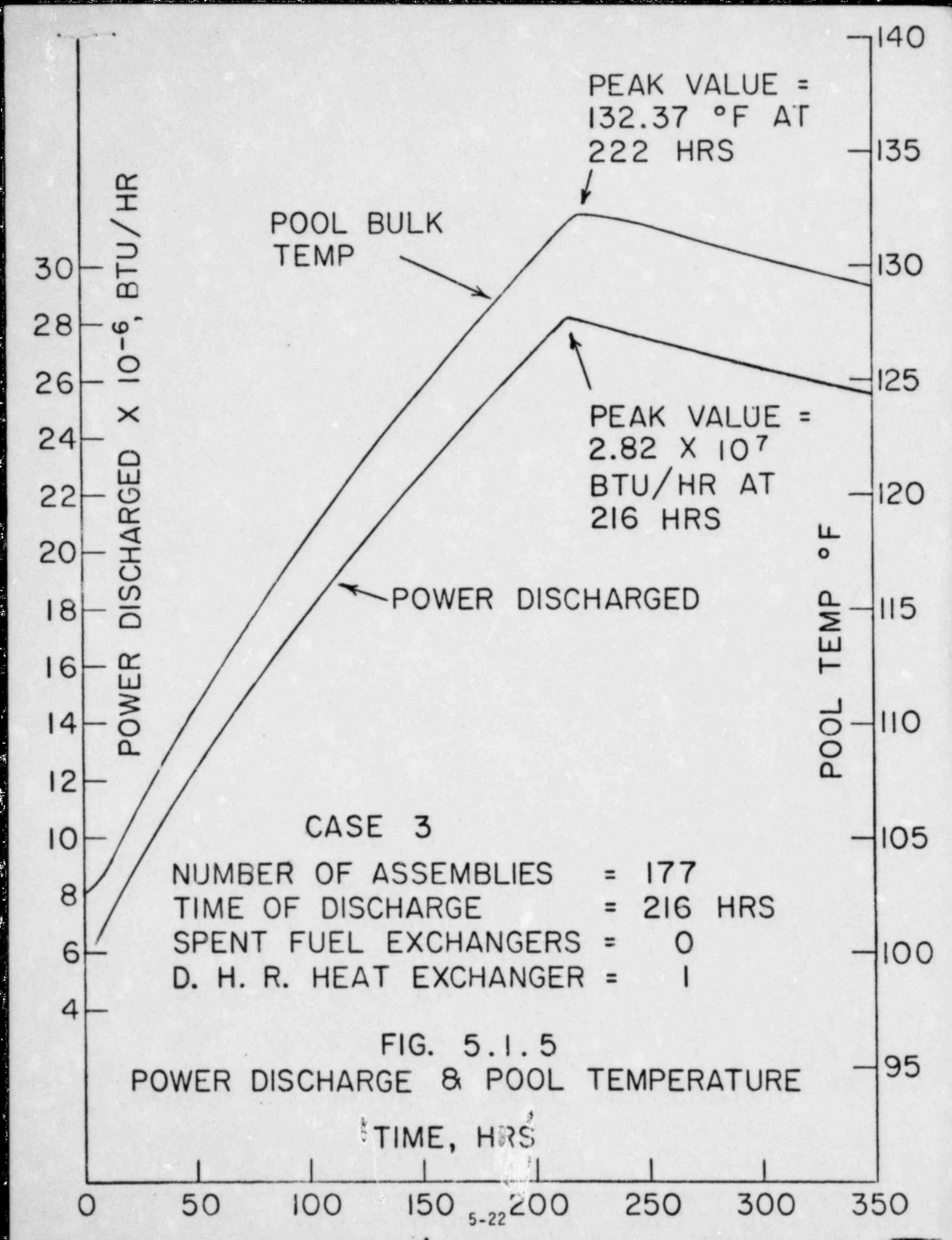

FIG. 5.1.5
POWER DISCHARGE & POOL TEMPERATURE

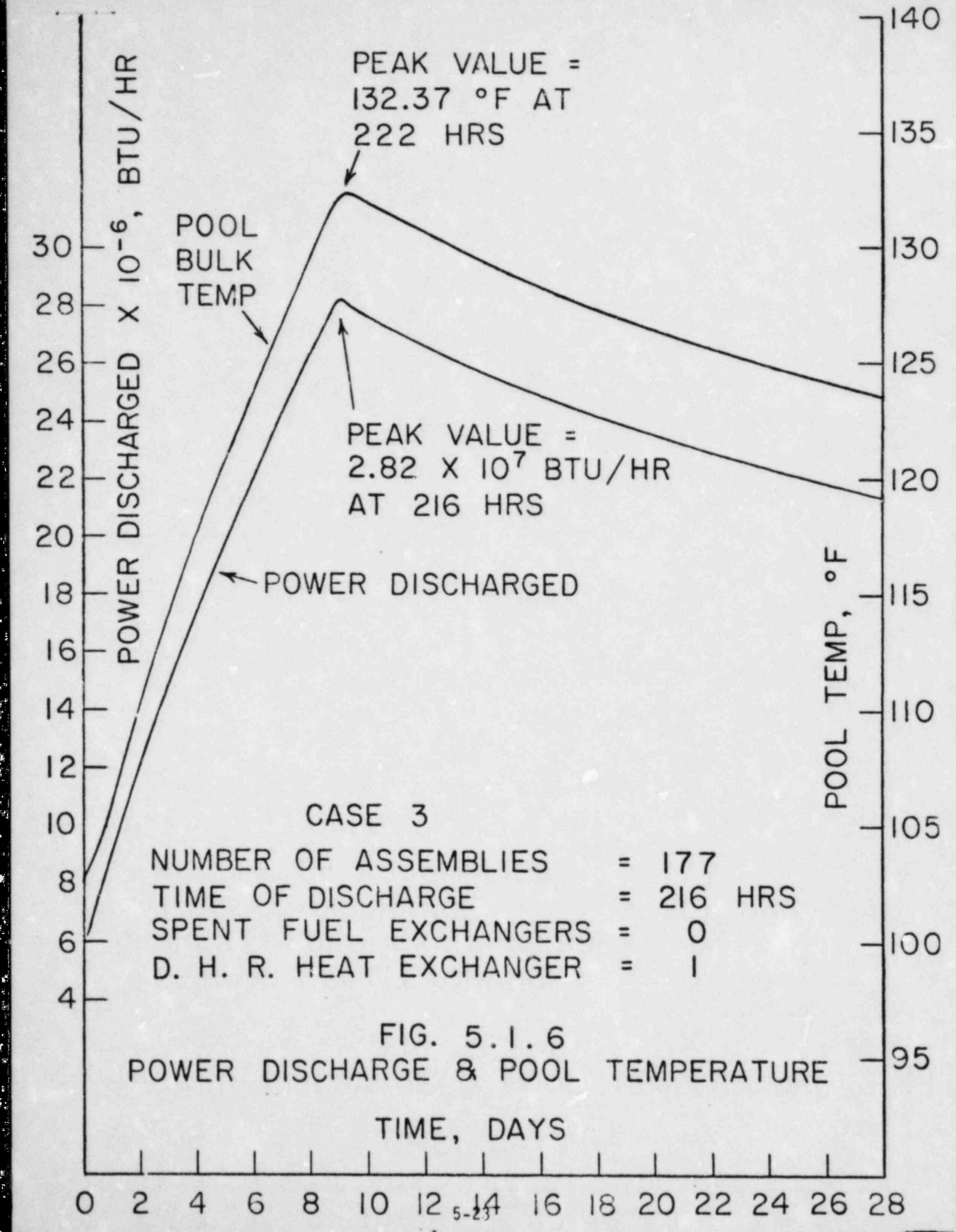

FIG. 5.1.6
POWER DISCHARGE & POOL TEMPERATURE

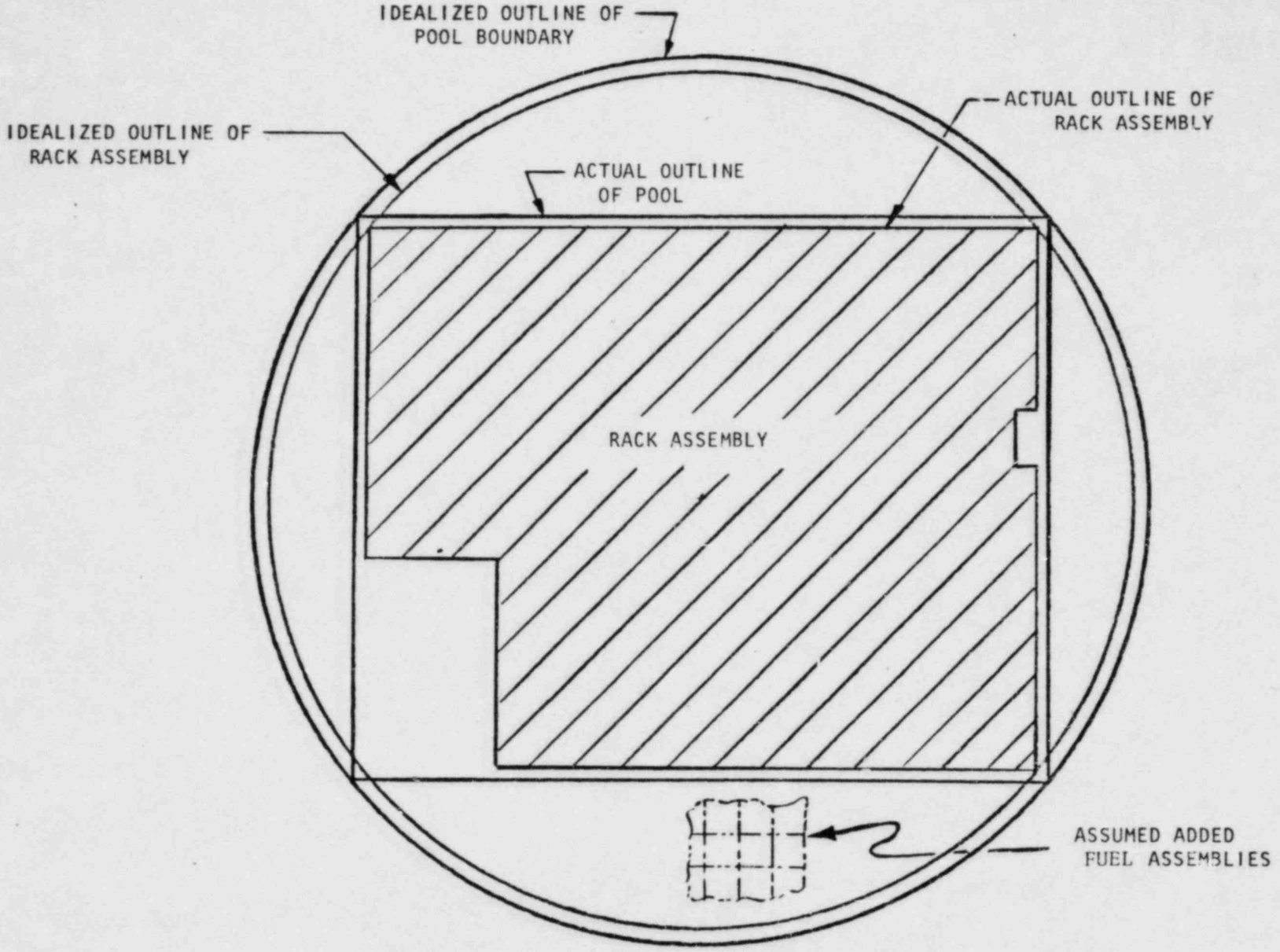

Figure 5.2.1 Rack Space Enveloping Cylinder
(Rancho SECO Nuclear Station)

6. STRUCTURAL ANALYSIS

The purpose of this section is to demonstrate the structural adequacy of the spent fuel rack design under normal and accident loading conditions. The results show that the high density spent fuel racks are structurally adequate to resist the postulated stress combinations associated with normal and accident conditions.

6.1 Analysis Outline:

The spent fuel storage racks are Seismic Category I equipment. Thus, they are required to remain functional during and after an SSE (Safe Shutdown Earthquake).[1] As noted previously, these racks are neither anchored to the pool floor, nor are they attached to the side walls. The individual rack modules are not interconnected. Furthermore, a particular rack may be completely loaded with fuel assemblies (which corresponds to greatest rack inertia), or it may be partially loaded so as to produce maximum geometric eccentricity in the structure. The coefficient of friction, μ, between the supports and pool floor is another indeterminate factor. According to Rabinowicz,[2] the results of 199 tests performed on austenitic stainless steel plates submerged in water show a mean value of μ to be 0.503 with a standard deviation of 0.125. The upper and lower bounds ($\mp 2\sigma$) are thus 0.753 and 0.253, respectively. Two separate analyses are performed for this rack assembly with values of μ equal to 0.2 (lower limit) and 0.8 (upper limit) respectively.

In summary, the following twelve separate analyses are performed on the largest rack module (Module A).

1. Fully loaded rack (all storage locations occupied), $\mu = 0.8$ (μ = coefficient of friction).
2. Fully loaded rack, $\mu = 0.2$.

3. Half-loaded rack to produce maximum geometric asymmetry about the major dimension of the rectangular rack, $\mu = 0.8$.
4. Half-loaded rack to produce maximum geometric asymmetry about the major dimension of the rectangular rack, $\mu = 0.2$.
5. Empty rack, $\mu = 0.8$.
6. Empty rack, $\mu = 0.2$.
7. Tipping and sliding study for Case 3 loading.
8. Full rack $\mu=0.8$; two dimensional ground motion (one vertical, one horizontal).
9. Half loaded rack to produce maximum asymmetry about a diagonal, $\mu = .8$.
10. Case No. 9 with $\mu=0.2$.
11. Case 1 except zero hydrodynamic coupling.
12. Case 2 except zero hydrodynamic coupling.

Cases 11 & 12 are strictly for sensitivity study purposes. The smallest module, Module C, is analyzed for those conditions which give maximum response in the above 12 cases for Module A.

The method of analysis employed is the time history method. The ground acceleration data are developed from the original plant design as reflected in the response spectra contained in the FSAR.

The object of the seismic analysis is to determine the structural response (stresses, deformation, rigid body motion, etc.) due to simultaneous application of the three orthogonal excitations. Thus, recourse to approximate statistical summation techniques such as "Square-Root-of-the-Sum-of-the-Squares" method [3] is avoided and the dependability of computed results is ensured.

The seismic analysis is performed in four steps as give below:

1. Development of nonlinear dynamic model consisting of beam, gap, spring, damper and inertial coupling elements.

2. Derivation and computation of element stiffnesses using a sophisticated elastostatic model.

3. Layout of the equations of motion, and inertial decoupling and solution of the equations using the "component element time integration" procedure[4,5] to determine nodal and element forces and displacements of nodes.

4. Computation of the detailed stress field in the rack structure, using the detailed elastostatic model, from the nodal forces calculated in Step III above. Determine if the stress and displacement limits,given in Section 6.5, are satisfied.

6.2 Non-Linear Dynamic Model

A brief description of the non-linear dynamic model consisting of beam, gap, spring, damper and inertial coupling elements is given in this section.

6.2.1 Fuel Rack - Fuel Assembly Model:

The following assumptions are made to construct a three dimensional multiple degree of freedom system model:

1. The fuel rack metal structure is represented by five lumped masses connected by appropriate elastic springs as shown in Figure 6.1. The spring rates simulate the elastic behavior of the fuel rack as a beamlike structure.

2. The fuel assemblies are represented by five lumped masses located, relative to the rack, in a manner which simulates either fully or partially loaded conditions.

3. The local flexibility of the rack-support interface is modeled conservatively in the analysis.

4. The rack base support may slide or lift off the pool floor.

5. The pool floor is assumed to have a known time history of ground accelerations along the three orthogonal directions.

6. Fluid coupling between rack and assemblies, and between rack and adjacent racks is simulated by introducing appropriate inertial coupling into the system kinetic energy.

7. Potential impacts between rack and assemblies are accounted for by appropriate spring gap connectors between masses involved.

8. Fluid damping between rack and assemblies, and between rack and adjacent rack is conservatively neglected.

9. The supports are modeled as extensional elements for dynamic analysis. The bottom of a support leg is attached to a frictional spring as described in Section 6.2.2. The cross section properties of the support beams are derived and used in the final computations to determine support leg stresses.

10. The effect of sloshing can be shown to be negligible at the bottom of a pool and is hence neglected.

6.2.2 Model Description

The absolute degrees of freedom associated with each of the mass locations i, i* are as shown in Table 6.1. These are also shown in Figure 6.1.

Table 6.1 Degrees of Freedom

Location (Node)	Displacement			Rotation		
	u_x	u_y	u_z	θ_x	θ_y	θ_z
1	p_1	p_2	p_3	q_4	q_5	q_6
1*	Point is assumed fixed to base at $X_B, Y_B, Z=0$					
2	p_7	p_9		q_{11}	q_{12}	
2*	p_8	p_{10}				
3	p_{13}	p_{15}		q_{17}	q_{18}	
3*	p_{14}	p_{16}				
4	p_{19}	p_{21}		q_{23}	q_{24}	
4*	p_{20}	p_{22}				
5	p_{25}	p_{27}	p_{32}	q_{29}	q_{30}	q_{31}
5*	p_{26}	p_{28}				

Thus, there are 32 degrees of freedom in the system. Note that elastic motion of the rack in extension is represented by generalized coordinates p_3 and p_{32}. This is due to the relatively high axial rigidity of the rack. Torsional motion of the rack relative to its base is governed by q_{31}.

The members joining nodes 1 to 2, 2 to 3, etc., are the beam elements with deflection due to bending and shear capability (see Reference 4,pp. 156-161.). The elements of the stiffness matrix of these beam elements are readily computed if the effective flexure modulus, torsion modulus, etc., for the rack structure are known. These coefficients follow from the elastostatic model as described later. The nodal points i (i = 1,2...5) denote the fuel rack mass at the 5 elevations.

The node points i* (i* = 1 , 2...5) denote the cumulative mass for all the fuel assemblies distributed at 5 elevations. The nodes i* are located at $X = X_B$, $Y = Y_B$ in the global coordinate system shown in Figure 6.1. The coordinates (X_B , Y_B) are determined by the center-of-mass of the set of fuel assemblies. For a completely loaded rack, $X_B = Y_B = 0$.

6.2.3 Fluid Coupling

An effect of some significance requiring careful modeling is the so-called "fluid coupling effect." If one body of mass m_1 vibrates adjacent to another body (mass m_2), and both bodies are submerged in a frictionless fluid medium, then the Newton's equation of motion for the two bodies have the form

$(m_1 + M_{11})\ \ddot{X}_1 - M_{12}\ \ddot{X}_2$ = applied forces on mass m_1

$-M_{21}\ \ddot{X}_1 + (m_2 + M_{22})\ \ddot{X}_2$ = applied forces on mass m_2

M_{11}, M_{12}, M_{21}, and M_{22} are fluid coupling coefficients which depend on the shape of the two bodies, their relatives disposition, etc. Fritz[6] gives data for M_{ij} for various body shapes and arrangements. It is to be noted that the above equation indicates that effect of the fluid is to add a certain amount of mass to the body (M_{11} to body 1), and an external force which is proportional to the acceleration of the adjacent body (mass m_2). Thus, the acceleration of one body affects the force field on another. This force is a strong function of the interbody gap,

reaching large values forms very small gaps. This inertial coupling is called fluid coupling. It has an important effect in rack dynamics. The lateral motion of a fuel assembly inside the storage location will encounter this effect. So will the motion of a rack adjacent to another rack. These effects are included in the equations of motion. The fluid coupling is between nodes i and i* (i =2,3...5) in Figure 6.1. Furthermore, nodal masses i contain coupling terms which model the effect of fluid in the gaps between adjacent racks.

Finally, fluid virtual mass is included in vertical direction vibration equations of the rack; virtual inertia is added to the governing equations corresponding to rotational degrees of freedom, such as q_4, q_5, q_6, q_{11}, etc.

6.2.4 Damping

In reality, damping of the rack motion arises from material hysteresis (material damping), relative intercomponent motion in structures (structural damping), and fluid drag effects (fluid damping). The fluid damping acts on the i and i* nodal masses. In the analysis, a maximum of 2% structural damping is imposed on elements of the rack structure during SSE seismic simulations. This is in accordance with NRC guidelines [7] and FSAR. Material and fluid damping are conservatively neglected.

6.2.5 Impact

The fuel assembly nodes i* will impact the corresponding structural mass node i. To simulate this impact, 4 impact springs around each fuel assembly node are provided (see Figure 6.2). The

fluid dampers are also provided in parallel with the springs. The spring constant of the impact springs is assumed equal to the local stiffness of the vertical panel computed by evaluating the peak deflection of a composite cell (Fig. 3.3) subject to a specified uniform pressure, and held at the diagonally opposite tips. A special purpose finite element program is used for this purpose.

6.2.6 Assembly of the Dynamic Model

The dynamic model of the rack, rack base plus supports, and internal fuel assemblies, is modeled for the general three dimensional (3-D) motion simulation, by five lumped masses and inertial nodes for the rack, base, and supports, and by five lumped masses for the assemblage of fuel assemblies. To simulate the connectivity and the elasticity of the configuration, a total of 37 linear spring dampers, 20 nonlinear gap elements, and 18 nonlinear friction elements are used. A summary of spring-damper, gap, and friction elements with their connectivity and purpose is presented in Table 6.2.

If we restrict the simulation model to two dimensions (one horizontal motion plus vertical motion, for example) for the purposes of model clarification only, then a descriptive model of the simulated structure which includes all necessary spring, gap, and friction elements is shown in Figure 6.3. The beam springs, K_Δ, K_B at each level, which represent a rack segment treated as a structural beam,[4] are located in Table 6.2 as linear springs 2, 3, 6, 7, 10, 14, and 15. The extensional spring, K_e, which simulates the lowest elastic motion of the rack in extension relative to the rack base, is given by linear spring 37 in Table 6.2. The remaining spring-dampers either have zero coefficients (fluid damping is neglected), or do not enter into the

two-dimensional (2-D) motion shown in Figure 6.3. The rack mass and inertia, active in rack bending, is apportioned to the five levels of rack mass; the rack mass active for vertical motions is apportioned to locations 1 and 5 in the ratio 2 to 1. The mass and inertia of the rack base and the support legs is concentrated at node 1.

The impacts between fuel assemblies and rack show up in the gap elements, having local stiffness K_I, in Figure 6.3. In Table 6.2, these elements are gap elements 3, 4, 7, 8, 15, 16, 19 and 20. The support leg spring rates K_δ are modelled by elements 9 and 10 in Table 6.2 for the 2-D case. Note that the local elasticity of the concrete floor is included in K_Δ. To simulate sliding potential, friction elements 2 plus 8 and 4 plus 6 (Table 6.2) are shown in Figure 6.3. The local spring rates K_f reflect the lateral elasticity of the support legs. Finally, the support rotational friction springs K_R, reflect the rotational elasticity of the foundation. The nonlinearity of these springs (friction elements 9 plus 15 and 11 plus 13 in Table 6.2) reflects the edging limitation imposed on the base of the rack support legs.

For the 3-D simulation, carried out in detail for this analysis, additional springs and support elements (listed in Table 6.2), are included in the model. Coupling between the two horizontal seismic motions is provided by the offset of the fuel assembly group centroid which causes the rotation of the entire rack. The potential exists for the assemblage to be supported on 1 to 4 rack supports during any instant of a complex 3-D seismic event. All of these potential events may be simulated during a 3-D motion and have been observed in the results.

A brief description of the elastostatic model now follows. This detailed model is used to obtain overall beam stiffness formulae for the rack dynamic model, and to determine detailed stress distributions in the rack from a knowledge of the results of the time history analysis.

6.3 Stress Analysis

6.3.1 Stiffness Characteristics:

The fuel rack is a multicell, folded-plate structure which has what is colloquially called a "honey-comb" configuration. This type of construction is very similar to the

(Text Continued on Page 6-14)

Table 6.2 Numbering System for Springs, Gap Elements, Friction Elements

I. Spring Dampers (37 total)

Number	Node Location	Description
1	1-2	X-Z rack shear spring
2	1-2	Y-Z rack shear
3	1-2	Y-Z rack bending spring
4	1-2	X-Z rack bending
5	2-3	X-Z rack shear
6	2-3	Y-Z
7	2-3	Y-Z rack bending
8	2-3	X-Z
9	3-4	X-Z rack shear
10	3-4	Y-Z
11	3-4	Y-Z rack bending
12	3-4	X-Z
13	4-5	X-Z rack shear
14	4-5	Y-Z
15	4-5	Y-Z rack bending
16	4-5	X-Z
17	1-5	Rack torsion spring
18*	1	Fluid damping of rack in torsion
19*	1	Fluid damping of rack in X direction
20*	1	Rack fluid damper in Y direction
21*	2	X direction rack fluid damper
22*	2	Y direction rack fluid damper
23*	3	X direction rack fluid damper
24*	3	Y direction rack fluid damper
25*	4	X direction rack fluid damper
26*	4	Y direction rack fluid damper
27*	5	X direction rack fluid damper
28*	5	Y direction rack fluid damper
29*	2,2*	X rack/fuel assembly damper
30*	2,2*	Y rack/fuel assembly damper
31*	3,3*	X rack/fuel assembly damper
32*	3,3*	Y rack/fuel assembly damper
33*	4,4*	X rack/fuel assembly damper
34*	4,4*	Y rack/fuel assembly damper

*Note: Dampers 18-36 assumed inactive.

Table 6.2 (continued)

Number	Node Location	Description
35*	5,5*	X rack/fuel assembly damper
36*	5,5*	Y rack/fuel assembly damper
37	1-5	Z rack extensional spring

* Note: Dampers 18-36 assumed inactive.

II. Nonlinear Springs (Gap Elements) (20 total)

Number	Node Location	Description
1	2,2*	X rack/fuel assembly impact spring
2	2,2*	X rack/fuel assembly impact
3	2,2*	Y rack/fuel assembly impact
4	2,2*	Y rack/fuel assembly impact
5	3,3*	X rack/fuel assembly impact
6	3,3*	X rack/fuel assembly impact
7	3,3*	Y rack/fuel assembly impact
8	3,3*	Y rack/fuel assemlby impact
9	Support S1	Z compression spring
10	Support S2	Z compression spring
11	Support S3	Z compression spring
12	Support S4	Z compression spring
13	4,4*	X rack/fuel assembly impact spring
14	4,4*	X rack/fuel assembly impact spring
15	4,4*	Y rack/fuel assembly impact spring
16	4,4*	Y rack/fuel assembly impact spring
17	5,5*	X rack/fuel assembly impact spring
18	5,5*	X rack/fuel assembly impact spring
19	5,5*	Y rack/fuel assembly impact spring
20	5,5*	Y rack/fuel assembly impact spring

III. Friction Elements (16 total)

Number	Node Location	Description
1	Support S1	X direction support friction
2	Support S1	Y direction friction
3	Support S2	X direction friction
4	Support S2	Y direction friction
5	Support S3	X direction friction
6	Support S3	Y direction friction
7	Support S4	X direction friction
8	Support S4	Y direction friction
9	S1	X Floor Moment
10	S1	Y Floor Moment
11	S2	X Floor Moment
12	S2	Y Floor Moment
13	S3	X Floor Moment
14	S3	Y Floor Moment
15	S4	X Floor Moment
16	S4	Y Floor Moment

so-called "stressed-skin" construction of ribs, spars, and cover plates which are widely used in aircraft construction. Techniques developed in the field of aircraft structural analysis are utilized herein in to find the stresses asnd deformations in such structures. These methods have been thoroughly tested and their reliability has been documented in a number of publications.[8-12]

Figure 6.4 shows two cross-sections of the fuel rack which is modeled as a rectangular network of plates interconnected along nodal lines shown as points in Figure 6.1. An arbitrary load with components $F_x i$, $F_y i$, $F_z i$ acts at an arbitrary elevation on one of the nodal lines. We find the displacements and stresses due to such a typical load according to the stressed-skin model as follows.

The torsional deformations are solved for by using the classical theory of torsion for multicelled, thin-walled, cross sections.[13]

The bending deformation is found by using the theory of shear flow[12] wherein all axial stresses are carried by the effective flanges (or stringers) formed by the intersections of the plates and all transverse shears are carried by the plates modeled as shear panels.

From a knowledge of the shear flows, the bending and torsional deformations, it is possible to provide a set of influence functions or the following section properties for the fuel rack as a whole:

$(EI)_{eq}$ = Bending rigidity (in two places)
$(GJ)_{eq}$ = Torsional rigidity
$(AE)_{eqs}$ = Extensional rigidity
k_s = Shear deformation coefficient

Such properties are used for the dynamic analysis of seismic loads and serve to establish values for the spring rates of the elastic beam elements representing each rack section.

6.3.2 Combined Stresses and Corner Displacements

The cross-sectional properties and the Timoshenko shear correction factor calculated in the previous section are fed into a dynamic analysis of the system shown in Figure 6.5, with a specified ground motion simulating earthquake loading. From the dynamic analysis, the stress resultants (F_x, F_y, F_z, M_x, M_y, M_z) act as shown in Figure 6.6 are computed for a large number of times $t = \Delta t$, $2\Delta t$, etc., at a selected number of cross sections. The displacements (U_x, U_y, U_z) at selected nodal points on the z axis are also provided by the dynamic analysis as well as the rotations (θ_x, θ_y, θ_z) of the cross sections at the nodes.

Figure 6.7 shows a typical subdivision of the structure into elements, nodes, and sections. The stresses are calculated at all sections and the displacements at all four corners of the racks are calculated at these elevations.

Since the axial stress varies linearly over the cross section and achieves its extreme values at one of the four corners of the rack, the shear stresses due to torsional loads (M_z) achieve their extreme values near the middle of each side. The shear

stresses due to lateral forces (F_x, F_y) will achieve their extreme values at the center of the cross section or at the middle of each side. Thus, candidates for the most critical point on any section will be the points labelled 1 through 9 in Figure 6.8. The expression for the combined stress and kinematic displacement for each of these points is written out. Similarly, the stresses in the support legs are evaluated.

A validated Joseph Oat Corporation proprietary computer program "EGELAST" computes the stresses at the candidate points at each level. It sorts out the most stressed location in space as well as time. The highest stress and maximum kinematic displacements are thus readily found.

6.4 Time Integration of the Equations of Motion

Having assembled the structural model, the dynamic equations of motion corresponding to each degree of freedom can be written by using Newton's second law of motion; or using Lagrange's equation. For example, the motion of node 2 in y-direction (governed by the generalized coordinate p_9) is written as follows:

The inertial mass is:

$m_{22} + A_{211} + B_{211}$

where m_{22} is the mass of node 2 for y-directional motion.

A_{211} is the fluid coupling mass due to interaction with node 2*, and

B_{211} is the fluid coupling mass due to interaction of node 2 with the reference frame (interaction between adjacent racks).

Hence, Newton's law gives

$$(m_{22} + A_{211} + B_{211})\, p_9 + A_{212}\, p_{10} + B_{212}\, u = Q_9$$

where Q_9 represents all the beam spring and damper forces on node 2, and A_{212} is the cross term fluid coupling effect of node 2*; B_{212} is the cross term fluid coupling effect of the adjacent racks. u represents the ground acceleration.

Let

$$q_9 = p_9 - u$$

$$q_{10} = p_{10} - u$$

That is, q_9 is the relative displacement of node 2 in x-direction with respect to the ground. Substituting in the above equation, and rearranging, we have:

$$(m_{22} + A_{211} + B_{211})\, q_9 + A_{212}\, q_{10} = Q_9 - (m_{22} + A_{211} + B_{211} + A_{212} + B_{212})\, u$$

A similar equation for each one of the 32 degrees of freedom can be written. The system of equations can be represented in matrix notation as:

$$[M]\,\{\ddot{q}\} = [Q] + \{G\}$$

where the vector [Q] is a function of nodal displacements and velocities, and {G} depends on the coupling inertia and the ground acceleration. Premultiplying above equation by $[M]^{-1}$ renders the resulting equations uncoupled in mass.

We have:

$$\{\ddot{q}\} = [M]^{-1}\,[Q] + [M]^{-1}\,\{G\}$$

The generalized force Q_9, which contains the effects of all spring elements acting on node 2 in the "direction" of coordinate q_9 (the relative displacement of node 2 in the y direction), can easily be obtained from a free body analysis of node 2. For example, in the 2-D model shown in Figure 6.3, contributions to Q_9 are obtained from the two shear springs of the rack structure, and the two impact springs which couple node 2* and node 2. Since each of these four spring elements contain couplings with other component deformations through the spring force-deformation relations, considerable static coupling of the complete set of equations results. The level of static coupling of the equations further increases when 3-D motions are considered due to the inclusion of rack torsion and general fuel assembly group centroid effect.

For example, referring to Figure 6.3, and Table 6.1, a 2-D simulation introduces static coupling between coordinates 2,9 and 15 in the expression for Q_9; this coupling comes from the shear springs simulating the rack elasticity which have constitutive relations of the form $|F| = K_S\,|(q_9 - q_2)|$, $K_S\,|(q_{15} - q_9)|$. Further, the impact springs introduce two additional forces having constitutive equations of the form $|F| = K_I\,|(q_9 - q_{10})|$. Of course, at any instant, these forces may be zero if the local gap is open. The local gap depends on the current value of $|q_9 - q_{10}|$.

It should be noted that in the numerical simulations run to verify structural integrity during a seismic event all elements of the fuel assemblies are assumed to move in phase. This will provide maximum impact force level, and hence induce additional conservatism in the time history analysis.

This equation set is mass uncoupled, displacement coupled, and is ideally suited for numerical solution using the central difference scheme. The computer program named "DYNAHIS", developed by General Electric Company, performs this task in an efficient manner.[4]

Having determined the internal forces as a function of time, the computer program "EGELAST" computes the detailed stress and displacement fields for the rack structure as described in the preceding section.

6.5 Structural Acceptance Criteria

There are two sets of criteria to be satisfied by the rack modules:

(a) Kinematic Criterion: This criterion seeks to ensure that adjacent racks will not impact during SSE (condition E'[14]) assuming the lower bound value of the pool floor surface friction coefficient. It is further required that the factors of safety against tilting[15] are met (1.5 for OBE, 1.1 for SSE).

(b) Stress Limits

(1) The stress limits of the ASME Code, Section III, Subsection NF, 1980 Edition were chosen to be met, since

this Code provides the most consistent set of limits for various stress types, and various loading conditions. The following loading cases[14] have been analyzed.

	SRP Designation	ASME Designation
(i)	D + L	Level A (normal condition)
(ii)	D + L + E	Level B (upset condition)
(iii)	D + L + T_o	No ASME designation. Primary membrane plus bending stress required to be limited to lesser of 2 S_y* and S_u*
(iv)	D + L + T_o + E	No ASME designation. Stress limit same as (iii) above.
(v)	D + L + T_a + E	No ASME designation. Stress limit same as above.
(vi)	D + L + T_a + E'	Level D (faulted condition)

where

D = Dead weight induced stresses

L = Live load induced stresses; in this case stresses are developed during lifting.

The conditions T_a and T_o cause local thermal stresses to be produced. The worst situation will be obtained when an isolated storage location has a fuel assembly which is generating heat at the maximum postulated rate. The surrounding

---

*S_y: Yield stress of the material; S_u: ultimate stress.

storage locations are assumed to contain no fuel. Furthermore, the loaded storage location is assumed to have unchanneled fuel. Thus, the heated water makes unobstructed contact with the inside of the storage walls, thereby producing maximum possible temperature difference between the adjacent cells. The secondary stresses thus produced are limited to the body of the rack; that is, the support legs do not experience the secondary (thermal) stresses.

(2) Basic Data: The following data on the physical properties of the rack material are obtained from the ASME Codes, Section III, appendices.

Table 6.3 Physical Property Data*

Property	Young's Modulus @ 200°F E	Yield Strength @200°F S_y	Ultimate Strength @200°F S_u	Allowable Stress @ 200°F S
Value	28.3×10^6 psi	25 KSI	71 KSI	17.8 KSI
Section III Reference	Table I-6.0	Table I-2.2	Table I-3.2	Table I-7.2

*Evaluated at 200°F. This temperature is higher than the pool water bulk temperature under any of the loading conditions under consideration.

(3) Stress limits for normal and upset, and faulted conditions: The following limits are obtained from NF-3230 in conjunction with Appendix XVII as modified by the NRC Regulatory Guide 1.124[16].

(3.1) Normal and upset conditions (level A or level B):

(i) Allowable stress in tension on a net section $= F_t = 0.6\ S_y$ or

$F_t = (0.6)\ (25000) = 15000$ psi

F_t is equivalent to primary membrane stresses

(ii) On the gross section, allowable stress in shear is $F_v = 0.4\ S_y$

$= (0.4)\ (25000) = 10000$ psi

(iii) Allowable stress in compression, F_a

$$F_a = \frac{[1-(\frac{Kl}{r})^2/2C_c^2]S_y}{[(\frac{5}{3}) + (3\frac{Kl}{r})/8C_c - (\frac{Kl}{r})^3/8C_c^3]}$$

where

$$C_c = \left[\frac{(2\pi^2 E)}{S_y}\right]^{1/2}$$

Substituting numbers, we obtain, for both support leg and "honey-comb" region:

$F_a = 15000$ psi

(iv) Maximum bending stress at the outermost fiber due to flexure about <u>one</u> plane of symmetry:

$F_b = 0.60\ S_y = 15000$ psi

(v) Combined flexure and compression:

$$\frac{fa}{Fa} + \frac{C_{mx} f_{bx}}{D_x F_{bx}} + \frac{C_{my} f_{by}}{D_y F_{by}} < 1$$

where

f_a: Direct compressive stress in the section.

f_{bx}: Maximum flexural stress along x-axis

f_{by}: Maximum flexural stress along y-axis

$C_{mx} = C_{my} = 0.85$

$$D_x = 1 - \frac{fa}{F_{ex}'}$$

$$D_y = 1 - \frac{fa}{F_{ey}'}$$

where

$$F'_{ex} = \frac{12\pi^2 E}{23\left(\frac{Kl_b}{r_b}\right)^2}$$

(vi) Combined flexure and compression (or tension)

$$\frac{fa}{.6S_y} + \frac{f_{bx}}{F_{bx}} + \frac{f_{by}}{F_{by}} < 1.0$$

The above requirement should be met for both direct tension or compression case.

(3.2) Faulted Condition:

F-1370 (Section III, Appendix F), states that the limits for the faulted condition are 1.2 $\left(\frac{S_Y}{F_t}\right)$ times the corresponding limits for normal condition. Thus, the multiplication factor is

Factor $= (1.2)\left(\frac{25000}{15000}\right) = 2.0$

(3.3) Thermal Stresses:

There are no stress limits for thermal (self-limiting) stresses in Class 3-NF Structures for linear-type supports. However, the range of primary and secondary stress

intensity is required to be limited to 3 S_m in the manner of Class 1 components; S_m is the allowable stress intensity of the rack material at the maximum operating temperature.

6.6 RESULTS

Input time history accelerations for the safe shutdown earthquake condition are shown in Figs. 6.9 and 6.10. The time histories correspond to the ground slab response spectra for the plant as given in the FSAR.

Since there are several rack module configurations (Fig. 2.1) it was decided to make an exhaustive analysis of one rack type. We note that module A is an above-average size module, and hence will produce above-average floor reaction and support stress levels. Module type A is also most numerous. Hence module A is chosen for performing extensive analyses. Appropriate simulations are also carried out for other limiting rack geometrics (e.g. tipping study for rack with low cross section to height aspect ratio, stress evaluations for the heaviest module, etc.). To determine the magnitude of structural dampers, free lateral vibration plots of the top of rack A (in X and Y directions) for fully loaded and empty conditions were developed. The dominant natural frequency of vibration thus evaluated enables computations of the linear structural dampers. The percentage structural damping for SSE condition is assumed to be 2% and modifications to the stiffness matrix to incorporate damping is based on the dominant frequency of 10 cps. Having determined the damper characteristic data, the dynamic analysis of the rack module is performed using the computer program DYNAHIS. To simulate a three dimensional analysis, two equal components of the SSE horizontal acceleration are applied in two orthogonal directions concurrently with the vertical seismic acceleration. Abstracted results for all twelve cases mentioned in Section 6.1 are reported in Table 6.4. Table 6.5 gives the maximum values of stress factors (R_i (i = 1,2,3,4,5,6). The values given in the tables are the maximum values in time and space (all sections of the rack). The various stress factors are listed below for convenience of reference.

R_1: Ratio of tensile stress on a net section to its allowable OBE value

R_2: Ratio of gross shear on a net section to its allowable OBE value

R_3: Ratio of net compressives stress to its allowable OBE value for the section

R_4: Ratio of maximum bending stress in one plane to its allowable value in OBE

R_5: Combined flexure and compressive factor

R_6: Combined flexure and tension (or compression) factor

The allowable value of R_i (i = 1,2,3,4,5,6) is 1 for OBE condition, and is 2 for SSE condition (see Section 6.5).

The displacement and stress tables given herein are for the SSE condition. It is noted that the maximum displacements are a fraction of the limiting value for inter-rack impact. The maximum stress factors (R_i) are well below (limiting value for SSE condition) in all cases, for all sections.

Seismic simulations for the tipping conditions are carried out by increasing the horizontal SSE accelerations by 50%.[15] The calculations indicate that the rack remains stable, and the gross movement remains within the limit of small motion theory. Thus the rack module is seen to satisfy both kinematic and stress criteria with large margins of safety.

Those loading cases which appear to give maximum response (displacement or stress) for module A, are also run for module C. Module C is the smallest module, and therefore is expected to provide, along with module A, the bound on the response of all modules.

As shown in tables 6.4 and 6.5 the margins of safety are quite large in all cases. Analysis of welded joints in the rack also show comparable margins of safety.

Table 6.4

Maximum Rack Module Displacement during SSE Condition

No. Module Type	Case No.	μ	Max. X - Dispt.† & Time U_x (max) (inch)	Time Instant (sec)	Max Y - Dispt.† & Time U_y (max) (inch)	Time Instant (sec)	Comments
A	1	.8	.064	7.74	.110	8.03	
A	2	.2	.058	7.24	.069	7.23	
A	3	.8	.038	7.99	.054	7.73	
A	4	.2	.063	9.72	.079	12.58	
A	5	.8	.031	7.75	.067	7.24	
A	6	.2	.082	9.70	.085	9.28	
A	7	.8	.074	7.75	.117	8.04	
A	8	.8	.050	6.25	0	0	
A	9	.8	.027	7.96	.036	7.96	
A	10	.2	.049	12.33	.052	14.68	
A	11	.8	.049	11.15	.062	4.07	
A	12	.2	.105	7.37	.127	13.14	
C	1	.8	.045	9.44	.053	5.67	
C	2	.2	.062	13.03	.071	12.59	
C	5	.8	.042	8.02	.035	8.00	

† There are maximum displacement due to sliding, twisting, bending and rigid body motion of the rack module. These numbers are extracted from over 100,000 values computed for each node at discrete time instants.

Table 6.5†

Maximum Stress Factors during SSE Condition

Module Type	Case No.	μ	R_1	R_2	R_4	R_4	R_5	R_6	Comments
A	1	.8	.220	.110	.910	.640	1.030	1.170	Fully loaded, μ = .8
A	2	.2	.114	.027	.218	.183	.331	.372	Fully loaded, μ = .2
A	3	.8	.118	.075	.375	.440	.601	.686	Half loaded, asymmetrical about major axis, μ = .8
A	4	.2	.084	.110	.143	.139	.223	.248	Half loaded, asymmetrical about major axis, μ = .2
A	5	.8	.049	.035	.237	.244	.304	.349	Empty rack, μ = .8
A	6	.2	.025	.007	.060	.041	.083	.093	Empty rack, μ = .2
A	7	←						→	Tipping & Sliding Study only (Case 3)
A	8	.8	.119	.078	0	.508	.526	.628	Full rack, μ = .8, Two-D motion (x-z vertical)
A	9	.8	.126	.056	.279	.315	.452	.510	One side of diagonal loaded, μ = .8
A	10	.2	.105	.025	.198	.137	.308	.344	Case 9 with μ = .2
A	11	.8	.165	.102	.627	.570	.763	.870	Case 1 except zero hydraulic coupling
A	12	.2	.144	.042	.388	.220	.457	.513	Case 2 except zero hydraulic coupling
C	1	.8	.107	.034	.310	.276	.446	.508	Same as Type A, Case 1
C	2	.2	.086	.019	.224	.182	.329	.372	Same as Type A, Case 2
C	5	.8	.040	.021	.167	.214	.263	.303	Same as Type A, Case 5

† These factors should be less than 2 for SSE loading. The above values of R for any case do not occur at the same rack section or at the same time. These are all maximax values.

REFERENCES TO SECTION 6

1. USNRC Regulatory Guide 1.29, "Seismic Design Classification," Rev. 3, 1978.

2. "Friction Coefficients of Water Lubricated Stainless Steels for a Spent Fuel Rack Facility," by Prof. Ernest Rabinowicz, MIT, a report for Boston Edison Company, 1976.

3. U.S. Nuclear Regulatory Commission, Regulatory Guide 1.92, "Combining Modal Responses and Spatial Components in Seismic Response Analysis," Rev. 1, February 1976.

4. "The Component Element Method in Dynamics with Application to Earthquake and Vehicle Engineering" by S. Levy and J.P.D. Wilkinson, McGraw Hill, 1976.

5. "Dynamics of Structures" b R.W. Clough & J. Penzien, McGraw Hill (1975).

6. R.J. Fritz, "The Effects of Liquids on the Dynamic Motions of Immersed Solids," Journal of Engineering for Industry, Trans. of the ASME, February 1972, pp. 167-172.

7. USNRC Regulatory Guide 1.61, Damping Values for Seismic Design of Nuclear Power Plants, 1973.

8. J.T. Oden, "Mechanics of Elastic Structures," McGraw Hill, N.Y., 1967.

9. R.M. Rivello, "Theory and Analysis of Flight Structures," McGraw-Hill, N.Y., 1969.

10. M.F. Rubinstein, "Matrix Computer Analysis of Structures," Prentice-Hall, Englewood Cliffs, N.J., 1966.

11. J.S. Przemienicki, "Theory of Matrix Structural Analysis," McGraw-Hill, N.Y., 1966.

12. P. Kuhn, "Stresses in Aircraft and Shell Structures," McGraw-Hill, N.Y., 1956.

13. S.P. Timoshenko and J.N. Goodier, "Theory of Elasticity," McGraw-Hill, N.Y., 1970, Chapter 10.

14. U.S. Nuclear Regulatory Commission, Standard Review Plan, NUREG-0800 (1981).

15. U.S. Nuclear Regulatory Commission, Standard Review Plan, Section 3.8.5, Rev. 1, 1981.

16. U.S. Nuclear Regulatory Commission, Regulatory Guide 1.124, "Design Limits and Loading Combinations for Class 1 Linear-Type Component Supports, November 1976.

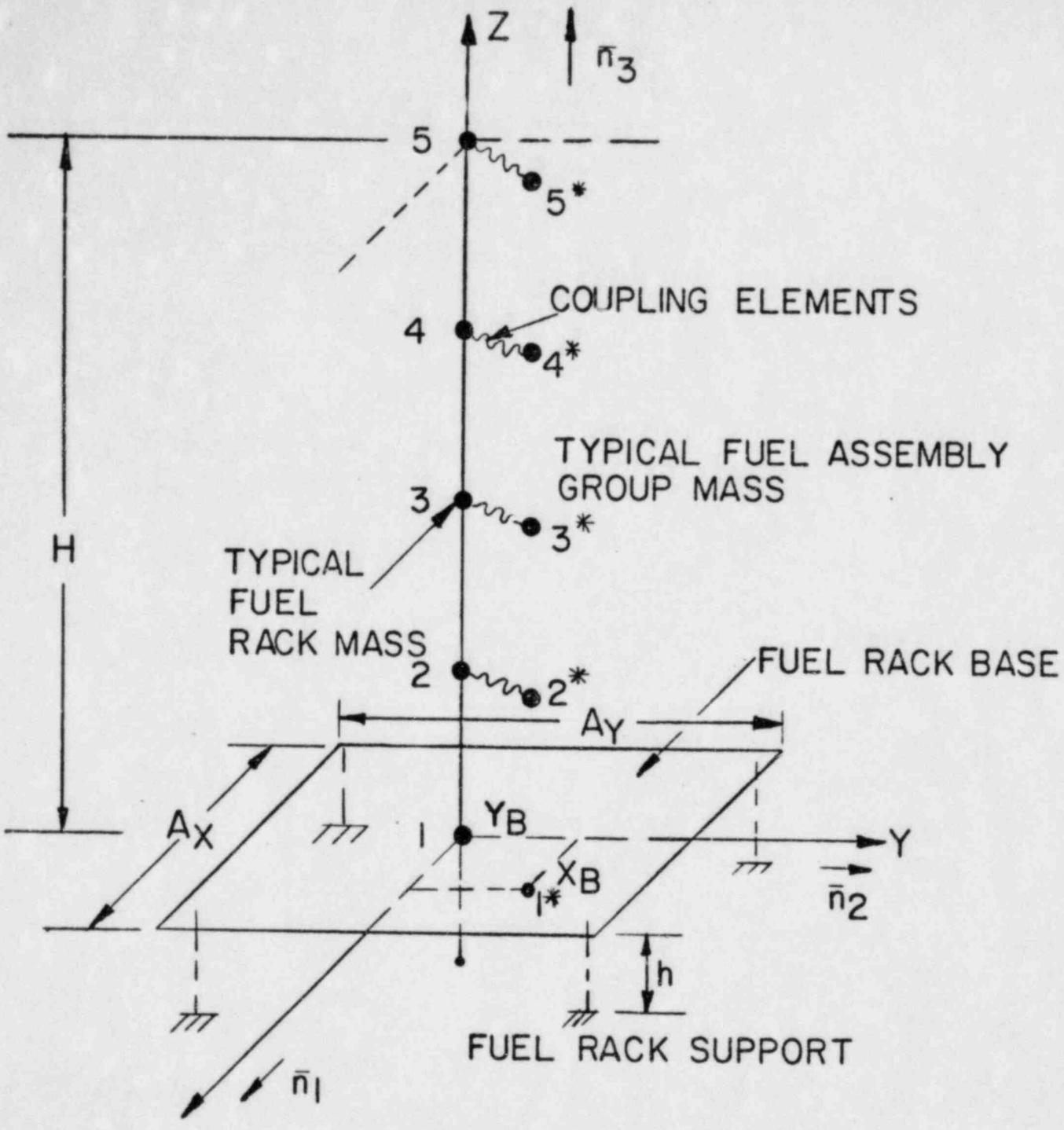

X_B, Y_B - LOCATION OF CENTROID OF FUEL ROD GROUP MASSES - RELATIVE TO CENTER OF FUEL RACK

n_i = UNIT VECTORS

FIG. 6.1 DYNAMIC MODEL

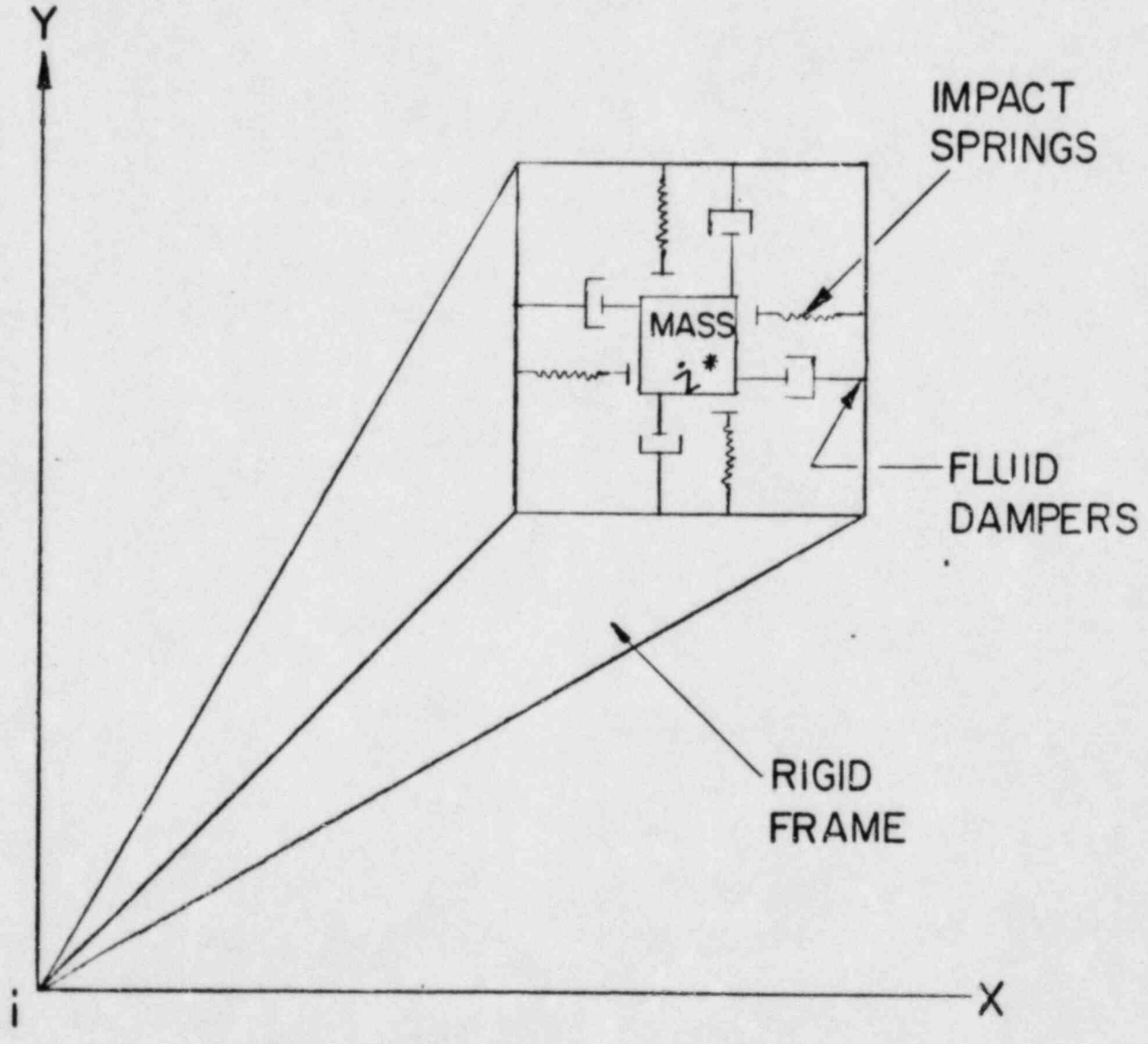

FIG. 6.2 IMPACT SPRINGS AND FLUID DAMPERS

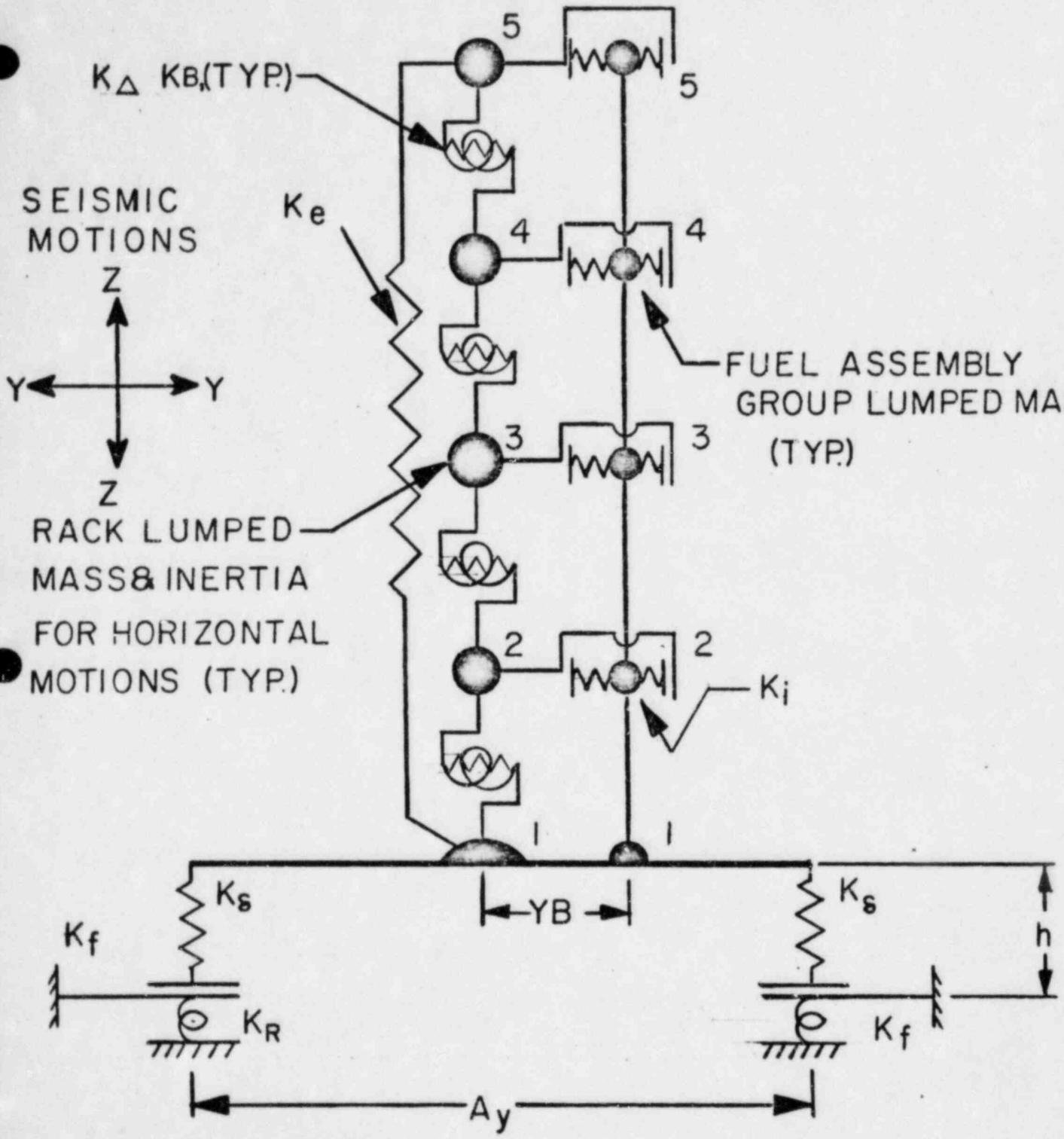

FIG. 6.3 SPRING MASS SIMULATION FOR A TWO DIMENSIONAL MOTION

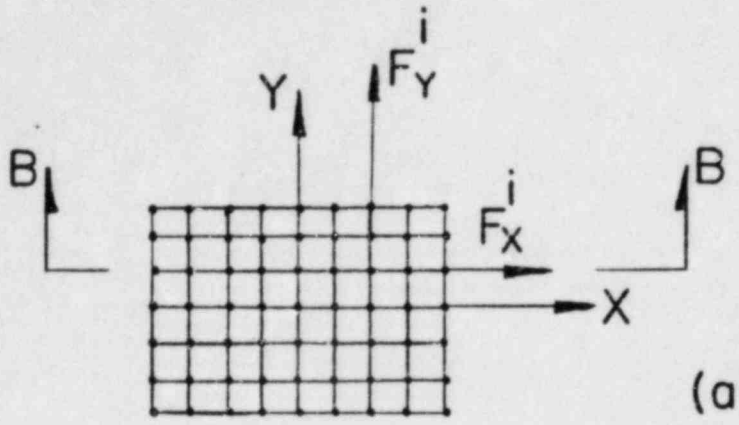

(a) TOP VIEW

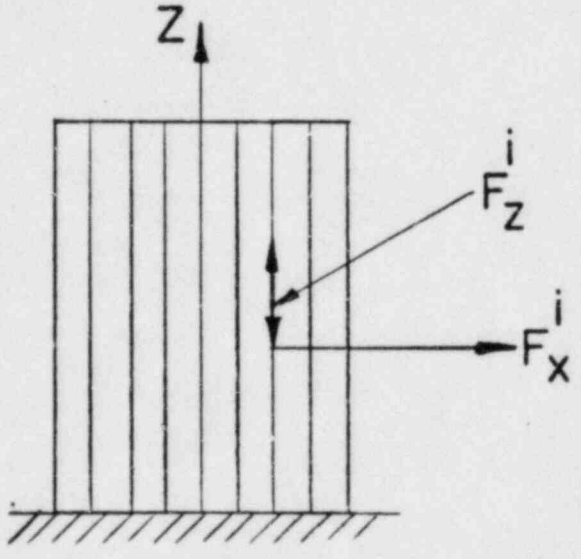

(b) AXIAL CROSS SECTION (B-B)

FIG. 6.4 (a) HORIZONTAL CROSS SECTION OF RACK
(b) VERTICAL CROSS SECTION OF RACK

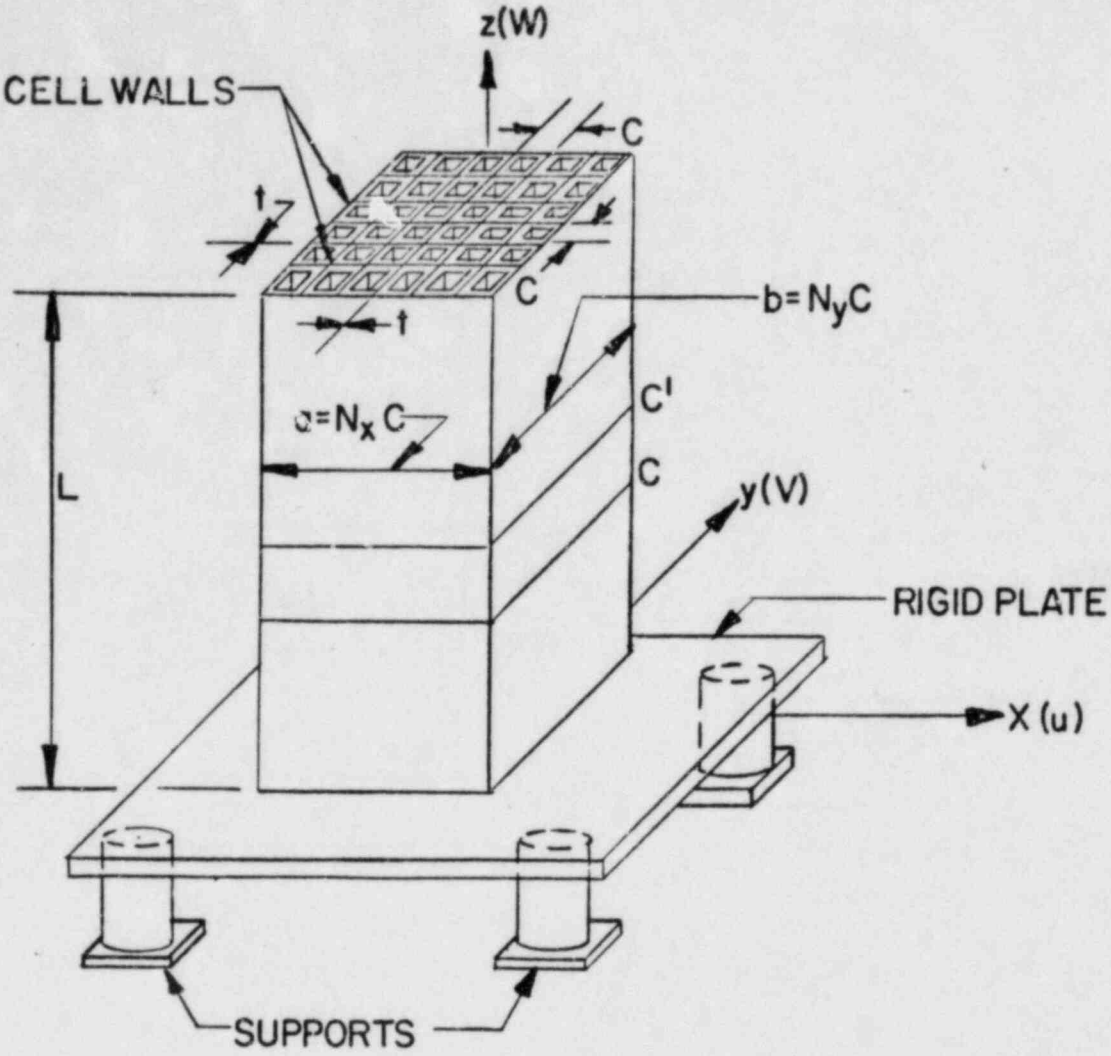
z(W)
CELL WALLS
C
t
C
t
b= NyC
a=Nx C
C'
C
L
y(V)
RIGID PLATE
X (u)
SUPPORTS

FIG. 6.5

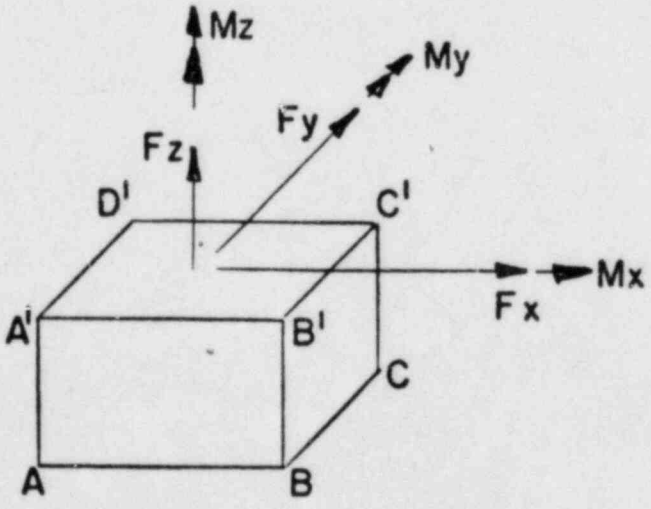
Mz
My
Fy
Fz
D'
C'
Mx
Fx
A'
B'
C
A
B

FIG. 6.6

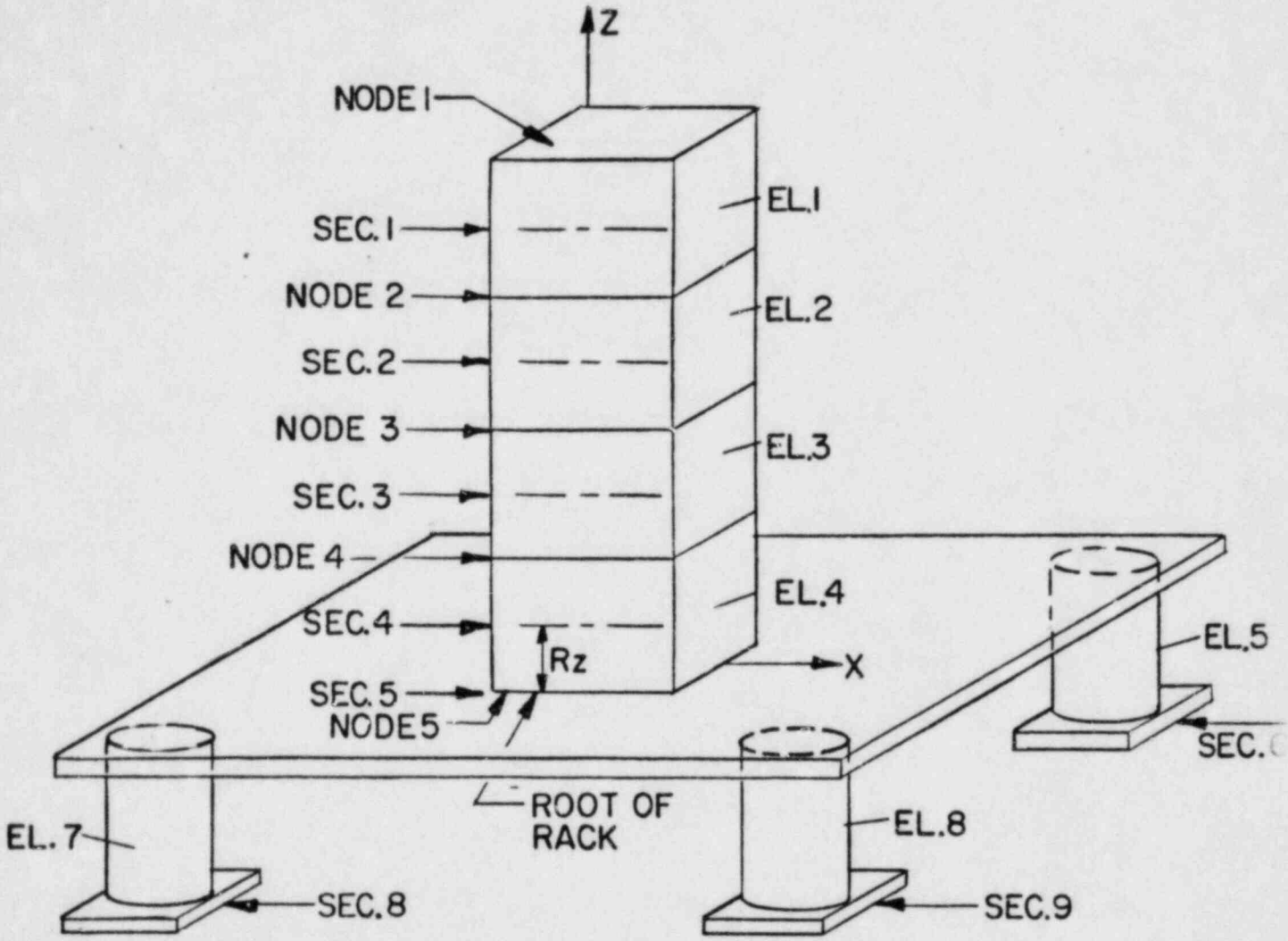

NO. OF ELEMENTS = 8
NO. OF SECTIONS = 9
NO. OF NODES = 5

FIG. 6.7

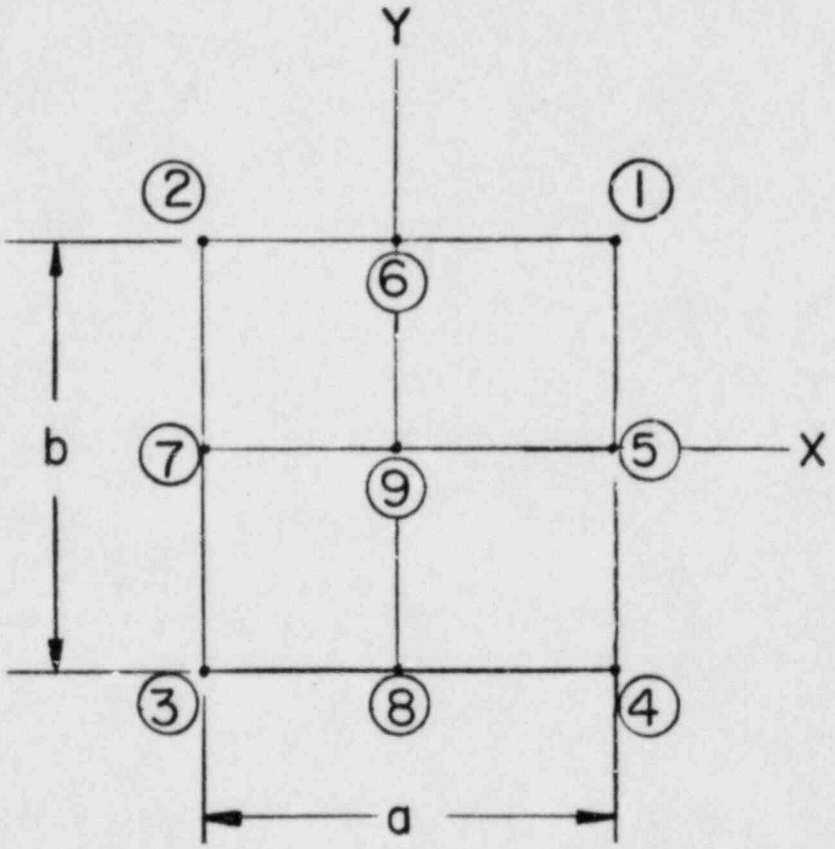

FIG. 6.8

Finite Element Model Cross Section

Figure 6.9

VERTICAL DIRECTION ARTEFICIAL TIME HISTORY
POOL FLOOR SLAB LEVEL
RANCHO SECCO STATION

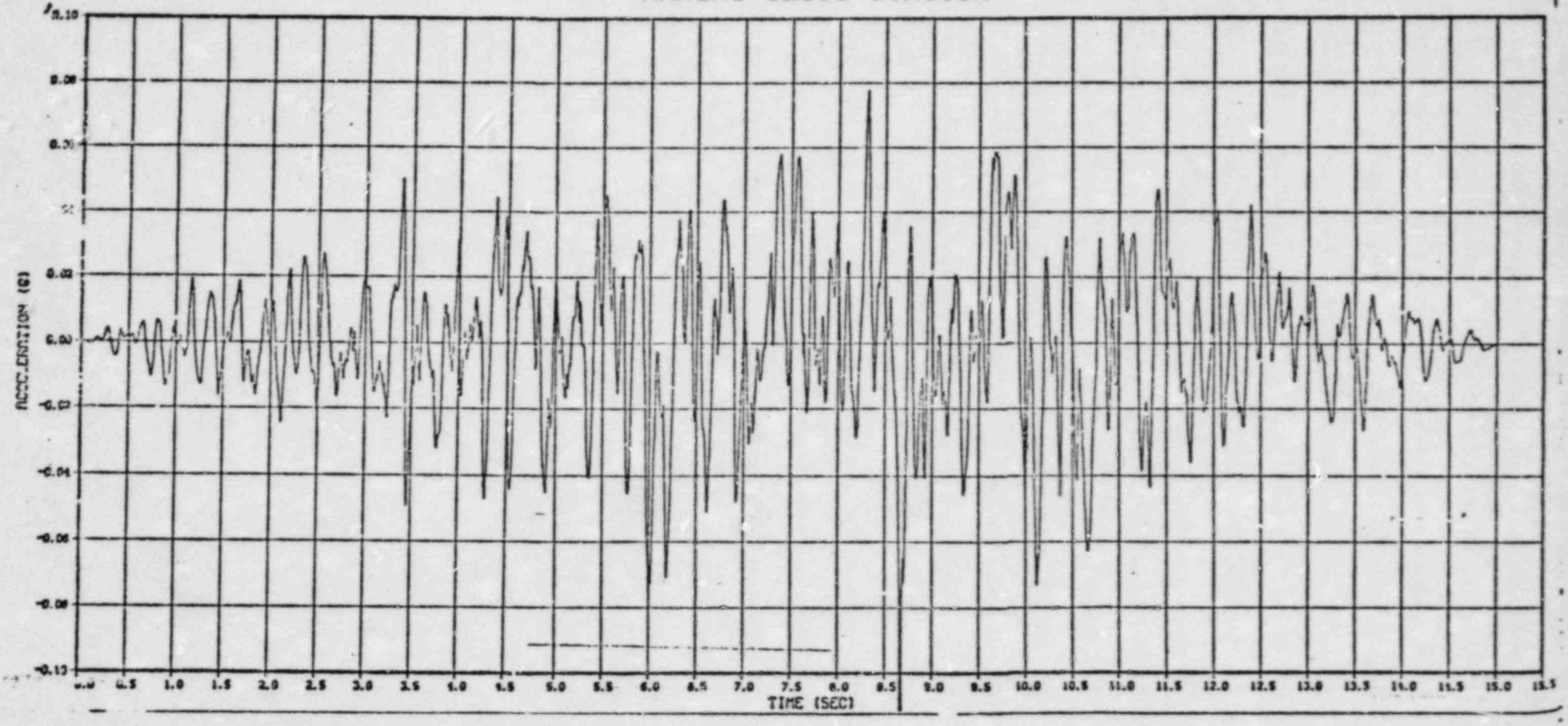

HORIZONTAL

Figure 6.10

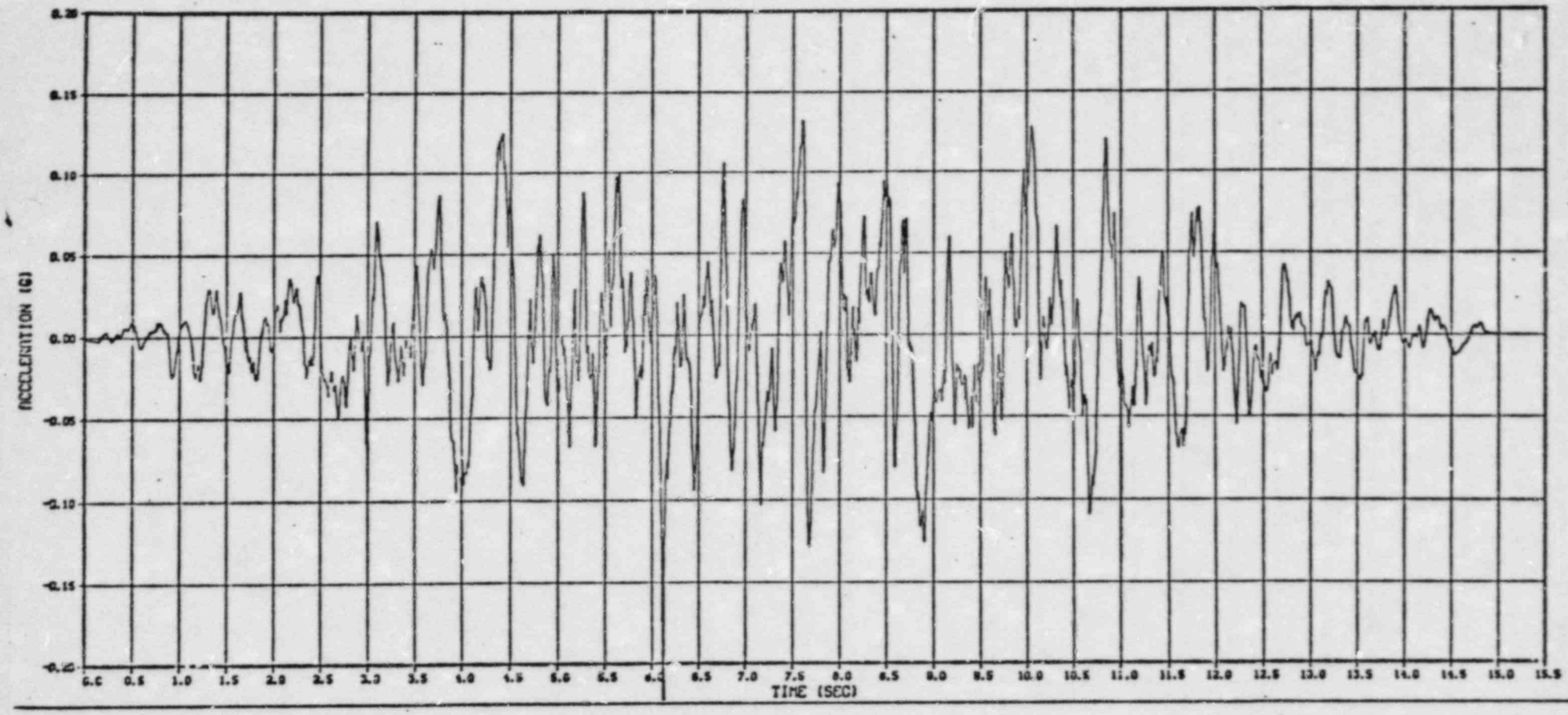

7. ACCIDENT ANALYSIS

7.1 Introduction:

In this section, a list of credible accidents with potential for affecting the performance of the spent fuel pool cooling system are described. The rack design features and method of analysis to evaluate the consequences of such accidents are also given. Since the installation of the proposed high density racks will enable the licensee to store increased amounts of fuel in the pool, it is important to review the accidents involving the pool region to ensure that the proposed pool modification does not reduce the degree of assurance of public health and safety. The following accidents are considered:

a. Fuel Pool - Earthquake loading.
b. Fuel Pool - Loss of cooling.
c. Refueling accidents
   - o Dropped fuel
   - o Jammed Fuel Handling Equipment
   - o Dropped gate
d. Radwaste leaks and spills
e. Turbine Missiles
f. Inadvertent placement of fuel assemblies

These are described in some detail in the following:

7.2 Results of Accident Evaluation:

a. Fuel Pool - Earthquake loading

The effect of earthquake loadings on the fuel racks is discussed in depth in section 6 of the Licensing Report. It is found that the stresses in the body of the proposed high density racks are a small fraction of the allowed limits of the ASME Code, Section III, Subsection NF.

b. Fuel Pool - Loss of Cooling:

If for some reason both primary and standby fuel cooling systems were to become unavailable, the temperature of water in the pool will begin to rise. It is found that the rate of temperature rise is hardly affected by the increased inventory of the spent fuel assemblies in the pool. Therefore, the thermal characteristics of the pool are essentially unaltered by the increased densification of storage.

c. Refueling Accidents:

The following four refueling accidents are considered possible.

(i) Dropped Fuel Accident I

A fuel assembly (weight - 1550 pounds) is dropped from 36 inches location and impacting the base. Local failure of the base plate is acceptable; however, a substantial impact with the pool liner is not acceptable. The subcriticality ofthe adjacent fuel assemblies is not to be violated.

(ii) Dropped Fuel Accident II

One fuel assembly dropping from 36 inches above the rack and hitting the top of the rack. Permanent deformation of the rack is acceptable, but is required to be limited to the top region such that the rack cross-sectional geometry at the level of the top of the active fuel (and below) is not altered.

(iii) Jammed Fuel-Handling Equipment and Horizontal Force

A 2000-pound uplift force and a 1000-pound horizontal force are applied at the top of the rack at the "weakest" storage location; the force is assumed to be applied on one wall of the storage cell boundary as an upward shear force. The damage, if any, is required to be limited to the region above the top of the active fuel.

(iv) Dropped Gate

The gate between the refueling transfer canal and the pool is conservatively assumed to fall from an elevation of 2' above the rack module. The gate is constructed of stainless steel and weighs 1600 lbs. in air. It is the largest and heaviest gate. Its minimum frontal areas corresponds to an upright vertical fall.
The mathematical model constructed to determine the impact velocity of the above falling object is based on several conservative assumptions, such as

1. The virtual mass of the body is conservatively assumed to be equal to its displaced fluid mass. Evidence in the literature[1] indicates that the virtual mass can be many times higher.

2. The minimum frontal area is used for evaluating drag coefficient.

3. The drag coefficients utilized in the analysis are lower bound values reported in the literature.[2] In particular, at the beginning of the fall when the velocity of the body is small, the corresponding Reynolds number is low resulting in a large drag coefficient.

4. The falling bodies are assumed to be rigid for the purposes of impact stress calculation on the rack. The solution of the immersed body motion problem is found analytically. The impact velocity thus computed is used to determine the maximum stress generated due to stress wave propagation.

The above loading conditions are analyzed to determine an upper bound on the plastic deformation zones. For the above conditions, it is shown that the plastic deformation is limited to the rack structure well removed from the active fuel regions. Thus, the subcriticality of the fuel arrays is not modified or violated.

d. Radwaste Leaks and Spills:
It has been determined that the spent fuel pool modification will not result in increased usage of the pool clean up system. Therefore, the analyses, which were conducted in the past on radwaste leaks are still valid.

e. Turbine Missiles:
Physical barriers between the pool and the turbine regions preclude the possibility of the racks being subject to turbine missile impact.

f. Inadvertent Placement of Fuel Assemblies:
Placement of fuel assemblies outside the designated storage locations, such as leaning against an exterior rack wall near the pool boundary, is a remote possibility.

REFERENCES TO SECTION 7

1. "Flow Induced Vibration" by R.D. Blevins, VonNostrand (1977).

2. "Fluid Mechanics" by M.C. Potter and J.F. Foss, Ronald Press, p. 459 (1975).

8. RADIOLOGICAL CONSEQUENCES

8.1 Summary and Conclusions

The high-density spent fuel storage racks will increase storage capacity in the Rancho Seco fuel pool from 579 to 1080 fuel assemblies. Radiological consequences of expanding the storage capacity of the Rancho Seco spent fuel storage pool have been evaluated with the objective of determining if there is significant additional radiological impact, onsite or offsite, relative to that previously reviewed and evaluated. In addition, the radiological impact to operating personnel has been assessed to insure that such exposure remains as low as is reasonably achievable.

The decay heat loading and the radiological burden to the spent fuel pool water are controlled almost entirely by refueling operations. The frequency and nature of refueling operations, however, are not related to or affected by the increase in spent fuel storage capacity, except as the increased capacity allows continued normal operation. Because of radioactive decay, aged fuel, which constitutes the bulk of the storage capacity (and will ultimately fill all the incremental capacity above that of the current design), will make only a minor contribution to the peak decay-heat loading on the pool water and an even smaller contribution to the radiological burden. Consequently, increasing the storage capacity of the spent fuel pool will neither significantly alter the operating characteristics of the current storage pool nor result in a measurable change in impact on the environment.

Based upon operating experience and evaluations discussed in more detail in subsequent sections, the following conclusions may be made relative to the increased spent fuel storage capacity.

- Due to the minor increase in radiological burden to the pool water, the existing spent fuel pool cleanup system (filter and demineralizer) is adequate to maintain the radionuclide concentration in the water at an acceptably low level.

- No appreciable increase in solid radioactive wastes (i.e., demineralizer resin and filter media) is anticipated.

- No increase in release of radioactive gases is expected, since any long-lived inert radioactive gas potentially available for release (i.e., Kr-85) will have leaked from the fuel (in the reactor core during operation, or in the first few months after removal from the core). Note that Kr-85 has not been detected in the atmosphere above the pool in previous operations.

- The existing spent fuel pool cooling system is adequate to maintain the bulk pool water temperature at an acceptable level (see Section 5 -- Thermal-Hydraulic Considerations), with an increase of only 1 to 2°F in bulk temperature of the pool water due to the increased storage capacity.

- No increase in corrosion of Zircaloy cladding is expected, and there is sufficient evidence of long-term fuel integrity to accommodate increased storage capacity.

- No buildup of crud along the sides of the pool, that might contribute to an increase in radiation dose to personnel, has been detected in prior operations. Consequently, there is no reason to expect this source to become significant in the future with increased pool capacity.

- The existing radiation protection program and monitoring system are adequate to detect and warn of any unexpected abnormal increase in radiation level and to provide assurance that personnel exposure can be maintained as low as is reasonably achievable.

- The total exposure to personnel occupying the fuel pool area for all operations in 1981 was 4.43 man-rem, and no significant increase in personnel exposure is expected as a result of the increased storage capacity.

- Expanding the storage capacity of the spent fuel pool will not increase the onsite or offsite radiological impact significantly above that of the currently authorized storage capacity, nor is any significant

increase in environmental impact anticipated, radiological or non-radiological.

The Final Generic Environmental Statement,[1] NUREG-0575, also provides general confirmation that high density spent fuel storage racks are an acceptable resolution of the problem of onsite storage of spent fuel, subject to the evaluation of specific rack designs at a particular plant.

Several options for removal and disposal of the existing racks are presently being evaluated. Similar operations have previously been performed successfully by a number of utilities, and this fact provides a credible basis for anticipating that an acceptable plan for re-racking can be developed with suitable consideration for ALARA exposure to personnel. Personnel exposures are expected to be less than 25 to 30 man-rem for the re-racking operation, including installation of the new racks.

The quantity of material removed for disposal will be a very small fraction of the total solid waste generated over the lifetime of the plant and therefore will result in a negligible additional environmental impact. Prior to re-racking, a detailed plan will be developed, based upon the disposal method selected and the best available estimates of dose rates and occupancy factors for specific job functions. This plan will be submitted for review and approval before actual re-racking operations begin.

8.2 Characteristics of Stored Fuel

The currently authorized storage capacity of the Rancho Seco spent fuel pool is 579 assemblies; when fully loaded, the pool would contain the 177 assemblies of a full core discharge and approximately 400 assemblies with cooling times ranging from 15 months to about 8 years.

An additional 501 fuel assemblies can be stored in the expanded capacity racks with cooling times greater than about 10 years, based upon an expected fuel cycle duration of 15 months and a corresponding discharge fuel burnup of 34,000 Mwd mtU.

Because of radioactive decay, the heat generation rate and the intensity of gamma radiation from the spent fuel assemblies decreases substantially with cooling time. Figure 8-1 shows the decay heat from an average fuel assembly (at a discharge burnup of 34,000 Mwd/mtU), calculated as a function of the time after reactor shutdown (cooling time) by the method of ASB Technical Position 9-2 (Rev. 2, 1981).

Reduced fuel burnup or increased cycle length would result in a lower fission-product inventory or longer storage (decay) periods respectively. Thus, the assumed storage pool composition should result in a conservative estimate of any additional thermal or radiological impact due to the expanded storage capacity.

After a cooling time of about 4 years, the decay heat generation rate is less than 2% of the rate at 10 days--the nominal time at which depleted fuel assemblies are transferred to the spent fuel pool. The intensity of gamma radiation is very nearly proportional to the decay heat and decreases with cooling time in a similar manner.

The expanded capacity storage racks are designed to accommodate fuel with an initial enrichment of 4 wt.% U-235, which could hypothetically achieve a discharge burnup as high as 50,000 Mwd/mtU. For this reason, a curve of the decay heat for fuel discharged at 50,000 Mwd/mtU is also shown on Fig. 8-1. The higher discharge burnup increases the decay heat rate at long cooling times but does not substantially change the maximum decay heat to the pool shortly after discharge of a full core loading.

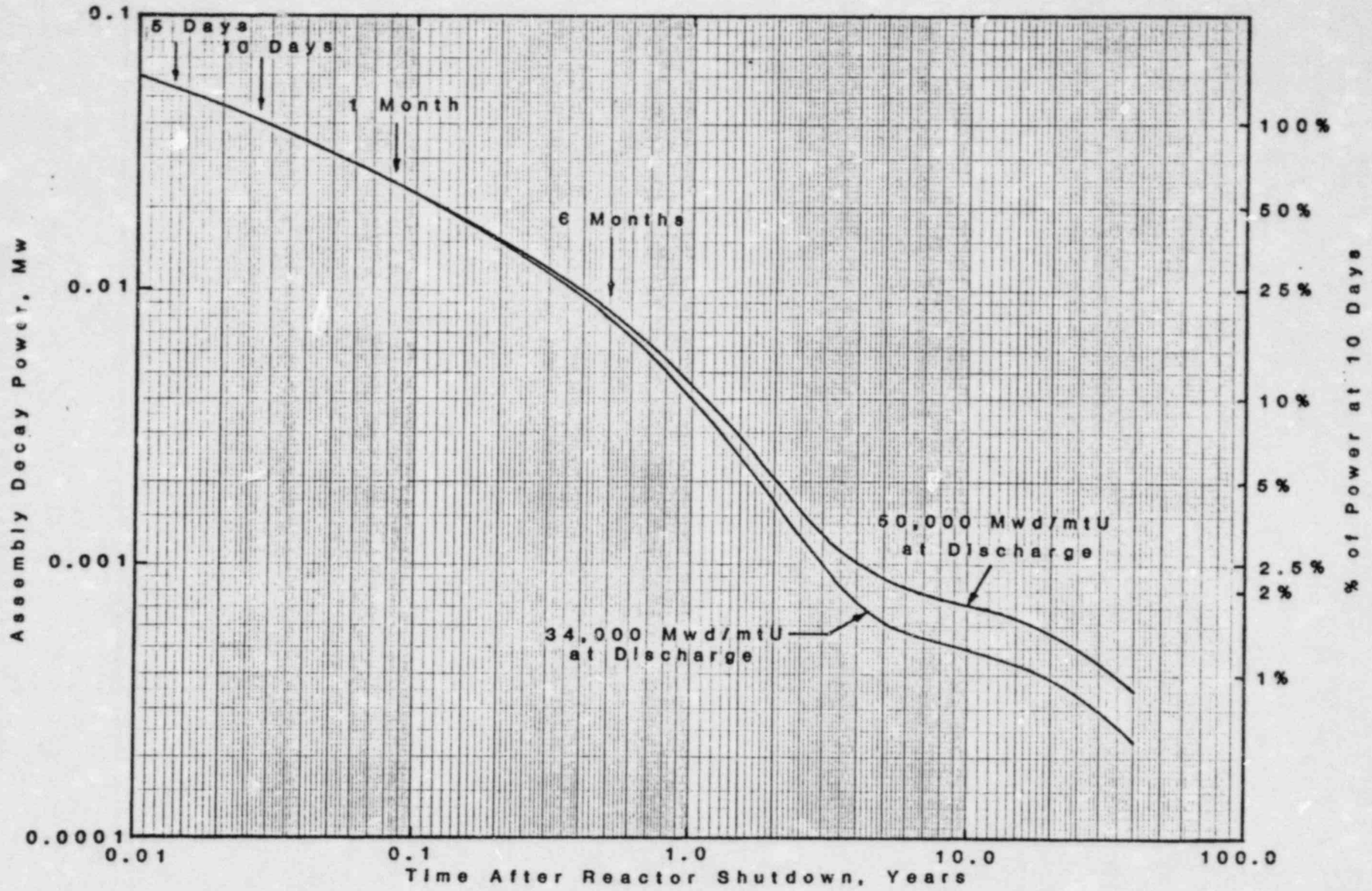

Fig. 8-1. Decay heat rate of an average fuel assembly as a function of cooling time (calculated by method of ASB9-2).

Figure 8-2 shows the total decay heat to the spent fuel pool water, illustrating the peaking in heat load at the time of refueling and the decay between refueling. The highest decay heat loading to the spent fuel pool occurs for a full core discharge at or near the end of a fuel cycle. Under these conditions, decay heat from the freshly discharged fuel (assumed at 10 days following reactor shutdown) accounts for the majority of the total heat load to the pool water. The total contribution of the aged fuel in the expanded capacity storage rack (approximately 501 assemblies with cooling times greater than 10 years) amounts to less than 4% of the maximum total decay heat to the pool water. A similar conclusion applies to the intensity of gamma radiation.

It is important to note that the aged fuel in the expanded capacity storage racks will not contain any radioactive iodine nuclides or any short-lived gaseous fission products. In the interval between refuelings, all of the radioiodine nuclides and short-lived gaseous fission products (Xe and Kr) will have decayed out, leaving Kr-85 as the only gaseous fission product remaining.

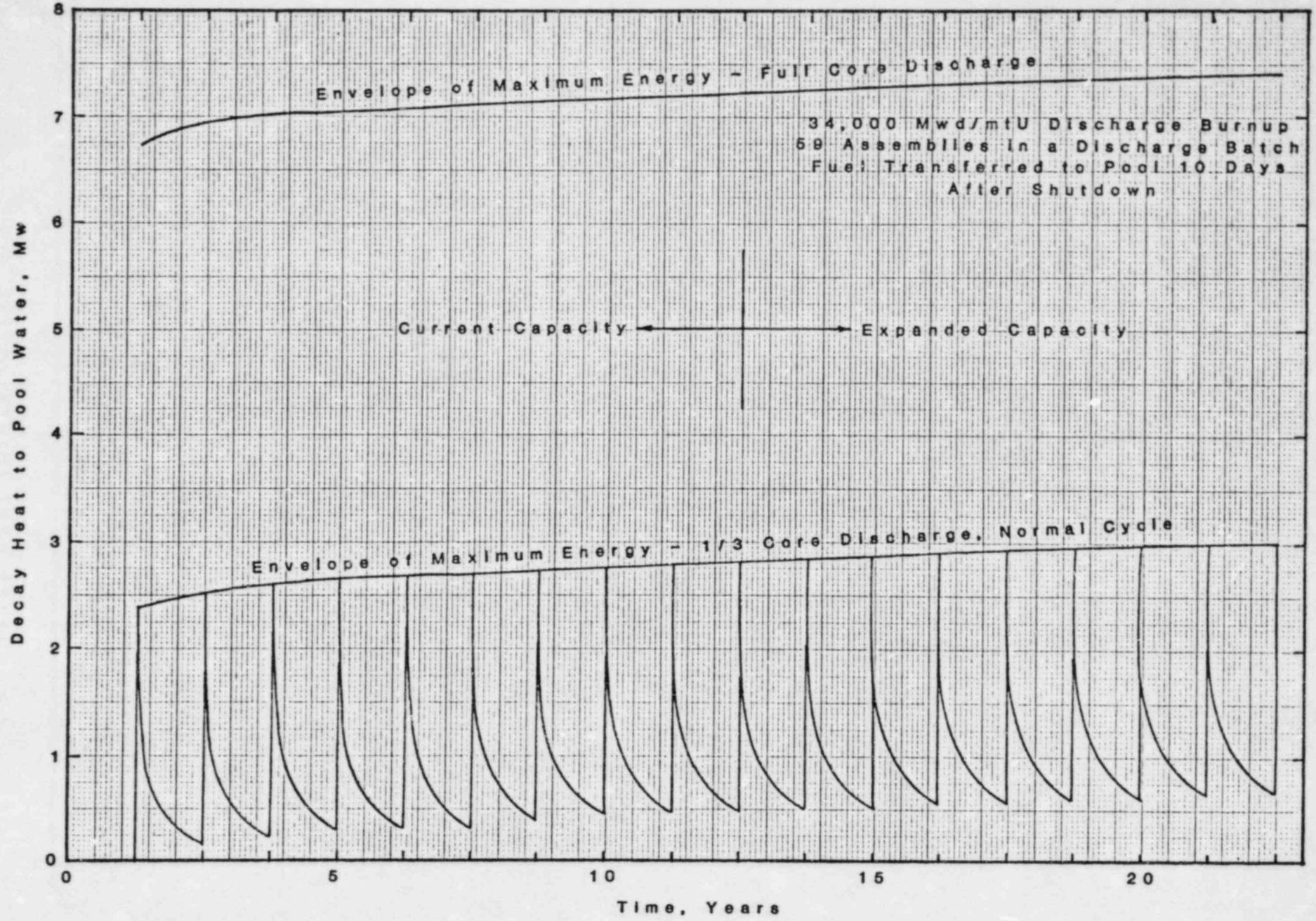

Fig. 8-2. Total decay heat for idealized fuel cycle with fuel discharged every 15 months at 34,000 Mwd/mtU burnup.

8.3 Operating Experience

8.3.1 Related Industry Experience

In a survey[2] of spent fuel storage pool experience, Johnson, at Battelle Pacific Northwest Laboratories, has shown that typical concentrations or radionuclides in spent fuel pool water range from 10^{-4} μCi/ml, or less, to 10^{-2} μCi/ml, with the higher value associated with refueling operations. Isotopic measurements of the nuclides confirm that a major fraction of the coolant activity results from activated corrosion products dislodged from fuel element surfaces during refueling operations or carried into the spent fuel pool water (with some fission-product radionuclides) by mixing of pool water with primary system water during refueling. These sources of storage pool radionuclides depend upon the frequency of refueling operations and are basically independent of the total number of fuel assemblies in storage.

Once fuel-handling operations are completed, the mixing of pool water with primary system water ceases and these sources of radionuclides decrease significantly; only dissolution of fission products absorbed on the surface of fuel assemblies and possible low-level erosion of corrosion-product (crud) deposits remain. For fuel aged for more than a few months, neither of the latter sources would be expected to contribute significantly to the concentrations of radionuclides in the storage pool.

Escape of fission products from failed fuel stored in the spent fuel pool might be thought to be a significant source of radionuclides to the pool water. However, industry experience and evaluations described below indicate that the radionuclide concentrations from failed fuel are considerably less than the concentrations of radionuclides from other sources, and, therefore, the aged fuel in the expanded storage pool will not contribute significantly to the onsite or offsite radiological impact.

The decay heat generated in spent fuel rapidly decreases (by radioactive decay) following removal from the reactor and, in an aged fuel assembly, will be very small (<2% of that in freshly-removed fuel). Fuel temperatures and internal gas pressures will correspondingly decrease with time. The release of fission products from failed fuel probably results from water-leaching or diffusion of material plated out or absorbed in the fuel-clad gap of the fuel element during operation in the reactor. Once the material in the gap is depleted, further release will be very small. Westinghouse, in capsule tests[3] with intentionally defected fuel, has shown that release of fission products from failed fuel decreases rapidly to essentially negligible levels shortly after shutdown. Most of the fission products are absorbed (retained) in the fuel matrix and can escape only by diffusion through UO_2. At the temperatures of the fuel in the spent fuel pool, the diffusion coefficient will be extremely small,[4] and any further release of fission products will be very low, if not negligible.

In his survey, Johnson indicates that numerous fuel assemblies with one or more defects have been stored in several spent fuel pools without requiring special handling. Detailed analysis of the spent fuel pool water confirmed that fuel elements with defects do not continue to release significant quantities of radionuclides for long periods of time following removal from the reactor. Johnson also cites evidence to confirm that UO_2 is inert to the relatively cool water (<150°F) of spent fuel storage pools. Therefore, the release rate of fission products from any defective rods among the aged fuel is expected to be negligibly small.

Both Johnson,[2] at Battelle, and Weeks,[5] at Brookhaven National Laboratory, have reviewed the corrosion properties of Zircaloy cladding and the integrity of spent fuel elements stored for long periods of time. They conclude that the corrosion of

Zircaloy cladding in spent fuel pool water is negligibly small and that there is sufficient evidence of satisfactory fuel integrity to justify expanded storage. The minor incremental heating of the pool water by the expanded storage capacity is far too small (~1-2°F) to materially affect the corrosion properties of Zircaloy cladding.

8.3. Rancho Seco Experience

Measurements have been made of the principal radionuclide concentrations in the Rancho Seco fuel storage pool with 196 spent fuel assemblies in storage. Table 8-1 summarizes these measurements.

Table 8-1 Observed Radionuclide Concentrations In Spent Fuel Storage Pool Water

Nuclide	Measured 5/20/81 *	Measured 1/6/82
I-131	4.7×10^{-4}	Not detected
I-133	2.1×10^{-4}	Not detected
Cs-134	1.6×10^{-3}	1.4×10^{-3}
Cs-137	2.4×10^{-3}	2.2×10^{-3}
Ag-110m	1.3×10^{-3}	2.2×10^{-4}
Co-58	3.5×10^{-3}	Not detected
Mn-54	1.4×10^{-4}	Not detected
Co-60	3.0×10^{-4}	2.6×10^{-5}

* Shortly after refueling

These observed radionuclide concentrations are generally comparable to industry experience in other spent fuel storage pools. Expanding the storage capacity of the Rancho Seco storage pool is not expected to significantly alter the general magnitude

of radionuclide concentrations, since the contribution from the aged fuel will be very low or negligible in comparison to that from recently discharged fuel or from primary system carry-over during refueling.

8.4 Fuel Storage Pool Purification System

The existing spent fuel purification system uses a small bypass flow (160 gpm) through a 3 micron (nominal) cartridge-type filter and mixed bed ion-exchange demineralizer, and is designed to process about half of the storage pool water in 24 hours. A skimmer loop is also provided to remove particulate matter floating on the surface (for water clarity) and to prevent pool overflow onto the pool area floor.

The frequency of filter and resin replacement is determined primarily by requirements for water clarity rather than the loading of fission product radionuclides. Experience has shown that filters are changed about three times a year and demineralizer resin about every two years. Frequency of change-out is not expected to be materially different with the expanded capacity storage pool. Originally (i.e., FSAR), the demineralizer resin (50 ft^3) was expected to be replaced annually, but experience has indicated the need for a lower frequency in practice.

The spent fuel pool water is sampled and analyzed periodically to confirm proper operation of the pool cleanup system. Table 8-2 summarizes the sampling frequency and lists pertinent limiting specifications.

If the limits are exceeded, operation of the cleanup system will be checked and the filter and/or ion-exchange resin changed as appropriate. Important operating parameters (i.e., pool temperature, differential pressures across the filter and demineralizer and pool area radiation levels) are monitored continuously

and displayed/alarmed in the reactor control room to enable prompt corrective action in the event of abnormal conditions.

Table 8-2 Pool Water Sampling Schedule and Chemical Limits

Analysis	Approximate Frequency*	Specification
Boron	Monthly and after make-up	1875 ppm B (min.)
	Weekly during refueling	1850 ppm B (min.)
Chloride	Weekly	0.15 ppm (max.)
Fluoride	Weekly	0.15 ppm (max.)
pH	Weekly	~4.5 - 4.6
Gross Beta	Weekly (daily (during refueling	NA
Gamma Spectra	Weekly	NA
Decontamination Factor	Monthly	NA
Tritium	Weekly	NA

*With spent fuel in the storage rack.

No problems with water clarity have been experienced, and the criteria for filter/demineralizer change-out are as follows:

Filter cartridges - differential pressure of 25 psi, or a radiation level of 1 R at 18 inches.

Demineralizer resin - differential pressure of 25 psi or loss in decontamination factor (D.F.).

Periodic measurements of the approximate decontamination factor across the demineralizers are made (approximately monthly), and the resin will be changed if there appears to be significant deterioration in decontamination factor.

The amount of suspended particulate material produced that must be removed is determined primarily by the frequency of refueling operations and is independent of the number of fuel assemblies stored. The expanded capacity of the Rancho Seco storage pool will not significantly alter either the frequency of resin or filter media replacement above that currently experienced, or the personnel radiation exposures during maintenance operations.

8.5 Fuel Storage Pool Cooling System

An analysis of the performance of the spent fuel pool cooling system, given in Section 5, confirms that the system can maintain the bulk water temperature within acceptable limits. Compared to the currently authorized storage capacity, the aged fuel in the expanded capacity rack, when completely filled, will increase the water temperature by less than 1° to 2°F (less than 4% of the temperature rise; see Section 8.2). This incremental temperature increase is too small to have an adverse effect on Zircaloy corrosion or on pool surface evaporation. Thus, it is concluded that the pool cooling system is adequate and will not require modification.

8.6 Fuel Pool Radiation Levels

The measured radiation dose at the 1 foot level above the Rancho Seco pool was 6-8 mr/hr (May 1982), except above the upender pit where higher levels were observed. Higher radiation dose rates above the pool are expected during refueling operations, decreasing soon after completion of refueling to the 6-8 mr/hr range.

Because of radioactive decay, the total contribution of all the aged fuel to the dose rate at the pool surface by direct radiation will be a very small (<4%) increase over that from the

more-recently-discharged fuel. Since the pool water affords adequate shielding and no significant increase in radionuclide concentrations in the pool water is expected, it is concluded that the occupational dose rate above the surface of the pool from direct radiation will be essentially the same as that for the currently authorized storage pool.

To confirm the absence of crud depositions on the pool walls, measurements were made above the center of the storage pool and at the pool edge. The observed values were essentially the same, indicating that there is no significant amount of crud deposited on the walls of the pool that might contribute to a higher dose rate at the pool edge. Visual observations also confirm the absence of any significant crud deposition on the pool walls. The pool cleanup system effectively prevents the accumulation of crud in the pool water which might lead to deposition on the pool walls. Operating experience has confirmed the absence of any significant crud buildup.

Radiological surveys around the perimeter of the spent fuel shield wall at several elevations indicate a radiation level of less than 2 mr/hr. The concrete shield wall (5 feet of concrete) of the pool and the water in the pool between the fuel and the wall afford more than adequate shielding. In the expanded capacity pool, the closest approach of stored fuel to the pool walls is very nearly the same as in the current rack. Consequently, no increase in dose rate through the shield wall will occur.

In view of the above, it is concluded that the additional storage capacity of the expanded spent fuel pool will not measurably alter the currently approved radiological impact or significantly alter the radiation dose to personnel occupying the fuel pool area.

8.7 Gaseous Radionuclides

Because of the half-lives of the gaseous radionuclides, only the release of Kr-85 ($T_{1/2}$ of 10.76 years) has the potential of increasing the radiological impact to the reactor building atmosphere as a result of expanding the capacity of the spent fuel storage pool. (Short-lived noble-gas radionuclides and other volatile fission products, such as iodine, are not present in the aged fuel.) Johnson concludes that the radioactive fission gases will have been largely expelled from defective fuel rods during reactor operation and, therefore, are not available for release during fuel storage. This is expected, since the noble gases are chemically inert, and there are no plate-out or hold-up mechanisms in the fuel-clad gap of the fuel element. Measurements above the Rancho Seco storage pools failed to detect any Kr-85 above the minimum detection level (approximately 5×10^{-6} μCi/cc).

The small amount of chemically-inert Kr-85 that might be absorbed on the surface of a fuel assembly and released slowly during storage is believed to be insignificant, particularly in the aged fuel. Since UO_2 is chemically inert to cool water, diffusion of Kr-85 entrapped within the UO_2 fuel matrix would be the remaining source for Kr-85 release. Based on the method outlined in the proposed ANS 5.4 standard[4] on fission gas release, the diffusion coefficient in the aged fuel at spent fuel pool temperatures will be negligibly small. Consequently, diffusion release of Kr-85 from aged fuel will be negligible in accord with Johnson's findings.

It is concluded that the incremental radiological impact from the release of volatile radionuclides with the expanded-capacity spent fuel storage pool will be negligibly small.

8.8 Radiation Protection Program

The total radiation exposure to personnel from all operations in the fuel pool area was 4.43 man-rem during 1981. No increase in personnel exposure due to operations with the expanded capacity storage racks is expected. (Re-racking operations are considered in Sec. 8.9, following). Area radiation monitors measure and record radiation levels in the spent fuel pool area in order to detect and alarm any abnormal conditions.

In view of the absence of any significant increase in direct radiation, radionuclide concentration in the pool water and/or volatile fission product release, the existing radiation program is adequate to assure the protection of personnel.

8.9 Re-racking Operation

The existing spent fuel racks will be removed, and the new racks will be installed in a manner which will minimize the environmental impact and maintain occupational exposure to levels as low as are reasonably achievable (ALARA). The following methods for the final disposal of the existing racks are currently under review:

- Crating and shipment of the racks in the "as-is" condition, with or without some cutting or shearing to reduce the size of individual modules.
- Dismantling and volume reduction (shredding and drumming), and shipment for ultimate burial as waste.
- Chemical and/or electrolytic decontamination, processing the decontamination chemicals as ordinary radwaste and disposing the bulk rack material as "clean" scrap. (Clean is defined as less than 200 DPM/100 cm^2 removable contamination (smear) and less than 1 mr/hr at the surface for non-removable contamination.

It is anticipated that after the evaluation is completed, re-racking will be handled by a contractor experienced in operations of this nature. Prior to re-racking, a detailed plan will be developed and submitted for review/approval, encompassing, as a minimum, the following:

- Assurance that personnel exposure will be maintained as low as is reasonably achievable (ALARA), identifying the step-by-step operations, including the number of personnel involved in each step, the anticipated dose rate, the time involved and the estimated man-rem exposure. At the present time, it is anticipated that the total personnel exposure can probably be maintained at less than 25-30 man-rem.

- Assurance that spent fuel stored in the racks is not within the area of influence of a potential rack-drop accident during removal of existing rack modules or installation of new ones.

- Assurance that operations or potential accidents (e.g., rack-drop) will not adversely affect any plant equipment needed to mitigate consequences of a reactor accident or necessary to maintain safe shutdown.

Similar operations have been successfully accomplished by a number of utilities in the past, and there is every reason to believe that a safe and acceptable re-racking plan can be developed, pending selection of the best method of removal and disposal of existing racks. The Generic Environmental Impact Statement (NUREG-0575, August 1979) also suggests that re-racking may be safely accomplished subject to evaluation of specific rack designs and factors enumerated above.

REFERENCES

1. USNRC, Final Generic Environmental Impact Statement on Handling and Storage of Spent Light Water Power Reactor Fuel, NUREG-0575, August 1979.

2. A. B. Johnson, Jr., "Behavior of Spent Nuclear Fuel in Water Pool Storage," BNWL-2256, September 1977.

3. J. M. Wright, "Expected Air and Water Activities in the Fuel Storage Canal," WAPD-PWR-CP-1723 (with addendum), undated.

4. ANS 5.4 Proposed Standard, "Method for Calculating the Fractional Release of Volatile Fission Products from Oxide Fuel," American Nuclear Society, issued for review 1981.

5. J. R. Weeks, "Corrosion of Materials in Spent Fuel Storage Pools," BNL-NUREG-2021 (Informal Report), July 1977.

9. NEUTRON ABSORBER MATERIAL

The material utilized for neutron attenuation in the racks is Boraflex; a proprietary product of Bisco, a Divisicn of Brand Industrial Services. This material is available in a sheet form which facilitates easy handling and close control of lateral dimensions during fabrication. This material has found wide-spread acceptance due to its durability, Boraflex retains its physical and mechanical properties remarkably when subject to high or low flux irradiation which are under typical fuel pool environments. A brief summary of the established information on this material is given in the following sections:

9.1 Chemical Composition

The elemental composition of the proposed Boraflex proposed can be divided into two categories, the polymeric matrix system and the boron carbide powder. The elemental composition of each to the nearest per centage by weight (∓0.5%) is given in Table I.

TABLE I

Elemental Composition of Boraflex Components by Weight

ELEMENT	POLYMER	B_4C
Silicon	41%	-
Oxygen	37%	-
Hydrogen	4.5%	-
Carbon	17.5%	23.5%
Boron	-	76%
Iron;soluble borons	-	0.5%

The elemental content of Boraflex based on this formulation would be as follows:

TABLE II
Elemental Composition of Boraflex Containing
49 wt. % B_4C (by wt. %)

Silicone	24.0
Oxygen	21.5
Hydrogen	2.5
Carbon	20.0
Boron	32.0

Iron, soluble boron - trace

Note that the isotopic B^{10} content expressed as wt. % of total boron is typically 18.33 ∓ .4.

9.2 Physical Properties

Boraflex has been extensively tested for physical and mechanical characteristics when subjected to high and low rate irradiation while contained in air, deionized water or borated water environments. Careful laboratory data on neutron attenuation, elemental boron leaching, residual activity, gas generation, etc. were also taken and documented. Bisco report 748-10-1 contains detailed description of the procedures and recorded results. It is shown that the exposure of boraflex in air to 2.81×10^8 rads gamma from a spent fuel source results in no significant physical changes nor in the generation of any gas. Irradiation to the level 1.03×10^{11} rads gamma with a

substantial concurrent neutron flux in air, deionized water, and borated water environments causes some increase in hardness and tensile strength of boraflex. During that irradiation a certain amount of gas is generated but beyond the level of 1×10^{10} rads gamma it drops off considerably. The rate of gas generation is found to be greater when B_4C is irradiated in deionized or borated water in absence of boraflex, thus confirming the function of boraflex polymer as an escapsulant which mitigates the interaction between boron carbide and the environment. Vent holes are provided on top of each storage cell compartment to eliminate gas entrapment.

Measurements of the specimen width, thickness, weight, specific grvity at pre-and-post irradiation stages indicated minuscule variation in these quantities.

Experiments also show that neither irradiation, environment nor boraflex composition has any discernible effect on the neutron transmission of boraflex. Tests also prove that boraflex does not possess leachable halogens that may be extracted into the pool environment in the presence of radiation. Similar conclusions are reached regarding leaching of elemental boron out of boraflex. The results attested to the efficient encapsulation function of the boraflex matrix in preventing dissolution of normally soluble boron species.

A critical examination of the voluminous body of evidence on the functional characteristics of boraflex has led Joseph Oat Corporation to recommend its use in the Fermi II racks. Following are the references which Joseph Oat Corporation used in citing the functional characteristics of the Boraflex.

BORAFLEX EXPERIENCE LIST

Wisconsin Electric — NRC License issued
Point Beach 1 (Docket 50-266) PWR

Wisconsin Electric — NRC License issued
Point Beach 2 °(Docket 50-301) PWR

Niagara Mohawk — NRC License issued
Nine Mile Point 1 (Docket 50-220) BWR

Niagara Mohawk — NRC License to be applied for
Nine Mile Point 2 (Docket 50-410) BWR

Consumer Power Company — NRC License pending
Midland Units 1 & 2 (Docket 50-329, 50-330) PWR

TVA — NRC License pending
Watts Bar Units 1 & 2 (Dockets 50-390),50-391) PWR

Louisiana Power & Light — NRC License Pending
Waterford Unit 3 (Docket 50-382) PWR

Duke Power
Oconee Units 11 & 2 (Docket 50-269,50-270) PWR License issued

Northern States Power
Prairie Island Units 1 & 2 (Docket 50-282,50-306) PWR License issued.

Detroit Edison
Fermi-2 (Docket 50-341) BWR License pending.

Baltimore Gas & Electric
Calvert Cliffs II (Docket 50-318) PWR License issued.

Commonwealth Edison Company
Quad Cities Units 1 & 2 (Docket 50-254,50-265) BWR License pending.

Carolina Power & Light Company
H.B. Robinson 2 (Docket 50-261) PWR License Pending.

Carolina Power & Light Company
Shearon Harris SUnit 1 (Docket 50-400) PWR* License to be applied for.

Northeast Nuclear Energy Company
Millstone Unit 3 (Docket 50-423) PWR* License to be applied for.

Gulf States Utilities Company
River Bend Unit 1 (Docket 50-458) BWR License pending.

* BWR & PWR Fuel Storage Capabilities

10. INSERVICE SURVEILLANCE PROGRAM FOR BORAFLEX NEUTRON ABSORBING MATERIAL

10.1 Program Intent:

A sampling program to verify the integrity of the neutron absorber material employed in the high-density fuel racks in the long-term environment is described in this section.

The program is intended to be conducted in a manner which allows access to the representative absorber material samples without disrupting the integrity of the entire fuel storage system. The program is tailored to evaluate the material in normal use mode, and to forecast future changes using the data base developed.

10.2 Description of Specimens:

The absorber material, henceforth referred to as "poison", used in the surveillance program must be representative of the material used within the storage system. It must be of the same composition, produced by the same method, and certified to the same criteria as the production lot poison. The sample coupon must be of similar thickness as the poison used within the storage system and not less than 6" x 6" inches on a side. Figure 10.1 shows a typical coupon. Each poison specimen must be encased in a stainless steel jacket of an identical alloy to that used in the storage system, formed so as to encase the poison material and fix it in a position and with tolerances similar to that designed used for the storage system. The jacket has to be closed by tack welding in such a manner as to retain its form throughout the test period and still allow rapid and easy opening without causing mechanical damage to the poison specimen contained within. The jacket should permit wetting and venting of the specimen similar to the actual rack environment.

10.3 Test:

The test conditions represent the vented conditions of the box elements. The samples are to be located adjacent to the fuel racks and suspended from the spent fuel pool wall. Eighteen test samples are to be fabricated in accordance with Figure 10.1 and installed in the pool when the racks are installed.

The procedure for fabrication and testing of samples is as given below:

a. The samples should be cut to size and weighed carefully in milligrams.
b. The length, width, and the average thickness of each specimen is to be measured and recorded.
c. The samples should be fabricated in accordance with Figure 10.1 and installed in the pool.
d. Two samples should be removed at each time interval according to the schedule shown in Table 10.1.

10.4 Specimen Evaluation:

After the removal of the jacketed poison specimen from the fuel pool at a designated time, a careful evaluation of that specimen should be made to determine its actual condition as well as its apparent durability for continued function. Separation of the poison from the stainless steel specimen jacket must be performed carefully to avoid mechanical damage to the poison specimen. Immediately after the removal, the specimen and jacket section should visually be examined for any effects of environmental exposure. Specific attention should be directed to the examination of the stainless steel jacket for any evidence of physical degradation. Functional evaluation of the poison material can be accomplished by the following measurements:

a. A neutron radiograph of the poison specimen aids in the determination of the maintenance of uniformity of the boron distribution.

b. Neutron attenuation measurements will allow evaluation of the continued nuclear effectiveness of the poison. Consideration must be given, in the analysis of the attenuation measurements, for the level of accuracy of such measurements as indicated by the degree of repeatability normally observed by the testing agency.

c. A measurement of the hardness of the poison material will establish the continuance of physical and structural durabiity. The hardness acceptability criterion requires that the specimen hardness will not exceed the hardness listed in the qualifying test document for laboratory test specimen irradiated to 10^{11} rads. The actual hardness measurement should be made after the specimen has been withdrawn from the pool and allowed to air dry for not less than 48 hours to allow for a meaningful correlation with the preirradiated sample.

d. Measurement of the length, the width, and the average thickness and comparison with the pre-exposure data will indicate dimensional stability within the variation range reported in the Boraflex laboratory test reports.

A detailed procedure paraphrasing the intent of this program will be prepared for step-by-step execution of the test procedure and interpretation of the test data.

TABLE 10.1

Date Installed_____

	SCHEDULE	INITIAL WEIGHT (mg/Cm^2-Yr)	FINAL WEIGHT (mg/Cm^2-Yr)	WEIGHT CHANGE (mg/Cm^2-Yr)	PIT PENETRATION mil/Yr
1					
2	90 day				
3					
4	180 day				
5					
6	1 year				
7					
8	5 year				
9					
10	10 year				
11					
12	15 year				
13					
14	20 year				
15					
16	30 year				
17					
18	40 year				

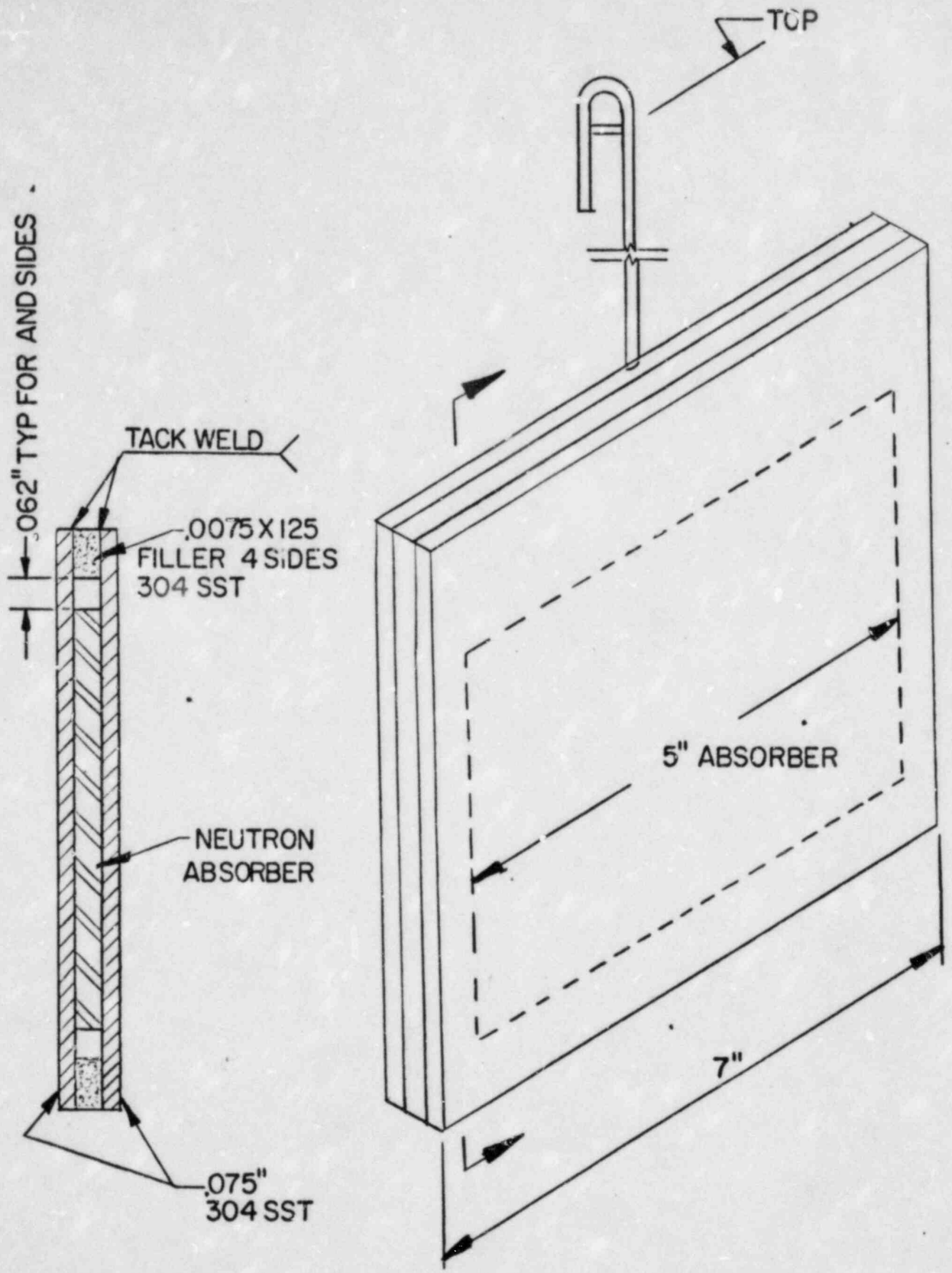
TOP
.062" TYP FOR AND SIDES
TACK WELD
.0075 X 125
FILLER 4 SIDES
304 SST
NEUTRON
ABSORBER
.075"
304 SST
5" ABSORBER
7"

FIG. 10.1

11. DESIGN CONTROL AND FABRICATION INTERFACE

11.1 Introduction

In this chapter, an abstract of the design control from Joseph Oat's Q.A. System is presented in a flow chart form. This program has been accepted by the ASME for engineered fabrication of ASME Section III, Class 1, 2, 3 and MC components. The program has been found to be acceptable to NRC audit teams, as well as to the special projects such as the CRBRP and the U.S. Department of Defense.

11.2 Personnel

The personnel categories involved in the operations are:

1. General Manager (G.M.)
2. Chief Engineer (C.E.)
3. Project Engineer (P.E.)
4. Professional Engineer
5. Designated Analysts (D.A.)
6. Designated Draftsman
7. Contract Administrator (C.A.)
8. Transmittal Clerk (T.C.)

The flow of work is shown in the following flow charts. Flow Chart #1 shows the job progress sequence from its initiation. Flow Chart #2 gives the operation sequence following customer feedback to the initial document and the customer generated documents.

All documents to be treated in course of a job are divided into five types as noted in the footnote of Flow Chart #2.

This operational flow chart gives the minimum number of steps required in the processing of a contract. Additional personnel may be called upon for expert help by the Project Engineer wherever deemed necessary. For example, the practical advice of the Shop Superintendent in determining the feasibility or economy of a

design or the advice of the Quality Control Manager regarding NDT and material testing requirements are frequent types of help sought by the Project Engineer. These are necessary steps for high quality design, although not essential for meeting quality assurance requirements.

The procedure itself is self-explanatory as laid out in the two Flow Charts.

11.3 Flow Charts:

The flow chart follows from pages 11-3 to 11-5, and in case of customer's comment for any document, the recycling channel is same as shown on page 11-5.

If there is any deviation in any dimension or tolerance according to the fabrication drawing, Q.C. sends a deviation notice to the Project Engineer. The Project Engineer evaluates and decides if it meets the customer's specification and drawings. If it does not meet the customer's specification, drawing, or both, the deviation notice is sent to the customer for evaluation. The final decision is based on customer's review.

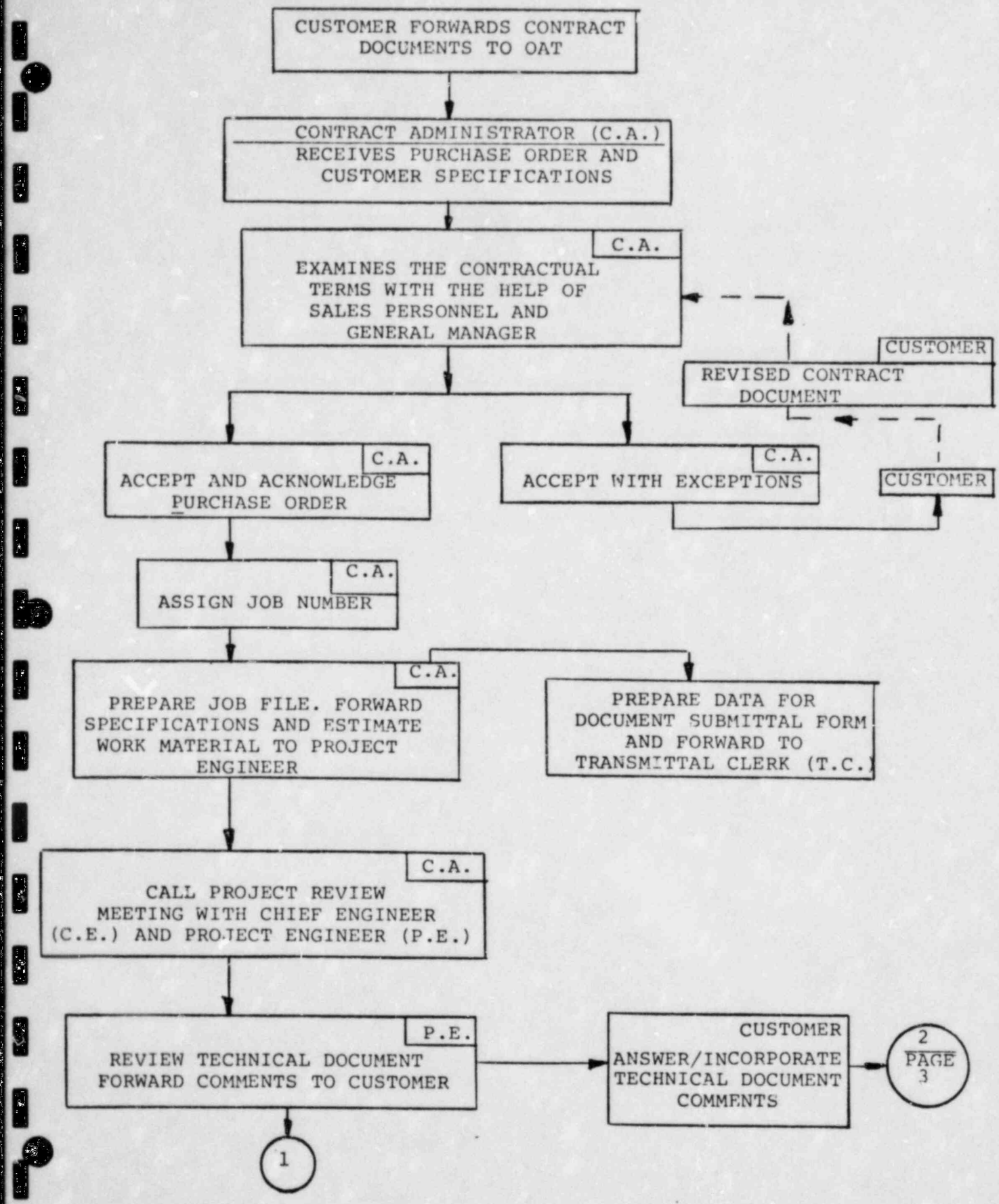
CUSTOMER FORWARDS CONTRACT DOCUMENTS TO OAT
CONTRACT ADMINISTRATOR (C.A.)
RECEIVES PURCHASE ORDER AND CUSTOMER SPECIFICATIONS
C.A.
EXAMINES THE CONTRACTUAL TERMS WITH THE HELP OF SALES PERSONNEL AND GENERAL MANAGER
CUSTOMER
REVISED CONTRACT DOCUMENT
C.A.
ACCEPT AND ACKNOWLEDGE PURCHASE ORDER
C.A.
ACCEPT WITH EXCEPTIONS
CUSTOMER
C.A.
ASSIGN JOB NUMBER
C.A.
PREPARE JOB FILE. FORWARD SPECIFICATIONS AND ESTIMATE WORK MATERIAL TO PROJECT ENGINEER
PREPARE DATA FOR DOCUMENT SUBMITTAL FORM AND FORWARD TO TRANSMITTAL CLERK (T.C.)
C.A.
CALL PROJECT REVIEW MEETING WITH CHIEF ENGINEER (C.E.) AND PROJECT ENGINEER (P.E.)
P.E.
REVIEW TECHNICAL DOCUMENT FORWARD COMMENTS TO CUSTOMER
CUSTOMER
ANSWER/INCORPORATE TECHNICAL DOCUMENT COMMENTS
2
PAGE 3
1

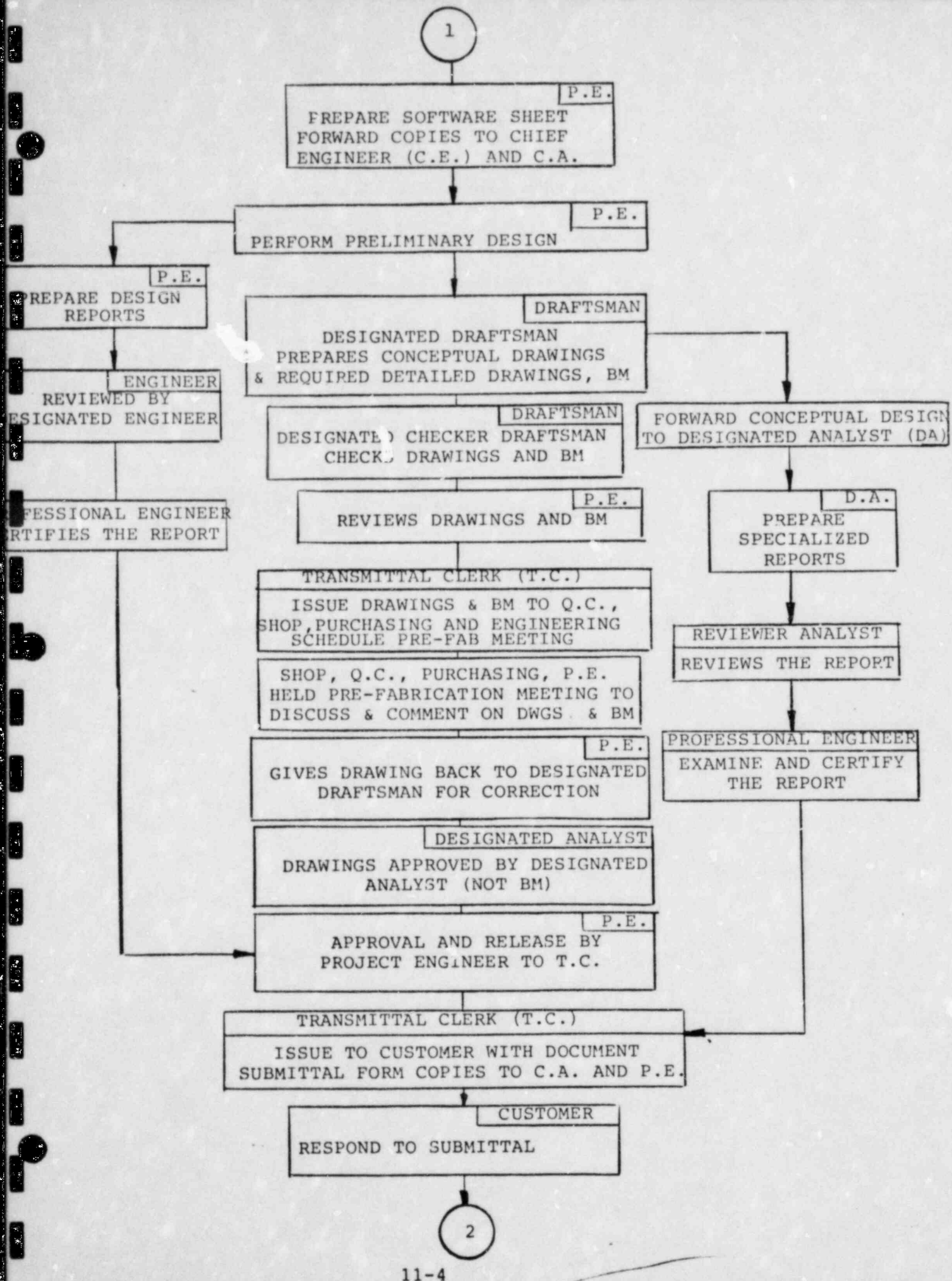
1
P.E.
PREPARE SOFTWARE SHEET FORWARD COPIES TO CHIEF ENGINEER (C.E.) AND C.A.
P.E.
PERFORM PRELIMINARY DESIGN
P.E.
PREPARE DESIGN REPORTS
DRAFTSMAN
DESIGNATED DRAFTSMAN PREPARES CONCEPTUAL DRAWINGS & REQUIRED DETAILED DRAWINGS, BM
ENGINEER
REVIEWED BY ESIGNATED ENGINEER
DRAFTSMAN
DESIGNATE) CHECKER DRAFTSMAN CHECK DRAWINGS AND BM
FORWARD CONCEPTUAL DESIGN TO DESIGNATED ANALYST (DA)
FESSIONAL ENGINEER RTIFIES THE REPORT
P.E.
REVIEWS DRAWINGS AND BM
D.A.
PREPARE SPECIALIZED REPORTS
TRANSMITTAL CLERK (T.C.)
ISSUE DRAWINGS & BM TO Q.C., SHOP, PURCHASING AND ENGINEERING SCHEDULE PRE-FAB MEETING
REVIEWER ANALYST
REVIEWS THE REPORT
SHOP, Q.C., PURCHASING, P.E. HELD PRE-FABRICATION MEETING TO DISCUSS & COMMENT ON DWGS & BM
PROFESSIONAL ENGINEER
EXAMINE AND CERTIFY THE REPORT
P.E.
GIVES DRAWING BACK TO DESIGNATED DRAFTSMAN FOR CORRECTION
DESIGNATED ANALYST
DRAWINGS APPROVED BY DESIGNATED ANALYST (NOT BM)
P.E.
APPROVAL AND RELEASE BY PROJECT ENGINEER TO T.C.
TRANSMITTAL CLERK (T.C.)
ISSUE TO CUSTOMER WITH DOCUMENT SUBMITTAL FORM COPIES TO C.A. AND P.E.
CUSTOMER
RESPOND TO SUBMITTAL
2

FLOW CHART #2

DOCUMENTS FROM CUSTOMER

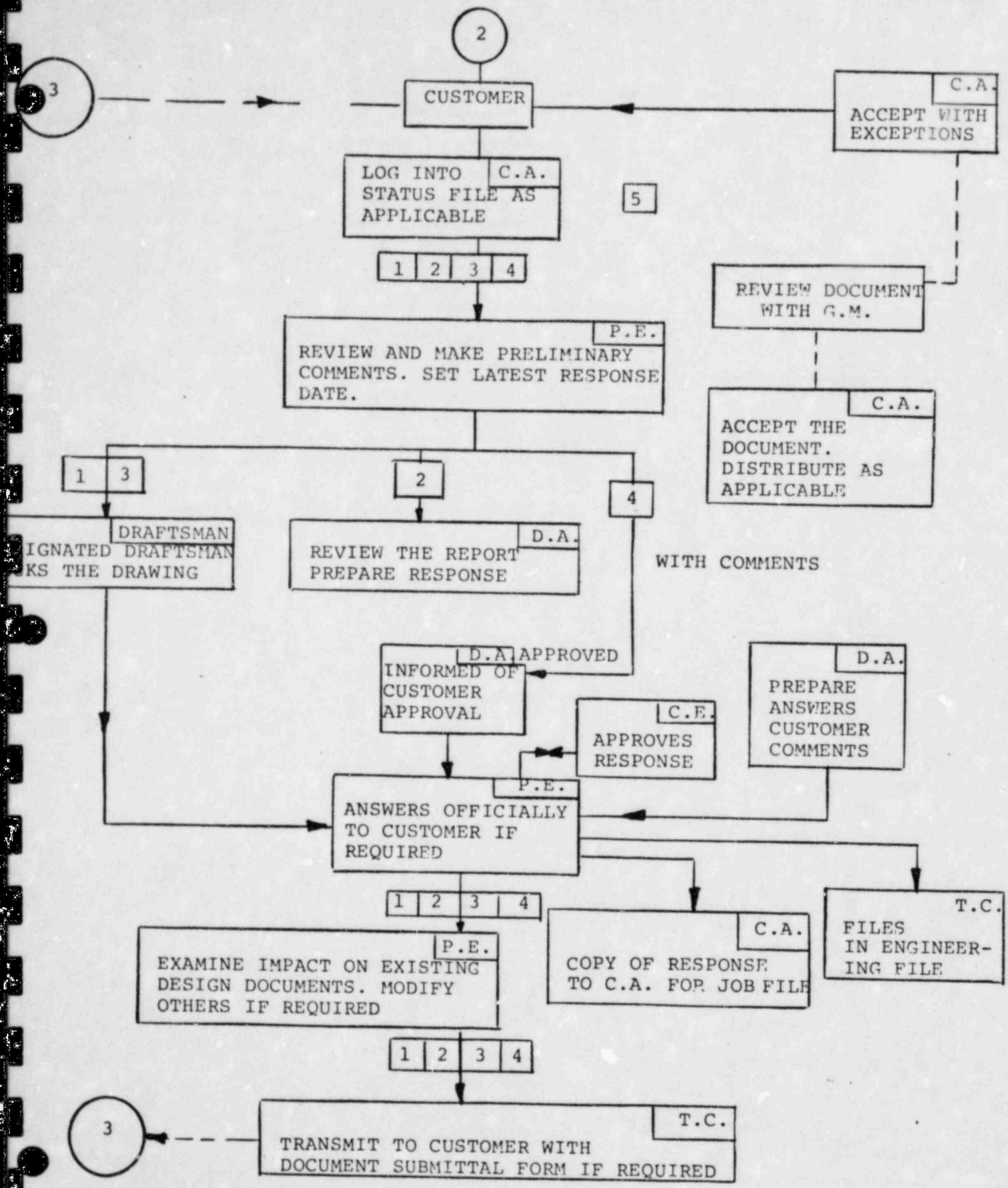

DOCUMENT TYPES:

CUSTOMER PREPARED DRAWINGS [3] OAT PPEPAPED DRAWINGS [5] CONTRACTUAL (NON-TECHNICAL) DOCUMENTS

CUSTOMER PREPARED REPORTS [4] OAT PREPAPED REPORTS

12. QUALITY ASSURANCE PROGRAM

12.1 Introduction

This chapter provides a general description of the Quality Assurance Program that is implemented to assure that the quality objectives of the contract specification are met.

12.2 General

The Quality Assurance Program used on this project is based upon the system described in Joseph Oat's Nuclear Quality Assurance Manual. This system is designed to provide a flexible, but a highly controlled system for the design, manufacture and testing of customized components in accordance with various Codes, specifications, and regulatory requirements.

The philosophy behind Oat's Quality Assurance System is that it shall provide for all controls necessary to fulfill the contract requirements with sufficient simplicity to make it functional on a day to day basis. As this system is applied to most of the contracts which Joseph Oat obtains, implementation of it is almost second nature to Oat's personnel. The system readily adapts to different designs and component configurations, making possible the construction of many varied forms of equipment. The highlights of this system, as addressed in the following paragraphs, provide an overview of the system and how it has been applied to the customer specifications and regulations.

12.3 System Highlights:

The design control section is organized to provide for careful review of all contract requirements to extract each individual design and quality criteria. These criteria are translated into design and quality control documents customized to the contract requirements and completely reviewed and approved by responsible personnel.

The system for control of purchased material entails generating detailed descriptions of each individual item of material along with specifications for any special requirements such as impact testing, corrosion testing, monitoring, or witnessing of chemical analysis, provision of overcheck specimens, special treatments or conditioning of material, source inspection, and provision of documentation of performance of any of the above.

Material receipt inspection includes a complete check of all material and its documentation. Upon acceptance, each item of material is individually listed on a control sheet issued once a week to assure that only accepted material goes into fabrication.

The fabrication control system provides that a shop traveler is prepared for each subassembly and assembly in each contract. The traveler is generated specifically to provide step by step instructions for fabrication, inspection, testing, cleaning, packaging, etc. which address all standard and special requirements of the contract specifications. Special attention is given to deployment of fabrication sequence and inspection steps to preclude the possibility of missing poison sheets or incorrect sheets (incorrect B^{10} loading).

Due to the tendency of contract specifications to require special examination techniques or test procedures, all nondestructive examination procedures and test procedures are custom written to apply to each given component within a contract.

The system provides for qualification and written certification of personnel performing quality related activities including nondestructive examination and fabrication inspection, welding, engineering, production supervision and auditing.

Other requirements of a solid quality control system are fully covered as specified in the Quality Assurance Manual including document control, control of measuring and test equipment, control of nonconforming material and parts, corrective action auditing and other areas as specified.

12.4 Summary:

Joseph Oat Corporation's Quality Assurance System provides the full measure of quality assurance required by the contract. All special requirements of the specifications are covered including source inspection of material and witnessing of material testing by the Engineer, furnishing of material certifications and test reports within five days of shipment, and obtaining verification of qualification testing of poison materials. We have a long history of providing excellent quality control over a wide range of equipment types such as the high density fuel racks.

13. PRODUCTION CONTROL

13.1 Introduction:

Production Control at Joseph Oat Corporation is based on the use of a critical path diagram (CPD). A critical path diagram is developed for each component manufactured at Joseph Oat Corporation. The critical path diagram consists of a detailed breakdown of the operations required to fabricate each part, subassembly and total assembly required to complete the finished product. The critical path diagram is arranged to show inter-relationship of all parts and sub-assemblies, including milestone dates for the completion of each operation to assure that all parts and subassemblies are completed in time to support the overall fabrication schedule.

13.2 Procurement:

A bill of materials is generated for every component to be manufactured. The bill of material is reviewed against the CPD to determine the required delivery date for each item of material. This information is given to the Purchasing Department to be used as the basis for purchase delivery requirements. The Purchasing Department has a full-time Expeditor to continuously review the scheduled delivery of all materials from suppliers. Problem items are reported to the Purchasing Agent who is responsible for assuring on-time delivery of all materials. Expediting visits to the supplier in question are performed by the Purchasing Agent or Expeditor whenever necessary. In addition, Production Control reviews the received materials on each component on a weekly basis. Any unreceived item of material which is within 2 weeks of its critical required date is reported to Purchasing and to the General Manager. The General Manager institutes the corrective action which is necessary to maintain the required delivery.

13.3 Shop Floor Planning:

Daily work assignments on the production floor are generated by the Plant Manager. All work assignments are planned out in writing a week in advance. Work assignments are based on completing the operations necessary to maintain the schedule required by the critical path diagrams. The work assignment sheet is checked each week by Production Control to assure that all required work is scheduled.

13.4 Operations Control and Coordination:

The critical path diagram for each component is monitored continuously by the Production Control Department. Once a week each component's status is determined and recorded on the CPD. The diagram is then reviewed to identify any operations which are not on or ahead of schedule. All such operations are reported to the General Manager, the Plant Manager, and to top management. Production Control meets with the Plant Manager to determine the action necessary to bring the operation back on schedule. The work schedule for the following week is revised as necessary to assure performance of the work required to support the delivery schedule.

13.5 Reporting:

The complete status of each component in the fabrication schedule is reported to management by Production Control every week in the form of updated critical path diagrams. This information is used by management for future work load planning, scheduling, and reporting status to the customer.

14. COST/BENEFIT ASSESSMENT

A cost/benefit assessment has been prepared in accordance with the requirements of Section V, Part 1.[1] The purpose of the assessment is to demonstrate that the installation of high-density spent fuel storage racks is the most advantageous means of handling spent fuel, considering the needs of our customers for a dependable source of electric power.

The material is presented to satisfy the NRC's need for information; it is the position of the District that no environmental impact statement need be prepared in support of the request, because that will be no significant impact on the human environment. However, an EIR was prepared in accordance with the California Environmental Quality Act of 1970 (CEQA). Similarly, NRC precedent establishes that alternatives and economic costs need not be discussed when there is no significant environmental impact.

14.1 Specific Needs for Spent Fuel Storage

No contractual arrangements exist for the storage or reprocessing of spent fuel from Rancho Seco. Accordingly, the storage of spent fuel from Rancho Seco, in the Rancho Seco spent fuel pool, is the only viable option being considered. Table 1.1 shows the schedule for refueling and indicates the discharge capability based on the following option:

- o Existing spent fuel
- o High-density spent fuel racks.

Based on the present lack of an alternative to onsite spent fuel storage, it is not possible to predict how long the additional spent fuel storage capability will be required. It is unlikely that an alternative to onsite spent fuel storage will be available before 1990. Based on Table 1.1, the proposed increase in storage

capacity would accommodate the refueling of Rancho Seco in the year 1997, but would not accommodate the refueling in the year 1998 if full core discharge capability is maintained.

14.2 Cost of Modification

The design and manufacture of the spent fuel storage racks will be undertaken by the organizations described in Section 1. It is expected that the total project cost will be between 4 and 5 million dollars.

14.3 Alternatives to Spent Fuel Storage Expansion

The District has considered the various alternatives to the proposed increase in spent fuel storage capacity. These alternatives are as follows:

- Shipment of fuel to a reprocessing or independent spent fuel storage facility

  No commercial spent fuel reprocessing facilities are presently operating in the United States. In addition, the District has not obtained commercial spent fuel storage commitments for fuel from Rancho Seco. The Department of Energy Away-From-Reactor Storage Program has been terminated, and no commercial independent spent fuel storage facilities exist.

- Shipment to another reactor site

  The District considers the storage of spent fuel at reactor sites to be a long-term option due to the lack of any reasonable alternatives. Shipments of fuel to another utility site would provide short-term relief; however, transshipment of spent fuel does not contribute to the long-term goal of providing adequate storage

capacity but merely serves to transfer the problem to another site. Accordingly, the District does not consider the transshipment of spent fuel to be an appropriate alternative to high-density spent fuel storage at the site.

- o Shutting down the reactor

  Shutting down Rancho Seco would result in an economic hardship that would be imposed on the Districts' customers. Moreover, as indicated in NUREG-0575, "Final Environmental Impact Statement on Handling and Storage of Spent Light Water Power Reactor Fuel,", the replacement of nuclear power by coal-generating capacity would cause excess mortality to rise from 0.59-1.7 to 15-120 per year for 0.8 GWY(e). Based on the above, shutting down Rancho Seco does not represent a viable alternative.

14.4 Resource Commitments

The expansion of the Rancho Seco spent fuel storage capacity will require the following primary resources (approximately):

- o Stainless steel - 250,000 pounds
- o Boraflex neutron absorber - 45,000 pounds of which 3,000 pounds is Boron Carbide (B_4C) powder.

The requirement for stainless steel represents a small fraction of the total domestic production of 175 million tons for 1980.[2] Although the fraction of domestic production of B_4C, required for the modification, is somewhat higher than that for stainless steel, it is unlikely that the commitment of B_4C to this project will affect other alternatives. Experience has shown that the production of B_4C is highly variable and depends on need, but could easily be expanded to accommodate additional domestic demands. The total boron production estimates for 1985 is 275 to 350 thousand tons.

14.5 Environmental Effects

An environmental impact report (EIR) has been prepared in accordance with the requirements of the California Environmental Quality Act.[3]. The EIR identifies the proposed project's features, potential environmental effects, the mitigation measures taken to ensure conformance with accepted safety design criteria, and alternatives to the project.

The ecological and health impacts of the handling and storage of spent fuel have been described in a generic environmental impact statement (EIS) prepared by the Office of Nuclear Material Safety and Safeguards of the U.S. Nuclear Regulatory Commission.[4] Based upon information from the generic EIS, the EIR concluded that storing additional spent fuel in the existing pool would have the following ecological impacts:

1. The amount of waste heat emitted by the plant would increase by less than one percent.

2. The amount of radioactive particulate matter accumulated in the pool filter and demineralizer, which are disposed of as solid radioactive waste, would increase. There would be no increase in the volume of radioactive waste shipped from Rancho Seco, however.

Based upon information from the generic EIS, the EIR concluded that the project would result in the following health impacts:

1. The dose rate in the pool area would increase by only a negligible amount because the radiological impact of aged spent fuel is significantly reduced, the depth of water in the pool provides adequate biological shielding and the pool cleaning system keeps the amount of contamination in the pool at a low level.

2. The potential radiological hazard to the public is increased by an extremely small amount because the radioactivity in spent fuel is not in a dispersible form and there is no credible mechanism available to cause the release of radiocactive material from the facility.

The EIR concluded that the project would have no significiant social impacts. Specifically, the project would not have an impact on the "Emergency Response Plan" or on other local services and facilities.

The EIR discussed the measures to be taken to minimize the environmental and health impacts of the project. These measures include the performance of criticality, seismic, and thermal hydraulic analyses to ensure conformance with the general design criteria of 10CFR50, Appendix A.

The EIR also discussed the methods to be taken to minimize radiation exposure to personnel during the installation of the new racks and the removal, decontamination, and disposal of the existing racks. Divers employed during the removal of existing racks and installation of new racks will wear dry suits covered by anticontamination suits and will maintain a minimum separation from the spent fuel in order to use the pool water for shielding. Decontamination of the existing racks may be performed with an underwater jet lancing process followed by the use of an electropolishing acid dip system.

The EIR examined the following alternatives to the project:

1. Shipment of fuel to an existing reprocessing or independent storage facility.

2. Volume expansion of existing pool.

3. Shipment of fuel to a new away from reactor wet storage facility.

4. Shipment of fuel to a new dry storage facility.

5. Shipment of fuel to another reactor site.

6. Modification of fuel management practices.

7. Termination of operations and construction of replacement coal-fired, photovoltaic, solar thermal, oil, gas, hydro, or geothermal power plants.

The EIR concluded that the above alternatives were either infeasible or would be more costly and involve more extensive environmental impacts.

REFERENCES TO SECTION 14

1. B.K. Grimes, "OT Position for Review and Acceptance of Spent Fuel Storage and Handling Applications," April 14, 1978.

2. "Mineral Facts and Problems," Bureau of Mines Bulletin 667, 1975.

3. Sacramento Municipal Utility District. May 1982. Draft Environmental Impact Report, Spent Fuel Pool Rerack.

4. U.S. Nuclear Regulatory Commission. August 1979. Final Generic Environmental Impact Statement on Handling and Storage of Spent Light Water Power Reactor Fuel. NUREG-0575.